Analysis of heterogeneously configured converter stations in HVDC grids under asymmetrical DC operation

by

Jesús Serrano Sillero

A dissertation submitted in partial fulfilment of the requirements for the degree of Doctor of Philosophy in

Electrical Engineering, Electronics and Automation

Universidad Carlos III de Madrid

Advisor:

Mª Ángeles Moreno López de Saá

Tutor:

Mª Ángeles Moreno López de Saá

May 2023

To my family/A mi familia

ACKNOWLEDGEMENTS

I would like to express my sincere gratitude to my supervisor, Dr. Mª Ángeles Moreno, who gived me the opportunity to do this work and helped me during all this time. I would also like to show my deep appreciation to Dr. Ana Morales for her contribution to part of this work.

I wish to extend my special thanks to Miriam, my family and my in-laws, who supported me and encouraged me during all this time.

Finally, I would like to thank all friends that have accompanied me at different times throughout this period.

PUBLISHED AND SUBMITTED CONTENT

- J. Serrano-Sillero, M. Á. Moreno, and A. Morales, "HVDC grids with heterogeneous configuration stations under DC asymmetrical operation," *International Journal of Electrical Power & Energy Systems*, vol. 113, 2019.
    - Published (https://doi.org/10.1016/j.ijepes.2019.05.053)
    - As first author, I conducted the analysis, calculations and simulations, and wrote the entire document.
    - Totally included in the thesis, Chapter 3.
    - The material from this source included in this thesis is not singled out with typographic means and references.
- J. Serrano-Sillero and M. Á. Moreno, "Small-signal stability analysis of the asymmetrical DC operation in HVDC networks," *Electric Power Systems Research*, vol. 214, p. 108942, Jan. 2023.
    - Published (https://doi.org/10.1016/j.epsr.2022.108942)
    - As first author, I conducted the analysis, the model development, the calculations and the simulations, and wrote the entire document.
    - Totally included in the thesis as part of Chapter 4, Chapter 5 and Appendix B.
    - The material from this source included in this thesis is not singled out with typographic means and references.

OTHER RESEARCH MERITS

- J. Serrano, M. Á. Moreno, A. Morales, and X. Robe, "*Reliability and security of unbalanced distribution grids based on probabilistic (n-1)-criterion with distributed renewable energy resources*," 2019, vol. Proc. of the 25th International Conference on Electricity Distribution, no. CIRED 2019 Conference. http://dx.doi.org/10.34890/603
- Cigré Working Group B4.72, "*DC grid benchmark models for system studies*," CIGRE Tech. Brochure, vol. 804, no. June 2020.

ABSTRACT

Additional technologies different from classical high voltage alternating current (HVAC) transmission are necessary to deal with the higher renewable energy integration in the current energetic framework. High voltage direct current (HVDC) transmission based on modular multilevel voltage source converters (MMC-VSC) is a promising alternative for some applications. Thus, the number of HVDC projects is increasing worldwide. This makes possible their future gradual interconnection to constitute an overlay DC grid that offers numerous additional advantages but still many challenges.

Even if the development of the HVDC technology overcomes all the present challenges in the future, the lack of standardisation will lead to a DC grid integrated by different HVDC station topologies, grounding schemes, DC-DC converters, or control strategies. During normal operation, the DC grid is assumed to work symmetrically, and some aspects, such as the topology or the grounding scheme, do not intervene in the system response. However, in case of working asymmetrically due to a fault or outage affecting a single pole of the DC network, all the aspects mentioned above affect the system operation.

However, such a heterogeneous DC grid under asymmetrical DC operation has yet to be addressed in the literature. Thus, it constitutes the general objective of this thesis. To achieve this objective, the asymmetrical DC operation in different heterogeneous DC systems is studied using load flow, dynamic EMT simulation, and small-signal stability analysis. The analysis of a system of these characteristics under asymmetrical DC operation is an original contribution of the thesis.

First, a DC grid connecting different AC zones and formed by different HVDC station topologies and DC-DC converters is modelled to perform the load-flow assessment. The asymmetrical DC operation is examined by causing an asymmetrical contingency in the DC network. The analysis is carried out considering different grounding resistances, control strategies, control parameters, and galvanic isolation ability of the DC-DC converters. The results obtained regarding DC current and voltage asymmetry, which are related to the overloading of elements and excessive voltage deviation, allow for assessing the impact of the asymmetrical operation under different circumstances.

Second, the dynamic assessment aims to identify the main aspects involved in the transient response during asymmetrical DC operation. The connection of a symmetrical monopolar station to a bipolar system is modelled, and the outage of one of the converters of a bipolar station is simulated. The effect of the grounding impedance and the control strategy on the dynamic response of the system is assessed. Therefore, the main system parameters and issues that may appear are identified. Furthermore, the effect of the connection of the symmetrical monopole station over the existing protections of the bipolar system is assessed by considering different grounding impedances in the monopolar station.

Finally, the small-signal analysis of a system composed of different topologies focuses on the asymmetrical DC operation. A new suitable model is developed and validated against EMT simulations. The small-signal analysis is carried out, and the main aspects that impact the small-signal stability during asymmetrical operation are identified. Furthermore, a new controller that enhances the system stability during asymmetrical DC operation is developed.

RESUMEN

Para hacer frente a la mayor integración de energías renovables en el marco energético actual se necesitan tecnologías adicionales distintas de la transmisión clásica en corriente alterna en alta tensión (HVAC). La transmisión de corriente continua en alta tensión (HVDC) basada en convertidores multinivel modulares de fuente de tensión (MMC-VSC) es una alternativa prometedora para algunas aplicaciones. Por tanto, el número de proyectos HVDC está aumentando en todo el mundo. Esto hace posible que se interconecten gradualmente en el futuro para formar una red de corriente continua (CC) que ofrece numerosas ventajas adicionales, pero todavía muchos retos.

Aunque el desarrollo de la tecnología HVDC supere todos los retos actuales en el futuro, la falta de normalización dará lugar a una red de CC integrada por diferentes topologías de estaciones HVDC, esquemas de puesta a tierra, convertidores CC-CC o estrategias de control. Durante el funcionamiento normal, la red de CC funciona simétricamente y algunos aspectos, como la topología o el esquema de puesta a tierra, no intervienen en la respuesta del sistema. Sin embargo, en caso de funcionamiento asimétrico, debido a una falta o desconexión que afecte a un solo polo de la red de CC, todos los aspectos mencionados anteriormente afectan al funcionamiento del sistema.

Este tipo de red de CC heterogénea en funcionamiento asimétrico aún no se ha abordado en el estado del arte. Por ello, constituye el objetivo general de esta tesis. Para lograr este objetivo, se estudia el funcionamiento asimétrico de CC en diferentes sistemas heterogéneos de CC utilizando diferentes enfoques como el flujo de cargas, la simulación dinámica EMT y el análisis de estabilidad de pequeña señal. El análisis de un sistema de estas características en funcionamiento asimétrico en CC constituye la principal contribución de la tesis.

Para realizar la evaluación del flujo de cargas, se modela una red de CC que conecta diferentes zonas de CA y está formada por diferentes topologías de estaciones HVDC y convertidores CC-CC. A continuación, se examina el funcionamiento asimétrico de CC provocando una contingencia asimétrica en la red de CC. El análisis se lleva a cabo considerando diferentes resistencias de puesta a tierra, estrategias de control, parámetros de control y capacidad de aislamiento galvánico de los convertidores CC-CC. Los resultados obtenidos sobre la asimetría de corriente y tensión en CC, relacionados con la sobrecarga de los elementos y la desviación excesiva de la tensión, permiten evaluar el impacto del funcionamiento asimétrico en distintas circunstancias.

La evaluación dinámica pretende identificar los principales aspectos que intervienen en la respuesta transitoria durante el funcionamiento asimétrico en CC. En primer lugar, se modela la conexión de una estación monopolar simétrica a un sistema bipolar. A continuación, se simula la interrupción de uno de los convertidores de una estación bipolar y se evalúa el efecto de la impedancia de puesta a tierra y de la estrategia de control en la respuesta dinámica del sistema. Por último, se identifican los principales

parámetros del sistema y los problemas que pueden aparecer. Además, se evalúa el efecto de la conexión de la estación monopolar simétrica sobre las protecciones existentes del sistema bipolar, considerando diferentes impedancias de puesta a tierra en la estación monopolar.

Por último, se realiza el análisis de pequeña señal de un sistema compuesto por diferentes topologías centrándose en el funcionamiento asimétrico en CC. Para ello, primero se desarrolla un nuevo modelo adecuado para este análisis y se valida con simulaciones EMT. A continuación, se lleva a cabo el análisis de pequeña señal y se identifican los principales aspectos que afectan a la estabilidad de pequeña señal durante el funcionamiento asimétrico. Además, se desarrolla un nuevo controlador que mejora la estabilidad del sistema durante el funcionamiento asimétrico en CC.

CONTENTS

LIST OF FIGURES

LIST OF TABLES

NOMENCLATURE

Acronyms:

AC	Alternating Current
AVM	Average Value Model
CCC	Capacitor-Commutated Converter
CSCC	Controlled Series Capacitor Converter
DC	Direct Current
DCCB	DC Circuit Breaker
DCS	DC System
EMT	Electromagnetic Transient
HVAC	High Voltage AC
HVDC	High Voltage DC
IGBT	Insulated-Gate Bipolar Transistor
LCC	Line-Commutated Converter
MMC	Modular Multilevel Converter
MTDC	Multi-Terminal DC
PLL	Phase-Locked Loop
SM	Submodule
VSC	Voltage-Source Converter

Superscripts:

*	Reference value.
+/-	Positive/negative pole of a direct current system.
b	Bipolar converter station.

j	Phase of an alternating current system.
m	Monopolar converter station.
Subscripts:	
$d,q,0$	Direct/quadrature/zero-sequence components.
o	Initial operating point.
Variables:	
e_0	Zero-sequence component of the inner voltage of a converter.
e^j	Inner voltage of a converter in the phase-*j*.
i_{ac0}	Zero-sequence component of the alternating current.
i_{ac}^j	Alternating current flowing through the phase-*j*.
i_{asy}	Current asymmetry between the positive and negative poles.
$i_{c,d}^{*m}$, $i_{c,q}^{*m}$	References for the direct/quadrature current components on the ac side of the monopolar converter.
$i_{c,d}^m, i_{c,q}^m, i_{c,0}^m$	Direct/quadrature/zero-sequence current components on the ac side of the monopolar converter.
i_c^{b+}, i_c^{b-}	Positive/negative pole current on the ac side of the bipolar converter.
i_c^m	Current on the ac side of the monopolar converter.
i_{dc}	Direct current on the dc side.
i_{dc}^{b+}, i_{dc}^{b-}	Positive/negative pole current on the dc side of the bipolar converter.
i_{dc}^{m+}, i_{dc}^{m-}	Positive/negative pole current on the dc side of the monopolar converter.
i_{diff}^j	Current flowing through the phase-*j* leg.
i_e	Earth current.
i_g^m, i_g^b	Current injected by the external ac grid on the ac side of the monopolar/bipolar station.

$i_{line}^{+}, i_{line}^{-}$	Positive/negative pole current on the dc line.
$i_{trf}^{b+}, i_{trf}^{b-}$	Current on the transformer of the positive/negative pole of the bipolar converter.
i_u^j, i_l^j	Upper and lower arm currents in phase-*j* of a converter
p_{asy}	Active power asymmetry between the positive and negative poles.
$p_{ctrl}^{*b}, q_{ctrl}^{*b}$	References for the active/reactive power of the controllers at the bipolar converter.
$p_{ctrl}^{*m}, q_{ctrl}^{*m}$	References for the active/reactive power of the controllers at the monopolar converter.
p_{dc}^{+}, p_{dc}^{-}	Active power injected in the positive and negative dc pole.
s_x	Insertion indexes of the submodules of each arm.
u_{ac0}	Zero-sequence component of the alternating voltage.
u_{ac}^j	Alternating voltage at the phase-*j*.
u_{asy}	Voltage asymmetry between the positive and negative poles.
u_l^j, u_u^j	Upper and lower arm voltages in phase-*j* of a converter
$v_{c,d}^m, v_{c,q}^m, v_{c,0}^m$	Direct/quadrature/zero-sequence components of the internal ac voltage of the monopolar converter.
v_c^{b+}, v_c^{b-}	Internal ac voltage of the positive/negative pole of the bipolar converter.
v_c^m	Internal ac voltage of the monopolar converter.
v_{com}^b	Voltage at the common point of the bipolar converter.
$v_{ctrl,d}^m, v_{ctrl,q}^m$	Direct/quadrature components of the ac voltage at the point controlled by the monopolar converter.
v_{ctrl}^{*m}	AC voltage reference for the monopolar converter controller.
$v_{ctrl}^{b+}, v_{ctrl}^{b-}$	AC voltage at the point controlled by the positive/negative pole of the bipolar converter.
v_{ctrl}^m	AC voltage at the point controlled by the monopolar converter.

v_{dc}	Direct current voltage
v_{dc}^{*m}	DC voltage reference for the monopolar converter controller.
v_{dc}^{b+}, v_{dc}^{b-}	Positive/negative pole voltage on the dc side of the bipolar converter.
v_{dc}^{m+}, v_{dc}^{m-}	Positive/negative pole voltage on the dc side of the monopolar converter.
v_g^m, v_g^b	AC grid Thevenin voltage on the ac side of the monopolar/bipolar station.
v_n	Difference between pole DC voltages of the monopolar converter.
θ_{pll}	Reference frame angle θ generated by the phase-locked loop of the converter.

Parameters:

c_c	Equivalent capacitance of converter submodules.
c_f	Fictitious capacitance located to make voltage a state variable.
c_{line}	Half capacitance of the π-model of the dc line.
k_{droop}	Droop coefficient of the DC voltage – active power droop control.
k_{p0}, k_{do}	Upper/lower path gains of the zero-sequence controller.
kp_{droop}, ki_{droop}	Proportional and integral gains of the DC voltage – active power droop control.
kp_i, ki_i	Proportional and integral gains of the inner controller.
kp_p, ki_p	Proportional and integral gains of the active power controller.
kp_q, ki_q	Proportional and integral gains of the reactive power controller.
kp_{vac}, ki_{vac}	Proportional and integral gains of the AC voltage controller.
kp_{vdc}, ki_{vdc}	Proportional and integral gains of the DC voltage controller.
l_{cc}	AC equivalent inductance from the converter to the controlled point.
l_e	Equivalent inductance of the grounding system.

r_{arm}, l_{arm}	Resistance and inductance of the converter arms.
r_e	Grounding resistance of the grounding system.
r_g, l_g	Thévenin resistance and inductance of the external AC grid.
r_{line}, l_{line}	Series resistance and inductance of the π-model of the dc line.
r_{trf}, l_{trf}	Series resistance and inductance of the converter transformer.
ω_b	Base frequency.
ω_g	Grid frequency.

CHAPTER 1. INTRODUCTION

This chapter establishes the context, background and importance of the thesis topic. Furthermore, it presents the main objectives of the research and the software and tools used. The chapter finishes with the thesis outline.

1.1. General background

1.1.1. Challenges for the transmission network in the current energy context

The present energy context is causing a rapid change in electricity networks worldwide. One of the main aspects behind this scenario is promoting renewable generation to move towards lower greenhouse gas emissions and higher independence from fossil fuel resources. Specifically in Europe, the goal of the European Union is to reach an emission reduction of 55% by 2030 and neutrality by 2050, which will also improve energy security and independence [1].

However, the significant increment of renewable energy projects, mainly solar photovoltaic and wind, poses a challenge for power systems in different aspects, primarily techno-economic, but also social and environmental [2].

On the one hand, renewable energy is mostly not dispatchable and intermittent. Consequently, there is an increment of the generation uncertainty in the network and a loss of power flow control by the operator. But on the other hand, this fact also involves an increase in the infrastructure required due to the further need for a backup generation [3], [4].

In addition, large-scale renewable energy plants are likely to be built in remote or unpopulated regions where the most optimal conditions for generation typically occur, usually far from main consumption centres, and energy has to be transmitted over long distances [4]. However, high voltage alternating current (HVAC) transmission is cost-effective for connecting remote-located power plants only in some cases. On the one hand, costs and energy losses increase with long distances and environmental concerns and policies make the construction of new HVAC overhead lines difficult. On the other hand, HVAC cables reduce the environmental impact and are the best technical solution to interconnect systems such as offshore wind power plants, but have higher losses and costs. This is mainly due to the higher amount of charge current, which involves a high reactive power flow through them, reducing the available cross-section to transmit energy and making necessary the use of compensation devices [4]. Although higher transmission voltages can mitigate this drawback, they pose a technical challenge, and commercial cable solutions have yet to be [5].

Consequently, HVAC transmission prevents power systems from utilising the many renewable energy resources available in those optimal areas.

Therefore, allocating the emerging renewable generation to comply with the social-environmental concern requires a substantial investment in enhancing present power systems and other technical solutions different from conventional HVAC transmission. In addition, the growth of the electricity network has to be made while guaranteeing the electricity supply since it is a crucial factor for citizens, industries, and the economy of countries.

1.1.2. HVDC transmission

High Voltage Direct Current (HVDC) transmission is a promising alternative to conventional HVAC transmission in the current scenario. During the last decades, HVDC transmission has been typically used for the interconnection of asynchronous systems, bulk power transmission over long distances, or underground and undersea connections through point-to-point links [3].

The advantages of HVDC against HVAC in these specific applications are due to the following inherent technical characteristics [6]:

- The charging current is zero in the case of Direct Current (DC) transmission, so it is free of reactive power flows. Thus, the optimal utilisation of the cross-section of the conductor to transmit energy poses a more cost-effective solution and reduces losses. This characteristic positions HVDC transmission as an alternative for bulk-power transmission over long distances, especially as a substitute for AC cables.
- The DC connection decouples interconnected AC systems, enabling the interconnection of asynchronous networks or systems with different rated frequencies. This aspect eases the connection of offshore systems with onshore synchronous areas.

Furthermore, HVDC transmission still presents more advantages, such as complete controllability of the transmitted active power in the connected systems. This provides a higher degree of control to system operators and can compensate somewhat for the loss of controllability caused by renewable generation. Active power control also enables additional services to AC systems where HVDC systems are connected, such as power-oscillation damping and preventing oscillations transmission from one AC system to another.

In addition, active power transmission through DC connections avoids stability constraints that limit the maximum active power transfer in AC, especially over long distances.

From an environmental point of view, the smaller number of conductors and the absence of proximity effect make DC transmission requires significantly less right-of-way than equivalent AC connections for both overhead lines and cables. This reduces the environmental impact of transmission, although the footprint of converter stations is larger. Nonetheless, considering the overall effect, DC transmission needs less space than AC transmission to transfer the same amount of power.

However, HVDC transmission also presents drawbacks when compared to classical AC transmission. One of them is that converter stations are still expensive. Therefore, investing in HVDC transmission depends on several factors, such as the breakeven distance, defined as the length from which HVDC transmission is more cost-effective than HVAC transmission. This breakeven distance depends on whether the transmission is done via overhead lines or cables, the amount of active power to transfer, the HVDC technology, and other technical aspects related to each project.

In addition, the experience in operating HVAC transmission systems is higher, so they are reliable and well-known. Typically, HVAC systems offer redundancy so the network can continue working correctly even in non-scheduled outages. In contrast, HVDC technology is still evolving and maturing as the number of HVDC projects increases. Indeed, most projects are point-to-point links, so the outage of an element, such as a converter, can produce the loss of half or total transmission.

Besides the advantages and drawbacks inherent in HVDC transmission, other specific aspects depend on the HVDC technology.

1.1.3. HVDC technologies

Two major converter technologies for HVDC transmission are line-commutated converter (LCC) and voltage-source converter (VSC).

Most HVDC links in operation use LCC, the first converter technology developed for HVDC transmission. Current LCC technology is based on thyristor-type valves. Therefore, the turn-on of the valves can be controlled, but the turn-off depends on the zero crossing of the alternating current.

The active power control is made by controlling the switching on of the valves through the firing angle, which is closely related to the power factor. This implies that the active and the reactive power at the AC side of the converter are not independent. The maximum active power leads to zero reactive power demand by the HVDC-LCC station, but any reduction in the transferred active power consequently involves reactive power consumption. Therefore, LCC-HVDC stations require reactive power compensation.

In addition, the need for an existing AC grid to turn-off the valves limits the connection of LCC-based HVDC stations to AC networks with a minimum short-circuit ratio. Thus, LCC technology cannot be connected to islanded or weak AC networks. However, there are advanced configurations based on LCC, such as capacitor-commutated converters (CCC) or controlled series capacitor converters (CSCC), that reduce the reactive power requirements and allow for converter operation in weaker AC grids [7].

In LCC-HVDC systems, the DC current is constant and unidirectional, so the DC voltage is adjusted to achieve the corresponding active power flow. As the DC current cannot be reversed, the direction of the active power flow can only change by reversing the polarity of the DC voltage. However, reversing voltage polarity is not a fast operation as it requires interrupting the LCC operation, de-energising the remaining charge in the DC poles, and energising them in the opposite polarity [4], [5].

VSC-HVDC systems are a more recent technology that offers benefits over LCC-HVDC systems. For example, VSC-HVDC systems use IGBTs instead of thyristors, and IGBTs are self-commuted, so their turn-on and turn-off can be fully controlled. This feature allows active and reactive power to be controlled independently, so reactive power compensation devices are no longer needed. Additionally, VSC-HVDC systems can be connected to weak or islanded AC networks as they do not require strong enough AC

grids for commutation. Thus, they provide additional services to AC systems, such as black start capability.

VSC-HVDC stations provide a constant voltage at the DC side and the DC current is adjusted to achieve the corresponding active power flow. Active power reversal is also possible by reversing the current flow without interrupting the operation. This is a valuable characteristic for building multi-terminal DC networks compared to former LCC-HVDC stations.

VSC-HVDC stations encompass different converters configurations: 2-level, 3-level, or modular multilevel converters (MMC). Although these configurations present specific differences, their operation in the power system is similar [3]. However, MMC-VSC-based HVDC stations are preferred due to additional advantages, such as low switching losses, high reduction of the harmonic content, and easy scalability [8], [9]. Besides, MMC configuration can be used with different submodule configurations, such as half-bridge, full-bridge, or hybrid [10], [11].

Compared with LCC-HVDC, VSC-HVDC stations have higher losses, lower ratings and are more expensive. This makes LCC-HVDC stations still a suitable solution for bulk power transmission over long distances [3], [4]. However, MMC-VSC HVDC stations have lower harmonic emissions, so they do not need the installation of harmonic filters. Furthermore, due to their superior controllability, they do not require reactive power compensation devices either. Both aspects lead to a smaller converter station footprint. Besides, the capability to provide a black start and not require strong AC networks to work appropriately makes MMC-VSC HVDC stations the best option to interconnect offshore systems [5].

Moreover, VSC-HVDC stations allow a straightforward connection of additional HVDC stations at the DC side since the current can be reversed at any moment, which eases the DC system operation. Compared with LCC-HVDC stations, this is a high advantage that enables the construction of a DC grid [12]–[14].

1.1.4. DC supergrid

Because of the mentioned advantages of HVDC transmission and VSC-HVDC technology, the number of projects has increased worldwide in the last few years [2], [15]–[22]. Moreover, the foreseen trend is that this number will increase further in the coming years. Particularly in Europe, the 10-years network development plan (TYNDP) published by ENTSO-E [23] indicates that more than 45 projects are under consideration, waiting for permission or under construction.

Most of these projects are point-to-point links. However, constructing these links will likely lead to future DC interconnections to form a multi-terminal meshed HVDC grid, or DC *supergrid*, that will constitute a new backbone for bulk power transmission [4], [24], [25]. This is expected to occur first in the North and Baltic seas due to the number of offshore wind power plants planned in these areas and, thus, the need to connect these

power plants to onshore AC systems [4]. In addition, projects on the European continent may lead to the development of an onshore HVDC grid.

Although there are already built some multi-terminal VSC-based HVDC systems [16], [17], [26]–[28], they are integrated into the existing AC networks and cannot be considered a backbone transmission system [29]. However, considering the mentioned aspects, developing an overlay backbone DC grid will bring numerous benefits.

On the one hand, HVDC transmission allows techno-economic access to renewable resources in remote locations not available with AC transmission. On the other hand, a DC grid takes more significant advantage of this and can facilitate the interconnection of large amounts of renewable energy resources over a wide area in Europe. Furthermore, this increased integration of renewable generation reduces uncertainty due to the probabilistic correlation between weather conditions over that wide area [3].

Furthermore, improved interconnection avoids the generation restriction in renewable power plants due to technical or stability constraints. This also positively impacts the economy, as energy demand can benefit from the cheapest energy at any time.

A DC grid can also relieve congestion on existing AC grids. This fact, together with the higher degree of interconnection and the complete controllability of the active power flow, can improve supply and grid security [3], [5].

Although much progress has been made in recent years in developing the necessary equipment, some technical and non-technical limitations still need to be overcome for an overlay DC grid to become a reality. Among the challenges to be solved, the most important can be summarised in the lack of standardisation and the further research and development required in the protection system of such grid [3], [29], [30]. At the same time, development must continue in AC-DC and DC-DC converters, lines and cables to offer higher capacities and voltages, lower losses and costs.

1.1.5. Need for standardisation

As this overlay DC grid is expected to evolve from previous point-to-point links towards a meshed grid through DC connections, equipment standardisation work is needed to guarantee multi-vendor operativity. In addition, standardisation brings many advantages, as it facilitates cost reduction, maintenance and operation, and reduces implementation time [31].

The recent publication of grid codes for HVDC in Europe is a step forward. Still, it is also necessary to establish standard control strategies, communication protocols, interfaces, calculation methodologies and procedures for planning. Among the calculation methods that need standardisation are the calculation of short-circuit currents, the design of the grounding system, and the management of faults in the HVDC network [30].

The topology of the future DC grid is also an aspect that needs to be defined since it can significantly impact the security of supply. Both monopolar and bipolar topologies are available. Although bipolar topology seems the most suitable due to its inherent redundancy, most projects currently use a monopolar one.

Furthermore, different grounding schemes can be implemented [32]–[34]. Since grounding methods impact DC currents and voltages during pole-to-ground faults, they also influence the protection system. Indeed, the main technical limitation regarding protection is the development of robust and reliable algorithms that detect and locate the fault in less than two milliseconds to keep protection coordination. Although several algorithms in the literature allow for fast fault detection and location, travelling-wave-based methods are the most promising option [35]. However, the grounding system can affect the performance of these algorithms. Therefore, standardisation of the grounding methods is also necessary.

DC circuit breakers (DCCB) are a key component for the future development of the DC overlay grid; therefore, there is a particular need to standardise them. Several prototypes with different topologies can be used to protect DC networks, such as mechanical, solid-state and hybrid circuit breakers. Nowadays, hybrid DCCBs, together with fault current limiter devices, seem to be the best alternative, although the DCCB technology is under continuous development [36]–[39].

In addition, the rated voltage of the DC system is not a standard value either. Future HVDC systems are expected to use higher DC voltages due to enhancements in converters and DC cables. Only DC systems using the same voltage level can directly connect via a cable or overhead line. Otherwise, a DC-DC converter is needed.

DC-DC converters are still subject of ongoing research and have yet to be implemented in actual projects. However, many possible topologies have been proposed in the literature for different applications [40]–[44]. Among them, modular topologies can be more easily standardised and adapted to different voltage levels and ratings.

DC-DC converters can also provide additional controllability to the DC network and, depending on the topology, fault-blocking capability or galvanic isolation. However, DC-DC converters are expensive, and they should be located in strategic locations.

Therefore, the interconnection of different DC systems to form the future supergrid can be challenging due to the number of components required and the wide variety of configurations and topologies for each. In addition, control interactions may appear [45]. Increased standardisation can facilitate these interconnections, but given the present scenario, different configurations, topologies, grounding schemes, etc., are likely to coexist.

In addition to the above, the control strategy of the HVDC network poses another degree of complexity, especially when different control strategies can be implemented in the subsystems inside the complete HVDC network. Furthermore, the role of each HVDC station inside the control strategy depends on the type of AC system to which it is connected [46]–[48].For that reason, one of the primary purposes of this dissertation is to analyse the behaviour of such a heterogeneous DC network and point out the possible issues that may arise.

1.2. Motivation

As mentioned, the lack of standardisation can conduct a future overlay DC grid to be integrated by different components and topologies. Such a system results very complexly for the analysis due to the high variability of factors involved. However, its study is still necessary for the future development of an overlay DC grid.

Most of the works dealing with the operation of DC networks consider a unique configuration: bipolar or monopolar [31], [49], [50]. In the same way, the focal point for most researchers has been the study of the system under balanced operation [32]–[34] or AC unbalanced operation [51]–[59]. Since it is assumed that bipolar HVDC stations operate symmetrically under normal conditions, i.e., like symmetrical monopolar stations, the inclusion of different topologies does not pose any difference under the balanced operation of the DC grid. [60]–[64]

Nonetheless, in the case of asymmetrical operation, the previous premise is no longer valid. Some of the causes behind an asymmetrical operation are the occurrence of a pole-to-ground fault [60]–[62], [65]–[68], a contingency affecting a single pole of the DC system [63], [64], [69], or an unbalanced operation at the AC side with a zero-sequence component [51], [70], [71]. In addition, converters may be required to deal with an asymmetrical operation of the DC grid for long periods due to different reasons [31], [72], [73]. Therefore, asymmetrical operation implies that the DC voltage and/or current are no longer symmetrical between both poles of the DC network. This directly involves a current or voltage across the grounding system of the HVDC stations. Although many works have also proposed algorithms and topologies that enhance the operation of HVDC stations facing such events [67], [74]–[77], permanent asymmetrical DC operation in heterogeneous DC grids has not been considered.

In the literature, the asymmetrical DC operation has been analysed for monopolar and bipolar systems separately, although. For symmetrical monopolar systems, the relationship between their operation and the grounding impedance was addressed in [72]. In addition, different rebalancing methods after clearance of a pole-to-ground fault were handled in [77]–[80]. As for bipolar HVDC stations, works [50], [69] studied their asymmetrical DC operation and the relationship with the grounding impedance and the control strategy of the system. The effect of the location of the earthing point in bipolar HVDC systems was also addressed in [31]. In addition, an optimisation of the grounding resistor of the Luxi back-back project considering DC voltage asymmetries was also addressed in [81].

However, the asymmetrical operation of DC grids formed by heterogeneously configured HVDC stations has yet to be addressed. Therefore, further research is needed to analyse the asymmetrical DC operation in grids with different topologies, grounding configurations, and control strategies, especially when this is expected to be the future scenario due to the lack of standardisation. In addition, this analysis should encompass different approaches to obtain complete information about the performance of the system.

First, DC networks should be subject to the N-1 criterion since the same degree of reliability as for conventional AC systems is required. Therefore, load-flow-based analysis of such DC grids should be carried out to identify operational constraints or limitations such as element overloading or excessive voltage deviations. It is highly recommendable that this type of analysis also includes the AC systems where the overlay DC grid is connected. This study can also aid in designing remedial actions after a contingency and support the design of the grounding scheme.

Second, analysing heterogeneous DC grids through electromagnetic transients (EMT) simulations during asymmetrical DC operation is also needed to correctly determine the transient response in such circumstances and the different factors involved in that response. EMT simulation is also the only method to accurately detect transient over/under-voltages or overcurrents that may endanger the system. Besides, asymmetrical DC operation is also needed to design the grounding system for conditions other than pole-to-ground faults, such as permanent asymmetrical operation, and to design and adjust protections.

Furthermore, although stability analysis of heterogeneous DC grids can also be addressed through dynamic simulations, these become very time-consuming in the case of large systems. In this sense, small-signal stability analysis is a powerful tool that identifies instabilities and underdamped oscillations. It may also assess the stability of large DC systems during asymmetrical DC operation.

The investigation of the asymmetrical operation of DC grids with different HVDC station configurations, topologies, grounding systems, and control strategies has motivated the work of this thesis.

1.3. Thesis objectives

The general objective of the thesis is to make progress in the study of the asymmetrical operation of heterogeneously composed DC systems from different approaches that include load flow, EMT dynamics and small-signal stability analysis.

Aiming this general objective, specific objectives are proposed for each approach.

- Specific objectives for the load flow analysis:
  - Define the steady-state equations that describe the asymmetrical operation of the elements composing the DC network.
  - Identify the main aspects involved in the steady-state reached during asymmetrical operation.
  - Perform N-1 analysis, including the asymmetrical DC operation.
  - Identify the impact of the asymmetrical operation on the system.
- Specific objectives for the dynamic (EMT) analysis:
  - Characterize the effect of the grounding impedance in the transient response during asymmetrical DC operation.
  - Identify the effect of different control strategies on the transient response.

  - Find the main issues that can appear during the transient response under asymmetrical operation.
  - Explore the effects of the connection of new stations on the protection systems.

- Specific objectives for the small-signal stability analysis:
  - Develop linear models valid during asymmetrical DC operation.
  - Validate the developed small-signal models against EMT dynamic simulations.
  - Identify the main elements involved in the small-signal stability during asymmetrical operation.
  - Examine the small-signal stability using different control strategies.

1.4. Software and tools employed

The thesis has been developed using different software and tools to carry out the following procedures:

- Matlab:
  - Modelling of the system presented in Chapter 2 and performing the load flow analysis.
  - Development of the small-signal model presented in Chapter 4 and its validation against EMT simulation.
  - Performing the small-signal analysis presented in Chapter 5.
- PowerFactory.
  - Dynamic modelling of the system presented in Chapter 3 to carry out the EMT dynamic simulations.
  - Dynamic modelling of the system presented in Chapter 4 to carry out the validation against the small-signal model.
- Python:
  - Scripting and automation of different tasks in PowerFactory.

1.5. Thesis outline

The thesis is structured into six chapters, including this introductory chapter.

Chapter 2 introduces the equations that define the behaviour of DC-DC converters and HVDC stations during asymmetrical DC operation from a steady-state perspective. In addition, the asymmetrical DC operation of an extensive DC system consisting of DC-DC converters and different configurations of HVDC stations is studied. Particular focus is put on the influence that galvanic isolation of DC-DC converters, grounding resistance, and control strategy of HVDC stations have over the asymmetrical DC operation. The main consequences of this asymmetrical DC operation are excessive DC voltage deviations and overloading of system components that can lead to a multi-contingency scenario if remedial actions are not provided. Control strategy and parameterisation determine the steady state reached during asymmetrical operation.

Chapter 3 introduces the dynamic equations that determine the behaviour of HVDC stations during asymmetrical DC operation. It also analyses the asymmetrical DC operation of a heterogeneous DC network from an EMT dynamic simulation perspective. Transient over/under-voltages, and overcurrents are identified, and the impact of inductance and ground resistance on the dynamic response of the system is highlighted. Different control strategies are also assessed, demonstrating that stability issues can appear during asymmetrical DC operation. In addition, the impact that the grounding impedance of symmetrical monopolar HVDC stations has over the short-circuit during pole-to-ground faults is studied.

Then, Chapter 4 provides the development of linearised models suitable for small-signal analysis of heterogeneous DC grids during asymmetrical DC operation. First, an equivalent circuit is introduced, and then equations and necessary linearisation are indicated. Finally, developed models are validated against EMT simulations using different control strategies, impedance values, and control parameters.

Chapter 5 takes advantage of the linearised models developed in the previous chapter and performs small-signal stability of a heterogeneous DC system paying particular attention to those dynamics involved during the asymmetrical DC operation. The impact of the grounding impedance, the control strategy, the operating point of the system and other system parameters on the system stability are identified. In addition, a controller that improves the system stability during asymmetrical operation is proposed from the small-signal stability analysis.

Chapter 6 gathers the main conclusions and contributions of the thesis. Additionally, areas for further research are identified.

Finally, Appendix A gives additional details about the data used in Chapter 2, and Appendix B provides further information on the parameters and equations used in Chapter 4 and Chapter 5.

CHAPTER 2. LOAD-FLOW ANALYSIS

During asymmetrical contingencies in a heterogeneous DC grid, the grounding scheme, the topology and the control strategy of each HVDC station are involved in the response of the system. Furthermore, if different DC systems are interconnected through DC-DC converters, their ability to provide galvanic isolation may influence that response. Therefore, this chapter mainly aims to assess the impact of these aspects on the whole DC grid under asymmetrical contingencies from a load-flow approach.

2.1. Introduction

As mentioned in Chapter 1, in the case of symmetrical contingencies, the configuration of the DC system (monopolar or bipolar), the grounding scheme or the galvanic isolation of the DC-DC converters does not affect the behaviour of the DC network during the contingency nor the steady-state operating point reached in the post-contingency scenario [69]. The loss of an entire HVDC station or the outage of an element in the AC grid to which an HVDC station is connected are examples of symmetrical contingencies.

In contrast, asymmetrical contingencies affect both poles of the DC network unequally. Their impact on different parts of the DC grid can vary in the case of heterogeneous DC grids. This inequality causes a divergence between the voltage magnitude of both poles and/or the DC current flowing through them [32], [33], [49], [78]. This divergence on the DC side appears on the AC side as a zero-sequence voltage and/or earth current, which is proportional to the asymmetry. A constant earth current flowing through the ground can cause detrimental effects on the system [82]–[84]. Therefore, the variation in the DC variables in the entire HVDC network depends on the grounding system of the HVDC stations, their configuration and, in the case of present DC-DC converters, whether they provide galvanic isolation.

Therefore, this chapter analyses from a load-flow perspective a multiterminal HVDC system formed by different station topologies and grounding configurations, which includes DC-DC converters. In addition, several control strategies of the DC grid are considered. The study aims to provide an overview of the challenges that may arise in such a heterogeneous multiterminal HVDC grid, specifically during contingencies affecting the DC network asymmetrically.

The chapter is organised as follows. Section 2.2 describes the methodology and the system used during the analysis. Section 2.3 introduces the behaviour of the main components of the DC grid during asymmetrical DC operation. Section 2.4 studies the asymmetrical DC operation considering different circumstances. Finally, the conclusions obtained are gathered in Section 2.5.

2.2. Methodology and system description

As mentioned, this chapter aims to analyse the operation of a heterogeneous HVDC network facing asymmetrical contingencies. This analysis is done from a load-flow perspective, focusing on the different steady-state operating points reached after an asymmetrical contingency in the HVDC network. The different post-contingencies scenarios are obtained by considering several combinations in terms of configuration and operation: a) different grounding systems, b) DC-DC converters with and without galvanic isolation, c) the effect on bipolar and monopolar DC systems, and d) the impact of the control strategy.

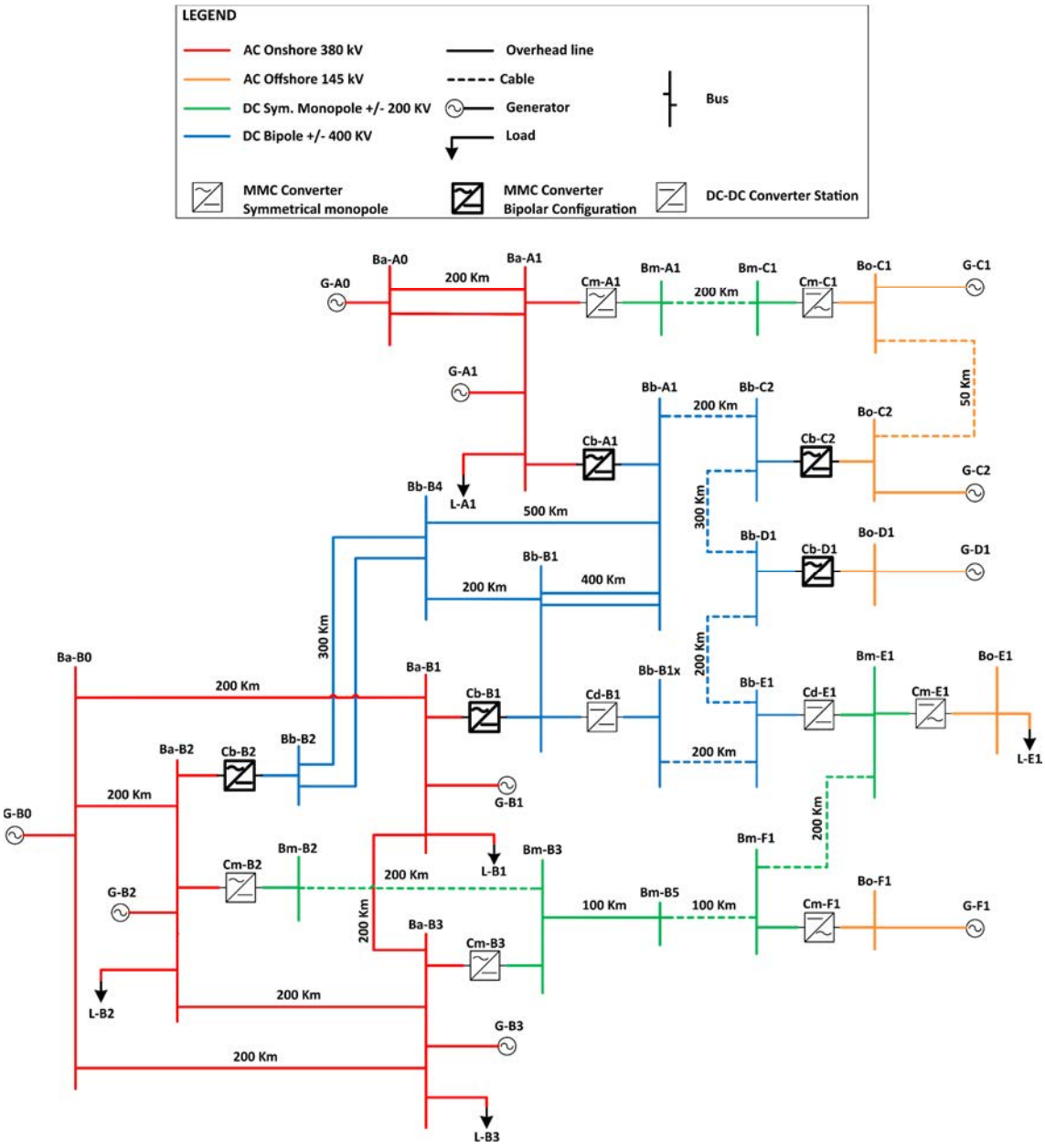

Figure 2.1 Test system used to study the DC asymmetrical operation.

The scope is to investigate how these factors can impact the entire HVDC network. For that, the test system used to carry out the study is the one presented by Cigré [85], depicted in Figure 2.1. This test system is composed of the following:

- 2 onshore AC systems;
- 4 offshore AC systems;
- 3 DC systems: DCS1, DCS2 and DCS3.

Furthermore, DCS1 is a symmetric monopole HVDC point-to-point link connecting the offshore generation at Bo-C1 to the onshore node Ba-A1; DCS2 is a 4-terminal symmetric monopole HVDC system connecting the offshore generation at Bo-F1 and the offshore load at Bo-E1 to the onshore nodes Ba-B2 and Ba-B3; and DCS3 is a 5-terminal bipole HVDC grid which contains an embedded DC-DC converter Cd-B1 for power flow

control. Besides, DCS2 and DCS3 are interconnected each other via the DC-DC converter Cd-E1.

2.3. Asymmetrical disturbances in HVDC networks

DC networks mainly consist of AC-DC converters, DC-DC converters, overhead lines, and cables. Besides, AC-DC converters need to be connected to an AC network to work correctly.

In this thesis, a DC network is considered symmetrical when the topology, the impedance, and the elements connected to one of the poles across the complete DC network are the same as in the other one. This involves that the analysis of one of the DC poles is sufficient to obtain the electrical variables.

Conversely, an asymmetrical DC operation implies that the electrical variables at one of the poles of the DC network are not the same as those at the other one. This can occur during regular operation of the DC network or due to a perturbation affecting a single pole.

During regular functioning, the asymmetrical operation of the DC network may occur due to the asymmetrical connection of elements (for example, connected between one pole and the ground instead of between both poles). Thus, the topological symmetry between poles is lost. This is the case with HVDC systems that include stations with asymmetrical monopolar configuration.

On the other hand, a disturbance affecting one pole can drive a symmetrical DC network into asymmetrical operation. This can be due to a fault or outage of an element on one of the poles only so that the symmetry in terms of topology or impedance is lost. The time that the DC network is operating asymmetrically after occurring these types of perturbations can vary depending on their origin.

In this document, the focus is on symmetrical DC systems that achieved asymmetrical operation after a disturbance. The purpose is to know how the DC system responds in those circumstances and the impact of the asymmetrical operation on the whole system.

The response of the DC system during an asymmetrical operation is influenced by the behaviour of AC-DC and DC-DC converters, responsible for controlling the entire HVDC system. For that reason, a brief description of the behaviour of these elements under these circumstances is given below.

2.3.1. Asymmetrical operation of HVDC stations

The network in Figure 2.1 consists of AC-DC stations formed by VSC-MMC converters with two configurations: symmetrical monopolar and bipolar. A schematic representation of both designs is depicted in Figure 2.2.

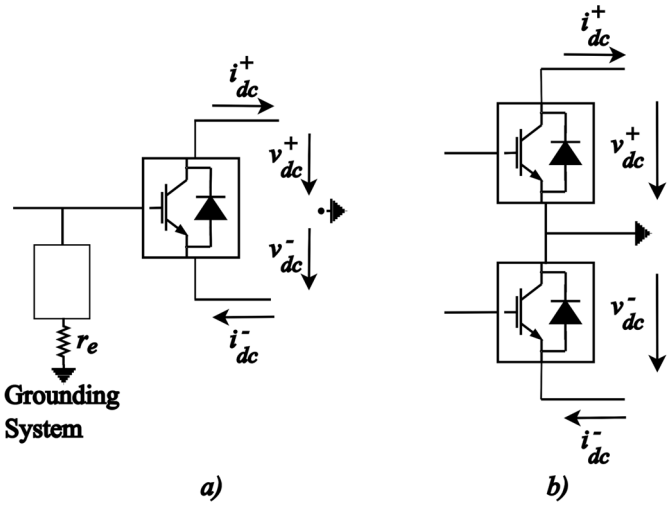

Figure 2.2. Schematic representation of HVDC station configuration: a) symmetrical monopolar and b) bipolar.

Each of these converters regulates its inner AC voltage magnitude and phase to control a) the DC voltage or the active power flow and b) the AC voltage or the reactive power flow. Since bipolar HVDC stations consist of one converter per DC pole, they can independently control active power or DC voltage in each pole. In contrast, symmetrical monopolar HVDC stations can only control the pole-to-pole DC voltage or the sum of the active power flowing through both poles.

Both bipolar and symmetrical monopolar configured HVDC stations represent a balanced element for the DC network where they are connected. Therefore, the voltage magnitude and current in each pole are the same as in the other one providing that the rest of the DC network is also symmetrical. This is also true in case of contingencies that affect both poles equally, such as pole-to-pole faults or the outage of a complete HVDC station.

However, the symmetry is lost in case of contingencies that affect a single pole (asymmetrical contingencies), and the response of each HVDC station is highly influenced by its configuration, grounding system and control.

The grounding of the HVDC stations of the network in Figure 2.1 is represented in Figure 2.2. The monopolar station is grounded at its AC side, whereas the bipolar design is solidly grounded at the common point of both converters.

Typically, symmetrical monopolar configurations can be grounded at their AC side through different systems, e.g., a start-point reactor or a zig-zag transformer. Nonetheless, all the grounding systems use a grounding resistance r_e that limits the ground current in case of pole-to-ground faults.

Bipolar configurations are usually solidly grounded so that, in the event of a pole failure, the healthy pole can continue to work as an asymmetrical monopolar station using the ground or a metallic return to close the circuit. Although it is possible to earth the bipolar station through a high resistance, the over-voltage reached in case of failure of one of the poles requires increasing the insulation of the equipment and, thus, the costs.

During a disturbance affecting a single pole, voltages and currents at the positive and the negative DC poles across the HVDC system become different. This difference can be defined in terms of DC current asymmetry (i_{asy}) and DC voltage asymmetry (u_{asy}) between poles according to (2.1) and (2.2), respectively.

$$i_{asy} = \frac{i_{dc}^{+} - i_{dc}^{-}}{2} \tag{2.1}$$

$$u_{asy} = \frac{v_{dc}^{+} - v_{dc}^{-}}{2} \tag{2.2}$$

where i_{dc}^{+}, i_{dc}^{-}, v_{dc}^{+}, v_{dc}^{-} represent the DC currents and voltages at each DC pole of an HVDC station following the sign criterion depicted in Figure 2.2.

Since the grounding system is the path through which the current difference between both poles returns, the asymmetry in the DC current injected into the DC network by an HVDC station is related to the zero-sequence current flowing through its grounding system ($3i_{ac0}$), according to (2.3).

$$3i_{ac0} = 2i_{asy} \tag{2.3}$$

Furthermore, in the case of symmetrical monopolar configurations, the steady-state current and voltage asymmetries are related to each other through the resistance of the grounding system (r_e) of the station, as expressed in (2.4),

$$u_{ac0} = u_{asy} = -3i_{ac0}r_e + e_0 \tag{2.4}$$

where u_{AC0} is the AC zero-sequence component of the voltage at the AC side of the converter and e_0 is the zero-sequence component of the inner voltage produced by the converter. Across this chapter, it is assumed that converters do not produce zero-sequence voltage at the AC side and, thus, e_0 is null.

Therefore, symmetrical monopolar HVDC stations do not have any control over the asymmetry. Once the asymmetry appears in the system, the level of asymmetry in the voltage and current in the steady state depends on their grounding resistance.

In contrast, DC current and voltage asymmetries are independent of each other in the case of bipolar configurations. That is, the resulting asymmetries are the consequence of the control action of each converter to maintain its corresponding setpoint. This fact is shown below.

The power asymmetry between both DC poles of a station can be defined as follows:

$$p_{asy} = \frac{1}{2}(v_{dc}^{+}i_{dc}^{+} - v_{dc}^{-}i_{dc}^{-}) \tag{2.5}$$

Substituting the definition of the voltage asymmetry u_{asy} and the current asymmetry i_{asy} given in (2.1) and (2.2) in equation (2.5) and rearranging, the active power asymmetry can be defined as presented in (2.6),

$$p_{asy} = i_{asy}\frac{(v_{dc}^{+} + v_{dc}^{-})}{2} + u_{asy}\frac{(i_{dc}^{+} + i_{dc}^{-})}{2} \tag{2.6}$$

where i_{dc}^{+} and i_{dc}^{-} , and v_{dc}^{+} and v_{dc}^{-}, represent the injected DC current and the DC voltage at the positive and negative poles of the HVDC station.

In addition, by defining an equivalent grounding resistance for the bipolar station using (2.3) and (2.4) and substituting in equation (2.6), the power asymmetry can be expressed as follows:

$$p_{asy} = i_{asy}\left[\frac{(v_{dc}^{+} + v_{dc}^{-})}{2} - r_e(i_{dc}^{+} + i_{dc}^{-})\right] \tag{2.7}$$

Equation (2.7) can be adapted for each bipolar station according to its control. This allows for finding the equivalent grounding resistance that describes the behaviour of a specific bipolar station as if it were a symmetrical monopolar station.

Thus, when bipolar HVDC stations control the active power, $p_{dc}^{+} = p_{dc}^{-}$ in steady-state and, therefore, the following constraint is added to equation (2.7):

$$p_{asy} = 0 \tag{2.8}$$

Substituting (2.8) in (2.7) and rearranging, r_e results in the following expression for bipolar stations controlling the active power flow:

$$r_e = \frac{v_{dc}^{+} + v_{dc}^{-}}{2(i_{dc}^{+} + i_{dc}^{-})} \tag{2.9}$$

In turn, when bipolar stations control the DC voltage, $v_{dc}^{+} = v_{dc}^{-}$ and $u_{asy} = 0$ in steady state. From (2.4), this yields to $r_e = 0$.. Therefore, bipolar stations controlling the DC voltage behave as symmetrical monopolar stations solidly grounded.

In case of bipolar stations that implement a distributed DC voltage droop control, then $p_{dc}^{+} = p_{ctrl} - \frac{v_{dc}^{+} - v_{ctrl}}{k_{droop}}$ and $p_{dc}^{-} = p_{ctrl} - \frac{v_{dc}^{-} - v_{ctrl}}{k_{droop}}$ in steady-state, thus, the power asymmetry can be defined according to the next expression:

$$p_{asy} = -\frac{u_{asy}}{k_{droop}} \tag{2.10}$$

Substituting (2.10) in (2.7) and rearranging, the equivalent grounding resistance r_e can be defined as follow for bipolar HVDC stations with distributed DC voltage droop control.

$$r_e = \frac{v_{dc}^{+} + v_{dc}^{-}}{2\left(i_{dc}^{+} + i_{dc}^{-} + \frac{1}{k_{droop}}\right)} \tag{2.11}$$

Hence, although bipolar HVDC stations cannot avoid the DC current and voltage asymmetry because of an asymmetrical perturbation in the DC network, the amount of power asymmetry and, consequently, the amount of voltage and current asymmetry depend on their control.

2.3.2. Asymmetrical operation of DC-DC converters

The system under study counts with two DC-DC converters. One of them is embedded in the bipolar DC system, and the other one connects the bipolar system with the symmetrical monopolar one.

Both DC-DC converters allow to control the active power transferred between their two terminals and represent a symmetrical element. Therefore, they do not introduce any asymmetry in the DC network.

Assuming lossless DC-DC converters, and that the active power is positive when it flows from the converter to the DC network, the power balance between their two terminals *i* and *j* follows the next expression:

$$p_{dci}^{+} + p_{dci}^{-} = -p_{dcj}^{+} - p_{dcj}^{-} \tag{2.12}$$

where p_{dci}^{+}, p_{dci}^{-} and p_{dcj}^{+}, p_{dcj}^{-} represent the active power entering through each pole of terminals *i* and *j*, respectively.

When the DC network works symmetrically, as there is neither DC voltage nor DC current asymmetry according to (2.1) and (2.2), the total transferred active power is equally distributed between both DC poles. However, when an asymmetry appears in the DC network due to a disturbance, the total active power transferred by DC-DC converters may not be equally distributed between their poles. Therefore, a power asymmetry between poles can be defined according to (2.6).

From (2.6), the asymmetry between the injected active power per each DC pole may be different in both DC terminals of a DC-DC converter since it depends on the current and voltage asymmetry at each of them, which may not be the same.

The relationship between the current and voltage asymmetry between the two terminals of a DC-DC converter mainly depends on whether it provides galvanic isolation.

When DC-DC converters provide galvanic isolation, the transmitted current asymmetry between their two terminals becomes zero, and thus, the DC current flowing through both DC poles is the same. This prevents the asymmetry in current from being transferred between two DC systems interconnected by a DC-DC converter.

However, when DC-DC converters do not provide galvanic isolation, the current and voltage asymmetry is transferred from one terminal to the other. Equations (2.13) and (2.14) describe the relationship between the current and voltage asymmetry in both DC-DC converter terminals.

$$i_{asy}^{i} = \frac{1}{m_{ij}} i_{asy}^{j} \tag{2.13}$$

$$u_{asy}^{i} = m_{ij} u_{asy}^{j} \tag{2.14}$$

where $m_{ij} = \frac{U_{rated}^{j}}{U_{rated}^{i}}$ is the rated transformation ratio of the DC-DC converter, being U_{rated}^{i} and U_{rated}^{j} the rated voltage of terminal *i* and *j*, respectively.

Therefore, DC-DC converters play a crucial role during the asymmetrical operation of the DC network since, depending on whether they have galvanic isolation, the spread of the asymmetry between the DC systems that they interconnect can be blocked or not.

2.4. Analysis of the asymmetrical operation of the DC network

This section analyses how different elements and circumstances can impact the post-contingency scenario after an asymmetrical contingency in the DC network. The impact of voltage magnitude and equipment loading in the DC network is assessed. Aspects analysed include the provision of galvanic isolation by DC-DC converters, the grounding resistance of symmetrical monopolar HVDC stations, or the control of the HVDC stations.

For that, the system in Figure 2.1 is configured to obtain the load flow results shown in Figure 2.3, which are used as the pre-contingency scenario and as a base to compare the different post-contingency scenarios studied across the section.

The control strategy in each of the three DC systems is set as follows:

- The point-to-point link (DCS1 system) applies a strategy based on centralised voltage control so that the HVDC station Cm-A1 controls the DC voltage and the station Cm-C1 the active power flow. Besides, both stations control the reactive power at their AC side.
- The multi-terminal symmetrical monopolar system (DCS2 system) uses a distributed DC voltage control between the HVDC stations Cm-B2 and Cm-B3, whereas the stations Cm-E1 and Cm-F1 control the voltage magnitude and the frequency at their AC side. In addition, Cm-B2 and Cm-B3 also control the reactive power flow at their AC side.
- The multi-terminal bipolar HVDC system (DCS3 system) also implements a distributed DC voltage control between the stations Cb-A1, Cb-B2, and Cb-B3.

Besides, they also control the voltage magnitude at their AC side. Stations Cb-C2 and Cb-D1 control the voltage magnitude and the frequency at their AC side.

Additionally, both DC-DC converters control the active power flow transmitted between their two terminals to a constant value. Further details about the parameters and system configuration can be found in Appendix A.

For the load flow calculation in Figure 2.3, the active power flow and DC voltage in the positive and negative poles are shown in the DC system. In contrast, the active and reactive power flows, and the voltage magnitude and phase angle are shown in the AC systems. In this initial scenario representing normal operation conditions, the values shown for the positive and the negative DC poles are equal. Still, they are delivered to ease the comparison with the post-contingency cases.

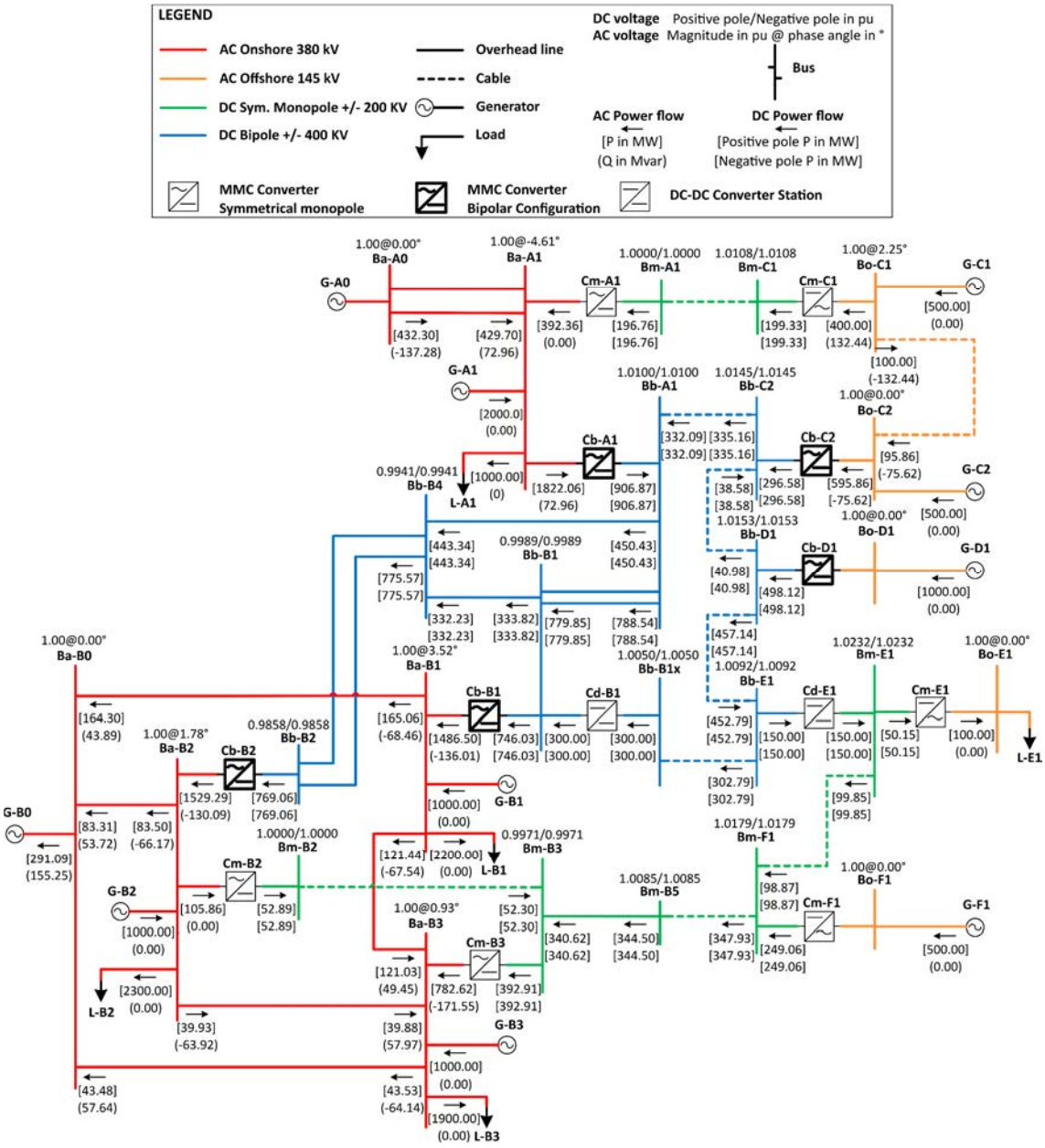

Figure 2.3. Pre-contingency scenario with the load flow calculation used as a base for comparison.

The results shown in Figure 2.3 for the DC network are depicted in Figure 2.4 in bar chart format. The voltage level in each DC pole of the system and the loading of each HVDC station and DC-DC converter are represented for each pole according to their rated DC current.

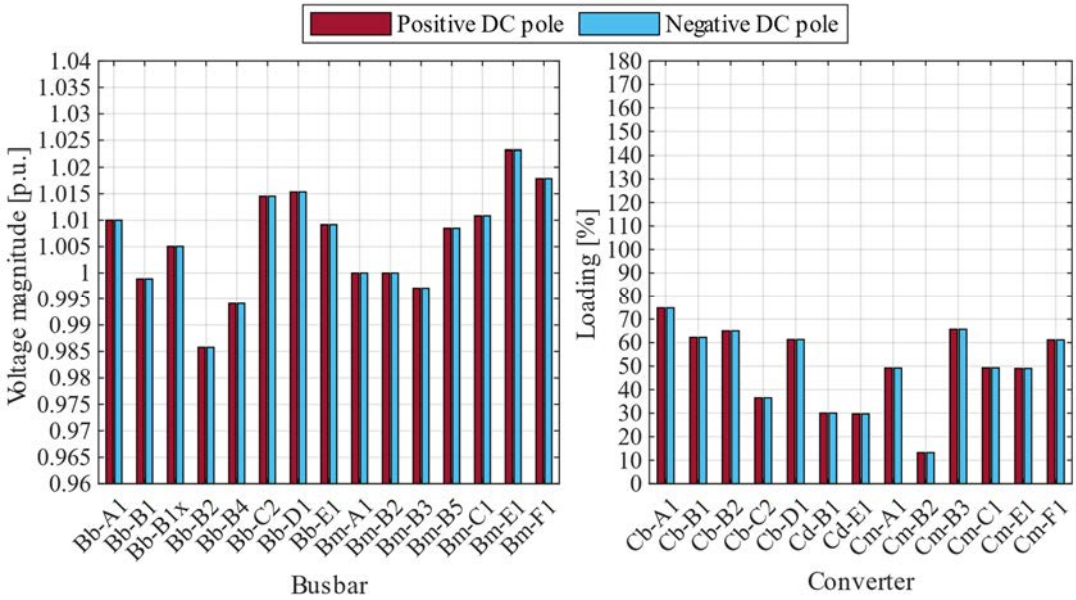

Figure 2.4. DC voltages and loading of converters in the pre-contingency scenario.

As shown in Figure 2.4, the voltage magnitude and loading between DC poles are the same for all the DC terminals and converters, respectively. In addition, there are neither overloaded converters nor voltage deviations larger than 5% in the DC busbars.

In the following sections, the post-contingency scenario after the outage of one of the converters forming the bipolar HVDC station Cb-C2, specifically that connected to the negative pole, is assessed considering different aspects.

2.4.1. Impact of the galvanic isolation of the DC-DC converters

First, the impact of using DC-DC converters with and without galvanic isolation is assessed. The purpose is to compare the impact of this capability on the system facing the same asymmetrical contingency. Specifically, the focus is on the voltage and current asymmetry, the voltage magnitude, and the loading.

2.4.1.1. DC-DC converters with galvanic isolation

As mentioned, DC-DC converters with galvanic isolation can block the transmission of asymmetrical current and voltage from one of their terminals to the other. This capability prevents one DC system from being affected by an asymmetrical disturbance in another when both systems are interconnected through a DC-DC converter. Figure 2.5 shows the post-contingency load flow of the system after the outage of the negative pole converter of the bipolar station Cb-C2.

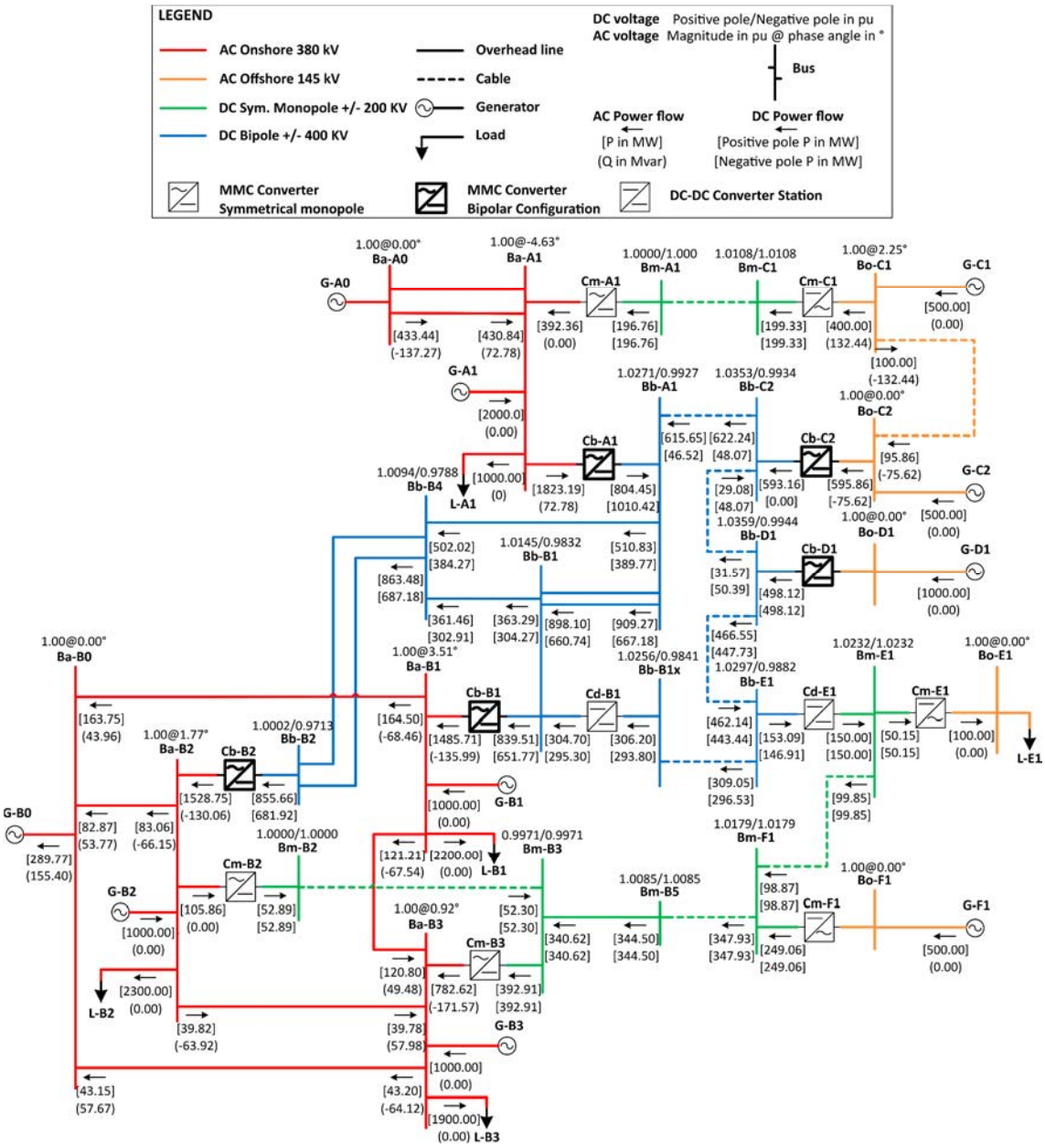

Figure 2.5. Post-contingency scenario in case of DC-DC converters with galvanic isolation after the outage of the negative pole converter of station Cb-C2.

Several conclusions can be drawn from the load flow results in Figure 2.5. As the Cb-C2 station controls the voltage magnitude and frequency at its AC side, once the negative pole converter is disconnected, the remaining positive pole converter has to transfer the total active power to maintain frequency control. This fact increases the loading of the positive pole converter of station Cb-C2, but it is still under its maximum loading. As a result, the contingency does not affect the load flow in that offshore AC area. The remaining offshore AC areas are not affected by the contingency either.

Regarding the DC network, it can be observed in Figure 2.5 that the bipolar DC system presents a considerable asymmetry between the positive and negative poles in terms of voltage magnitude and power flow. This asymmetry can have harmful effects on the system.

On the one hand, the current asymmetry can cause the overloading of cables, overhead lines, and converters. In the worst scenario, double the rated current can circulate through them. This high current can provoke the tripping of certain protections leading to a multi-contingency scenario that endangers the working of the complete system. In addition, this current asymmetry causes a constant current flowing through the earth or the ground conductor, which can have other important implications for the entire system.

On the other hand, the voltage asymmetry is also damaging for the system since the voltage magnitude is the variable used by the HVDC stations involved in the DC voltage control to balance the active power flow in the DC system. Therefore, increasing the voltage at one pole and reducing it at the other causes an active power asymmetry mainly distributed between the HVDC stations participating in the DC voltage control. In addition, high voltages can cause protection tripping to protect the equipment. Still, low voltages limit the active and reactive power capability, preventing the converter from working properly and keeping its corresponding setpoint.

Figure 2.6 shows the voltage magnitude at the positive and negative poles of each busbar of the DC network and the loading of each pole converter. A green busbar representing the value in the pre-contingency scenario is also depicted to facilitate the comparison.

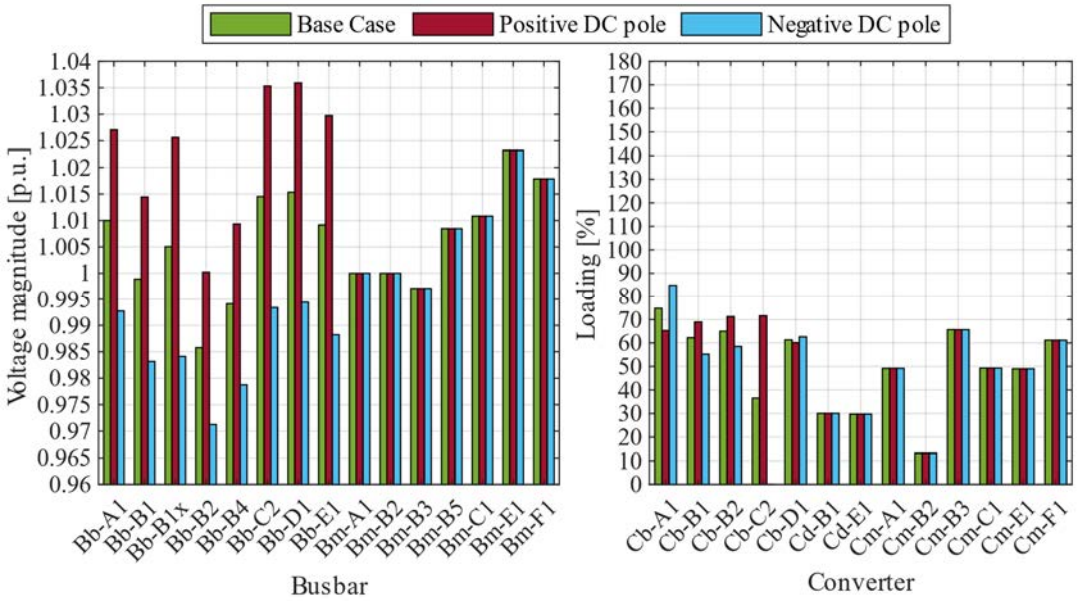

Figure 2.6. DC voltages and loading of converters when DC-DC converters provide galvanic isolation.

As shown in Figure 2.6, the outage has caused significant voltage asymmetries between the positive and negative poles in the bipolar system due to the change in the active power injected into each of them.

The loading in Figure 2.6 shows that the outage of the negative pole converter of the Cb-C2 station is mainly compensated by the three stations participating in the DC voltage control (Cb-A1, Cb-B1, and Cb-B2). Therefore, one of the poles increases its loading, and the other reduces it due to the different power flow through them.

In addition, observe that the voltage and the loading of the two symmetrical monopolar systems remain unchanged. In the case of the point-to-point link, the lack of a direct DC connection with the perturbated system avoid any impact on it.

In the case of the multi-terminal monopolar DC system, despite it being connected to the bipolar system through the DC-DC converter Cd-E1, the disturbance is not transmitted due to two main reasons:

1. The DC-DC converter directly controls the active power flow. Therefore, the DC-DC converter will continue transferring its pre-contingency active power if it does not overpass its current limit.
2. The galvanic isolation prevents the DC voltage and current asymmetry from being transferred from the bipolar system to the symmetrical monopolar one.

Therefore, the galvanic isolation in DC-DC converters, specifically in Cd-E1, avoids affecting the symmetrical monopolar system by the asymmetrical contingency in the bipolar system.

2.4.1.2. DC-DC converters without galvanic isolation

As previously mentioned, if DC-DC converters do not provide galvanic isolation, the DC voltage and current asymmetries are transmitted from one system to another through the DC-DC converter. This behaviour is shown in Figure 2.7, where the same contingency as in the previous case is shown without considering galvanic isolation in the DC-DC converters.

As can be observed, the load flow calculation without galvanic isolation in Figure 2.7 is different from that obtained with galvanic isolation in Figure 2.5. One of the main differences is that the multi-terminal monopolar system is affected by the outage of the negative pole converter of the HVDC station Cb-C2.

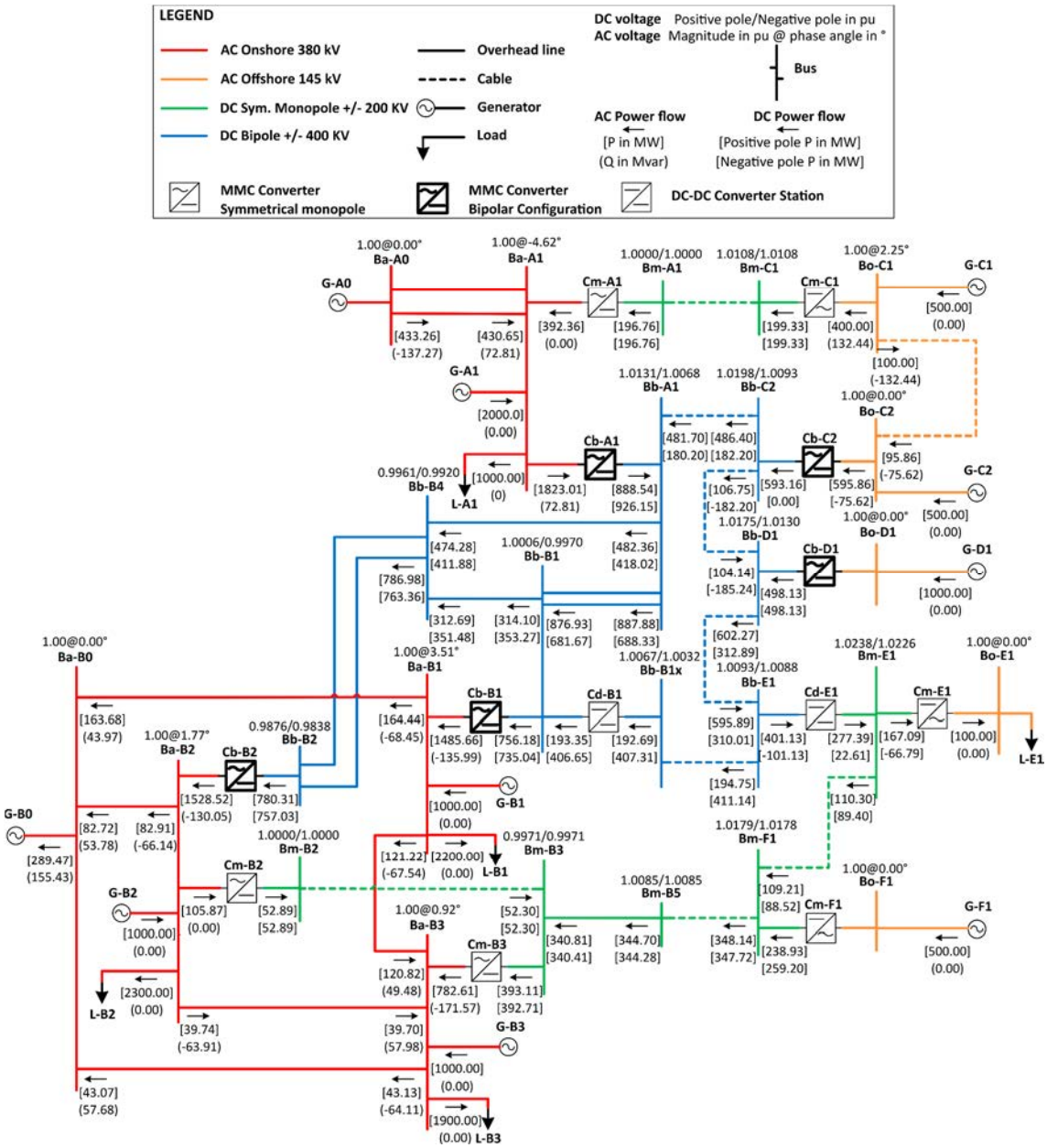

Figure 2.7. Post-contingency scenario in case of DC-DC converters without galvanic isolation after the outage of the negative pole converter of station Cb-C2.

Note that the power flowing through the positive and negative poles of each of the two terminals of both DC-DC converters is different from each other due to the different voltage and current asymmetry in each terminal. However, the sum of the active power of both DC poles is the same.

Figure 2.8 gathers the DC busbar voltages and the converter loading. It demonstrates that the voltage deviation is lower without galvanic isolation than with galvanic isolation. It also shows that the power asymmetry is distributed differently than in the previous case.

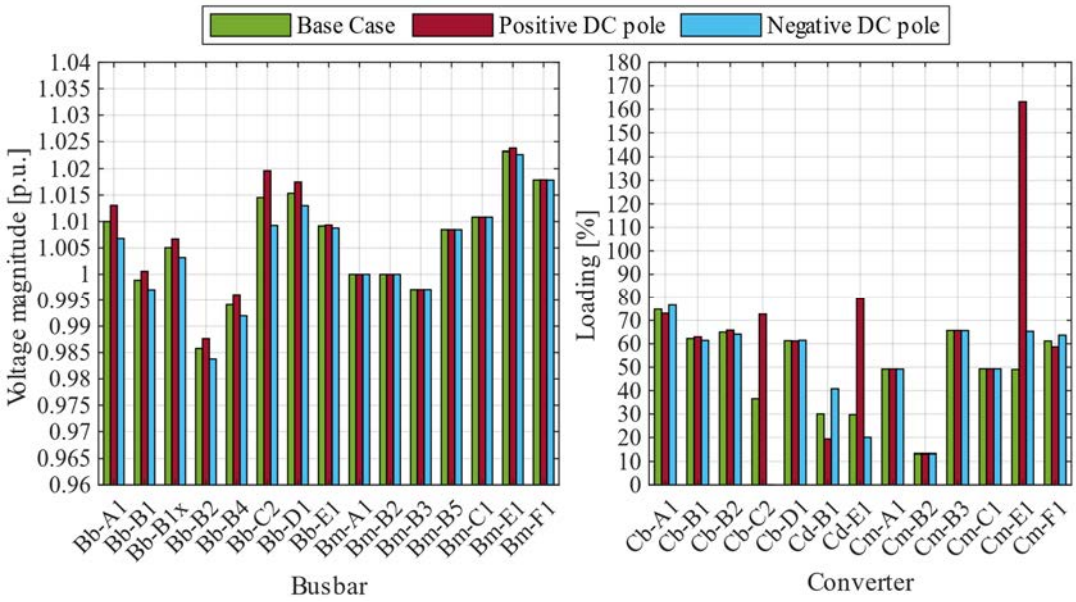

Figure 2.8. DC voltages and loading of converters when DC-DC converters do not provide galvanic isolation.

These results can be explained by the lack of galvanic isolation and the grounding resistance installed in the stations forming part of the multi-terminal symmetrical monopolar system.

Regarding the symmetrical monopolar station Cm-E1, equation (2.4) proves that its voltage and current asymmetry are related through the zero-sequence resistance. As the grounding resistance is considered zero in this case, this zero-sequence resistance only consists of the equivalent resistance of its arms, which is very small. This fact implies that the voltage asymmetry is almost zero and, thus, the power asymmetry is mainly due to the current asymmetry.

The current asymmetry is closely related to the current flowing through the grounding system, as expressed in (2.3). Therefore, this asymmetry in current is distributed across the monopolar system following the minor resistive path. As the grounding resistance of station Cm-E1 is zero, almost the total current asymmetry flows from the DC side to its grounding system, causing the overload of its positive arm in this case. As can be seen, the voltage magnitude and the loading of the remaining stations forming the multi-terminal monopolar system keep their pre-contingency value.

The smaller resistive path posed by the Cm-E1 station for the current asymmetry also explains the results obtained in the bipolar system. Furthermore, since the voltage and current asymmetry at the bipolar side of the DC-DC converter Cd-E1 depends on the current and voltage asymmetry at its monopolar side, according to (2.13) and (2.14), Cd-E1 also becomes the minor resistive path for current asymmetry in the bipolar system.

Therefore, the amount of current asymmetry absorbed by the bipolar HVDC stations participating in the DC voltage control is much smaller compared to the previous case, where DC-DC converters provided galvanic isolation. Thus, the voltage deviation caused by their voltage droop-based controller on the system is also minor.

Once the reason behind the results obtained is explained, it is essential to highlight the strong influence that the galvanic isolation and the grounding resistance of the monopolar HVDC station have over the whole system.

Whereas in the previous case with galvanic isolation, the loading of the converters did not exceed their maximum value, in this case, the station Cm-E1 is overloaded due to the high amount of current asymmetry flowing to its grounding system. Suppose station Cm-E1 trips as a result of the high current. In that case, it is likely that station Cm-F1, which is also grounded through a zero-resistance, becomes in the same situation, thus, causing a cascade outage of the stations in the monopolar system.

It is also important to note that the active power transmitted to the two onshore AC systems in the post-contingency scenario is mostly the same despite the significant change in the load flow results in the DC network.

2.4.2. Influence of the grounding configuration of the system DCS2

2.4.2.1. Influence of the grounding resistance value

The grounding resistance has been demonstrated to be behind the reduction of the voltage asymmetry in the DC system and the overloading of the station Cm-E1 when the DC-DC converter Cd-E1 does not provide galvanic isolation. Therefore, in this section, it is also considered that DC-DC converters do not provide galvanic isolation to explore further the influence of the grounding resistance in the post-contingency scenario.

First, the post-contingency scenario, considering that the symmetrical monopolar HVDC stations are grounded through a 5 kΩ resistance, is presented in Figure 2.9. Observe that the load flow results in Figure 2.9 are very different compared to those obtained with a zero-grounding resistance in Figure 2.7.

Since symmetrical monopolar stations use a high grounding resistance, the current asymmetry caused by station Cb-C2 because of the contingency is hardly transferred to the symmetrical monopolar system. Therefore, the asymmetry in current is conducted to ground almost totally by the bipolar HVDC stations.

The asymmetry distribution among all the bipolar stations depends on their equivalent resistance, which is related to their respective control. Therefore, the asymmetry in current flows from station Cb-C2 to the ground through the different ground paths according to their resistance.

From (2.9) and (2.11), bipolar HVDC stations with DC voltage droop control offer a smaller resistive path to ground than stations implementing an active power control in the same conditions. The smaller the droop coefficient k_{droop}, the smaller the equivalent grounding resistance of a bipolar station.

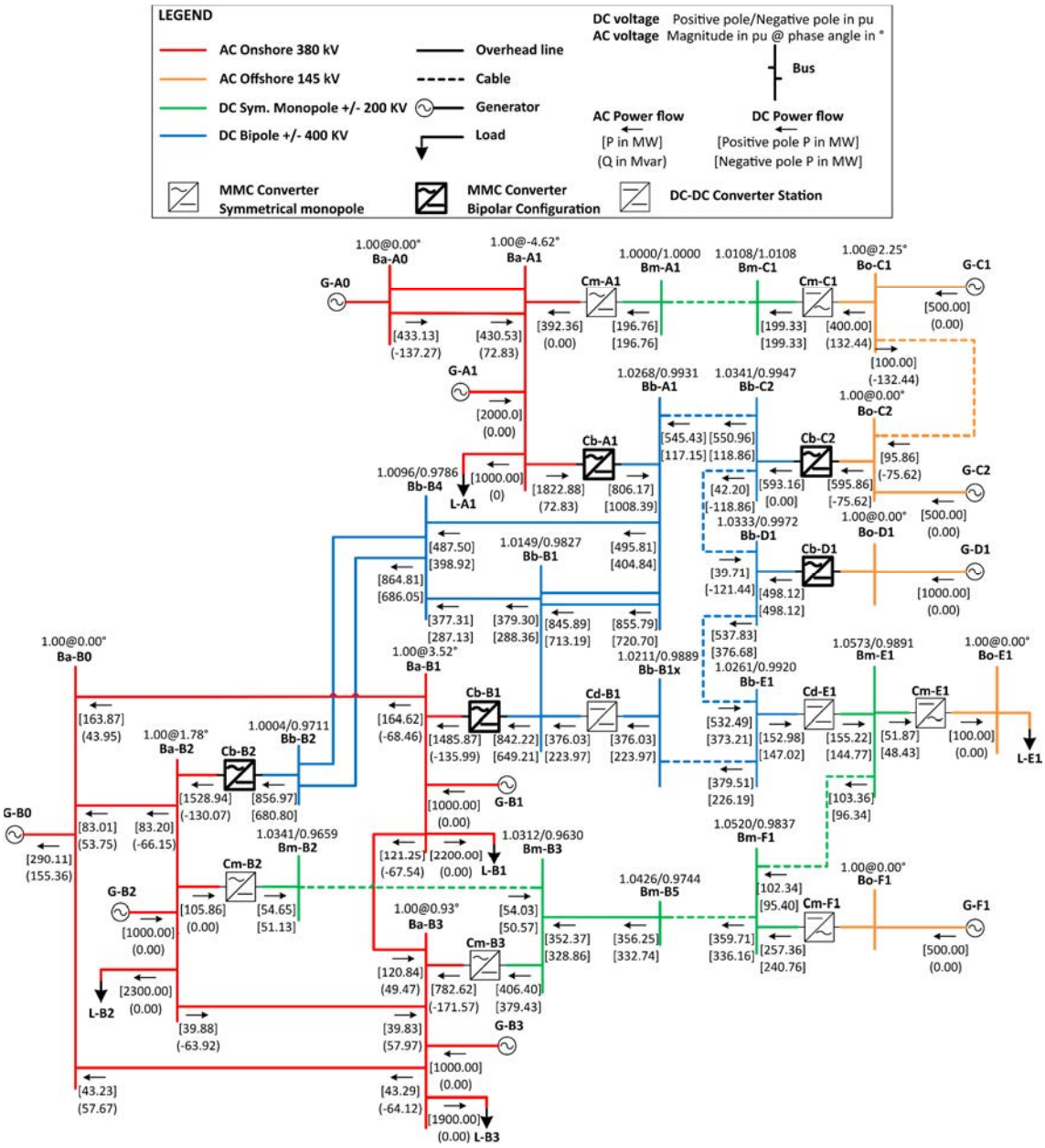

Figure 2.9. Post-contingency scenario in case of DC-DC converters without galvanic isolation after the outage of the negative pole converter of station Cb-C2. Symmetrical monopolar stations grounded through a 5 kΩ resistance.

Therefore, the current asymmetry is conducted to ground almost totally by the bipolar HVDC stations participating in the DC voltage control as in the case where DC-DC converters provided galvanic isolation in Figure 2.5.

Regarding the symmetrical monopolar multi-terminal system (DCS1), although the amount of the transferred current asymmetry is small due to the high grounding resistance, it causes a high voltage asymmetry. Figure 2.10 shows the voltage magnitude of the DC terminals for each pole and the loading of the converters in this scenario.

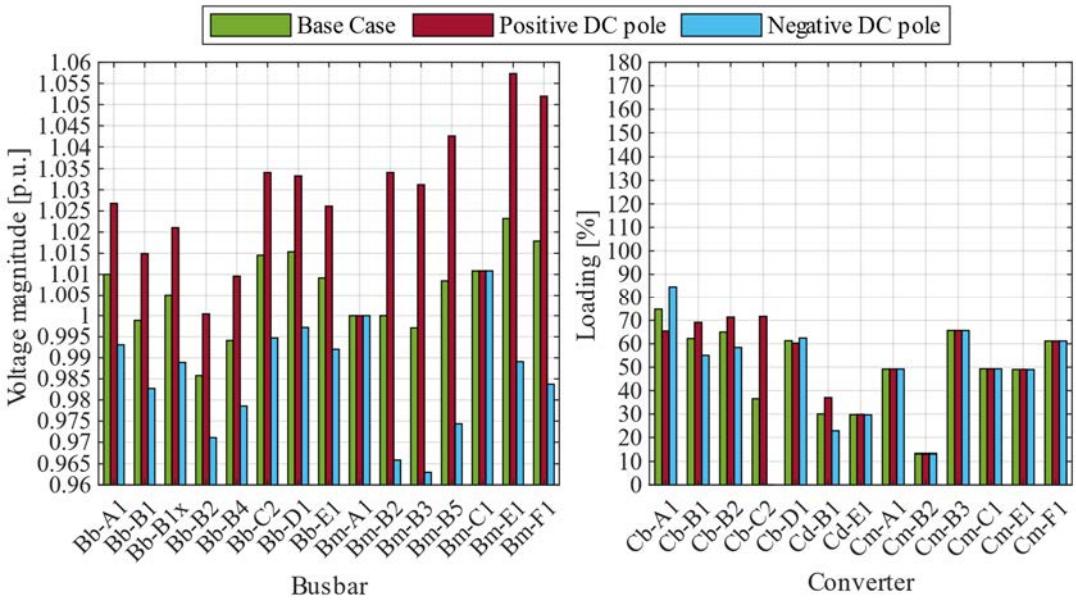

Figure 2.10. DC voltages and loading of converters when DC-DC converters do not provide galvanic isolation. Symmetrical monopolar HVDC stations are grounded through a 5 kΩ resistance.

As can be seen, the voltage asymmetry appears both in the bipolar and the symmetrical monopolar multi-terminal systems. The highest voltage asymmetry appears in the symmetrical monopolar stations where voltages above 5% of the rated voltage are far exceeded in the case of the terminal Bm-E1, where station Cm-E1 is connected.

As for the loading, it is almost equal for both poles of the symmetrical monopolar stations because of the small amount of current asymmetry transferred from the bipolar system. The asymmetry in the loading appears mainly in the stations Cb-A1, Cb-B1, and Cb-B2, which are responsible for the DC voltage control in the bipolar system.

Therefore, the impact of the grounding resistance in the post-contingency scenario after an asymmetrical contingency has been demonstrated from the analysis of a zero and high resistance scenario.

However, to provide higher sensitivity about the proper value of grounding resistance from the perspective of the asymmetrical operation of the DC system, the evolution of the voltage and current asymmetry in both DC systems is plotted in Figure 2.11 as a function of the grounding resistance.

As expected, the voltage asymmetry increases with grounding resistance in both DC systems. However, the trend of the current asymmetry differs between DCS2 and DCS3 systems. As the resistance increases, the current asymmetry tends to follow the path to ground offered by the bipolar stations instead of flowing through the higher grounding resistance of the symmetrical monopolar stations.

DC-DC converters transmit the current asymmetry but do not pose a direct path to the ground like HVDC stations, so they only transmit the current asymmetry from one part of the system to another. Specifically, DC-DC converter Cd-E1 transmits the current asymmetry that has not been conducted to ground by HVDC stations participating in the DC voltage control in DCS3 to the system DCS2.

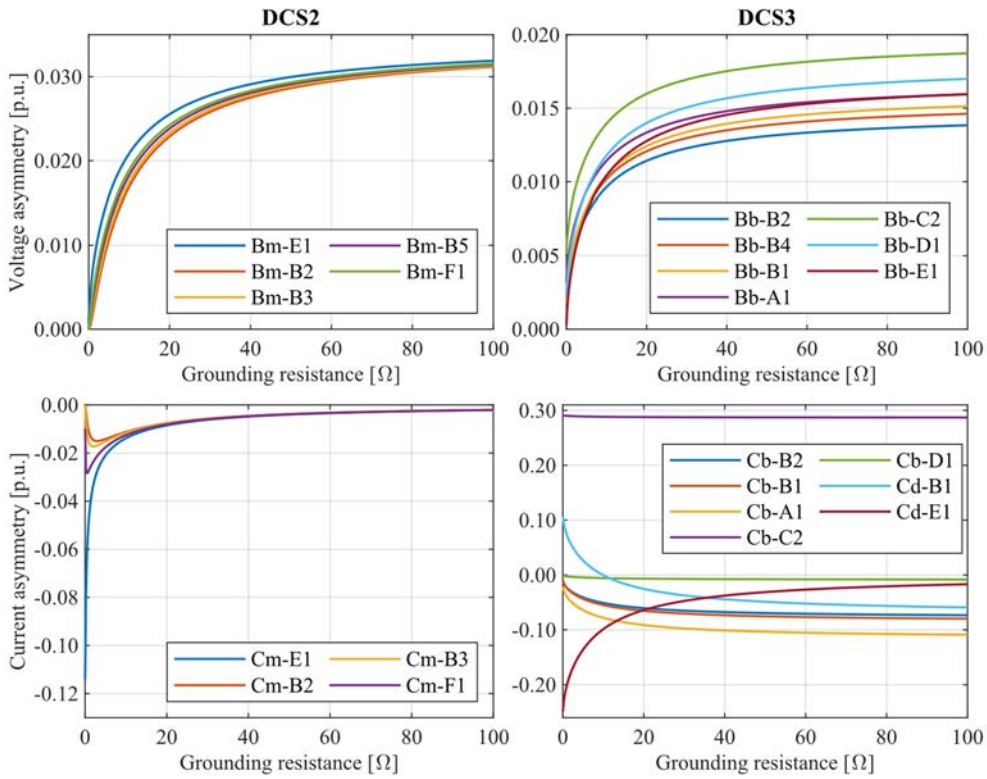

Figure 2.11. Current and voltage asymmetry in the DC systems DCS2 and DCS3 as a function of the grounding resistance of the symmetrical monopolar HVDC stations.

Both current and voltage asymmetry can harm the system due to the overloading of elements caused by the former or the high and low voltages provoked by the latter. Since this asymmetry cannot be suppressed in case of asymmetrical contingencies, the grounding resistance value should also be designed considering the asymmetrical DC operation.

In the case of the system DCS2, a grounding resistance value between 10 and 20 Ω achieves a current asymmetry below 2% and a voltage asymmetry below 2.6% for all the HVDC stations. Note that as the base power of the system is 1000 MW, a 2% current asymmetry implies 20 MW of power asymmetry at the rated voltage.

However, the same grounding resistance range between 10 and 20 Ω in symmetrical monopolar stations causes a current asymmetry of up to 10% in bipolar HVDC station Cb-A1 and a voltage asymmetry below 1.7% in the system DCS3. In this case, a 10% current asymmetry represents a power asymmetry of 100 MW at rated voltage.

Therefore, defining a grounding resistance for symmetrical monopolar stations from the perspective of the asymmetrical operation of the DC network when there is no galvanic isolation is not straightforward, as it also requires checking the effect of all the possible contingencies in the DC network. In addition, if the power asymmetry is more significant for the same contingency, the current and voltage asymmetry impact is also greater.

2.4.2.2. Effect of different grounding resistance among the stations

The previous analysis was performed assuming that the grounding resistance in all the stations in the system DCS2 is the same. However, this assumption may only be met in some cases.

For that reason, this section analyses the response of the network when all the stations in the symmetrical monopolar system are grounded through a 5 kΩ resistance, except station Cm-B2, which is solidly grounded.

The load flow results for the complete network are depicted in Figure 2.12 and are very different from those obtained in Figure 2.9, where all stations were grounded through a 5 kΩ resistance.

One of the main differences is the high-power asymmetry in all the lines and cables of the system DCS2 from station Cd-E1 up to station Cm-B2. Station Cm-B2 presents a high-power asymmetry due to the zero-grounding resistance. However, the rest of the stations in the system DS2 offer a slight power asymmetry.

Figure 2.12 also shows that the further away a busbar is from station Cm-B2, the higher the voltage asymmetry between its two DC poles. The voltage asymmetry in the DCS3 system is also reduced compared with the previous case.

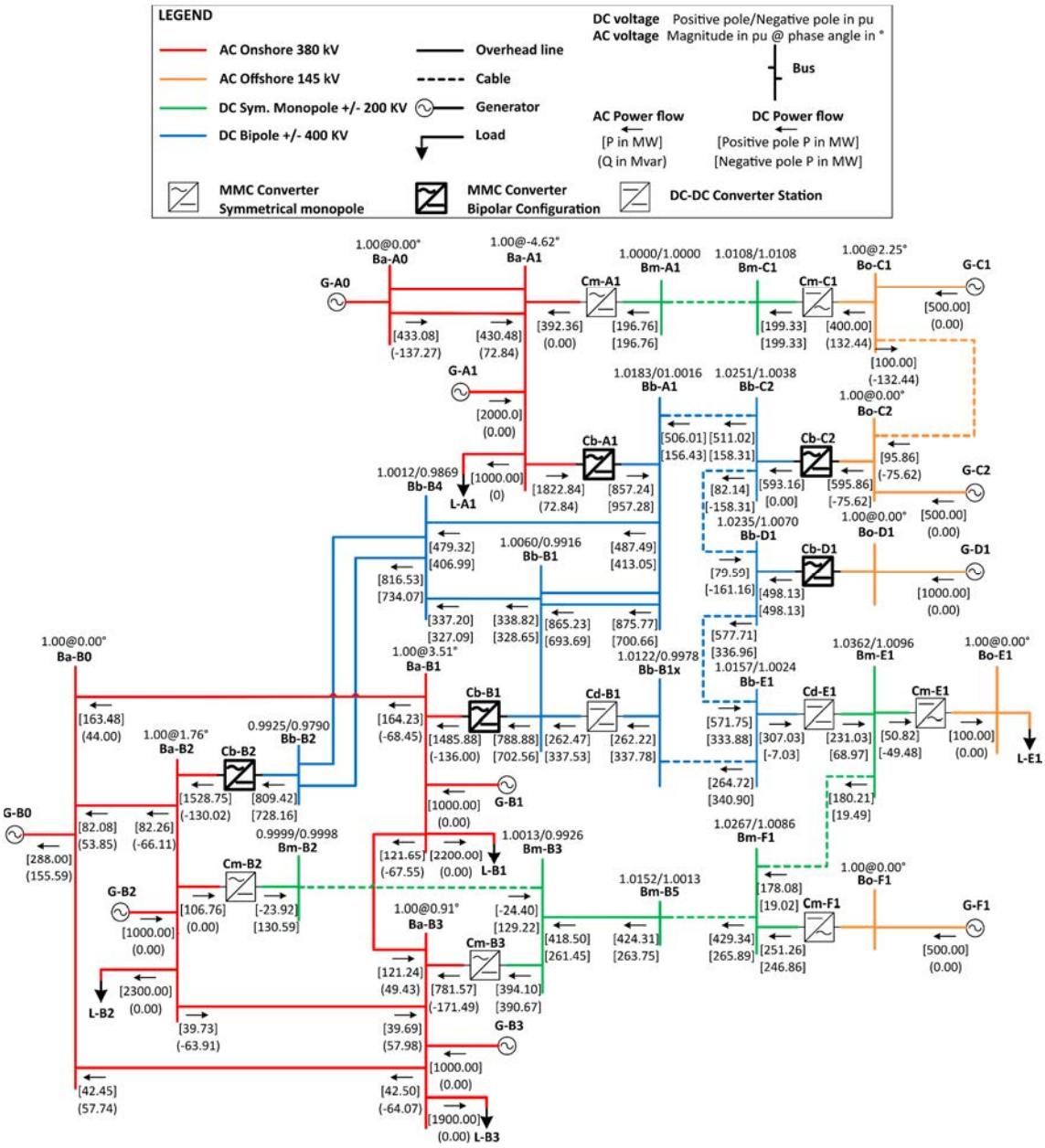

Figure 2.12. Post-contingency scenario in case of DC-DC converters without galvanic isolation and symmetrical monopolar stations grounded through a 5 kΩ resistance (Cm-B2 solidly grounded).

Figure 2.13 shows the voltage magnitude of each pole of the DC terminals and the loading of the converters in each pole. Observe that there are neither excessive voltages in any terminal nor elements overloading in this case.

Although station Cm-B2 exhibits a significant power asymmetry between the power flowing for its positive and negative pole, it remains under limits due to its low initial loading. Nonetheless, the same contingency would result in an overload station for higher initial loading.

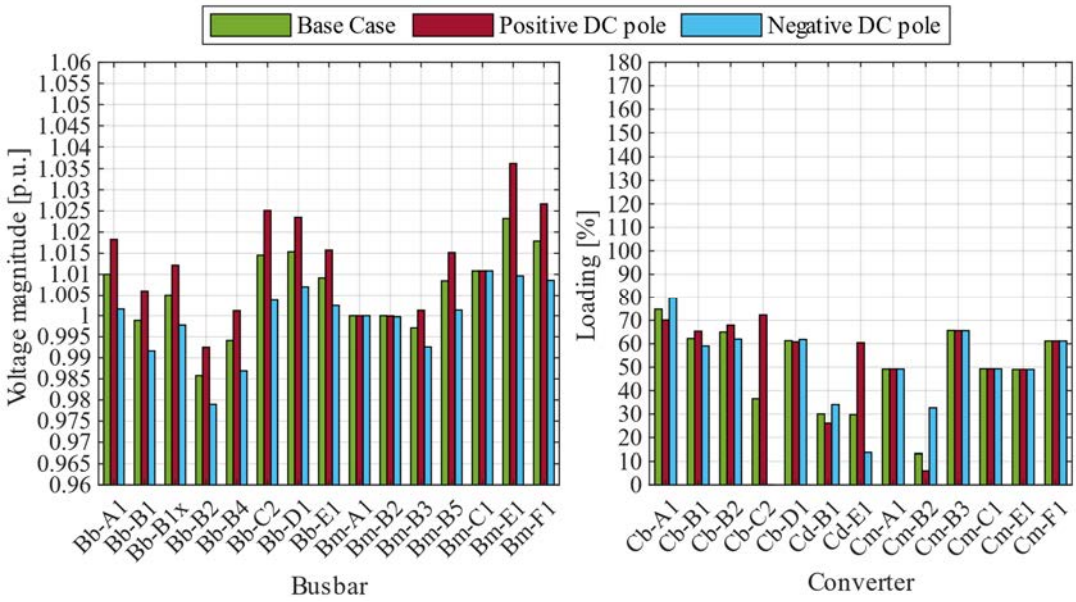

Figure 2.13. DC voltages and loading of converters when DC-DC converters do not provide galvanic isolation. Symmetrical monopolar HVDC stations are grounded through a 5 kΩ resistance, except station Cm-B2, which is solidly grounded.

Therefore, it is not only important the grounding resistance value of the complete symmetrical monopolar system but also the individual grounding resistance of each station since each combination in the configuration of the grounding system of the DCS2 system can consequently lead to different post-contingency scenarios.

2.4.3. Influence of the control of the DC network

The last section demonstrated the influence of the grounding resistance on the post-contingency steady state following an asymmetrical disturbance. However, as the equivalent grounding resistance of bipolar stations depends on their respective control, it is expected that a change in the control strategy of the network also influences its asymmetrical operation. Therefore, this aspect is addressed in this section.

2.4.3.1. Influence of the droop coefficient in the case of distributed DC voltage control

First, the role of the control strategy of the DCS3 is addressed considering that DC-DC converters provide galvanic isolation. Therefore, the grounding resistance of the symmetrical monopolar stations is not involved in this case.

As was seen in the previous sections, the DC voltage regulation in DCS3 is carried out by stations Cb-A1, Cb-B1, and Cb-B2 through a distributed DC voltage droop control. The equivalent grounding resistance of each station depends on the droop coefficient k_{droop} according to (2.11).

Therefore, the impact of the droop coefficient k_{droop} in the current and voltage asymmetry in the DCS3 system is shown in Figure 2.14.

As expected from (2.11), the smaller the droop coefficient, the smaller the equivalent grounding resistance. Thus, small droop coefficients provoke small voltage asymmetries at the DC busbars.

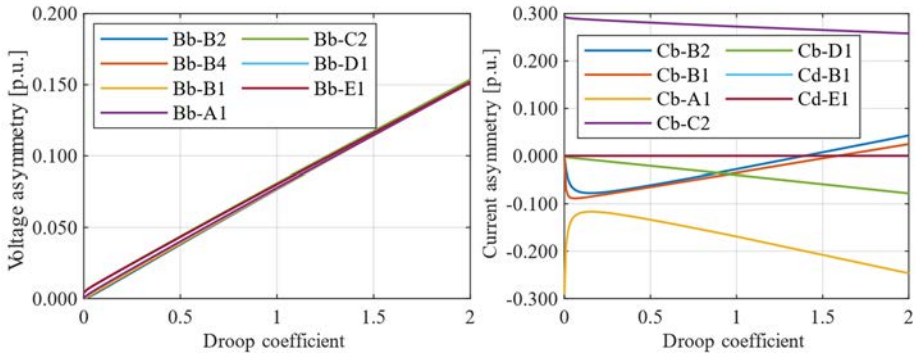

Figure 2.14. Current and voltage asymmetry as a function of the droop coefficient in the system DCS3 when DC-DC converters provide galvanic isolation.

However, the current asymmetry is not equally distributed between the stations participating in the DC voltage control since the current asymmetry tends to circulate through the path to ground whose electrical distance to station Cb-C2 is smaller.

This fact implies that almost the total current asymmetry flows through station Cb-A1 for very small droop coefficients. This can cause excessive overloading of one of the converters of this station and another outage in the system. Besides, the tripping of the DC line connecting station Cb-A1 with Cb-C2 can also occur for the same reason.

As the droop coefficient rises, the behaviour of the stations with a distributed DC voltage droop control tends to be similar to those performing active power control. Therefore, station Cb-D1, which transfers a constant active power to the DC network, increases its participation in the current asymmetry. The asymmetrical voltage also increases linearly as the droop coefficient rises.

For high droop gains, (2.11) tends to be (2.9). Thus, the equivalent resistance of bipolar stations mainly depends on their active power setpoint. Since higher setpoints imply lower equivalent resistance, Cb-D1 and Cb-A1 absorb the current asymmetry. As station Cb-A1 has a higher setpoint, its absorption of asymmetrical current is more elevated.

On the other hand, stations Cb-B1 and Cb-B2 have a negative active power setpoint from the point of view of the DC network, i.e., they act as DC loads. Therefore, they behave as an equivalent negative resistance for high droop coefficients according to (2.9), and, thus, they work as sources of asymmetrical current. This is shown in Figure 2.14. For droop coefficients above 1.5, their current asymmetry has the same sign as the current asymmetry created by the outage of the negative pole converter of station Cb-C2. This behaviour of stations Cb-B1 and Cb-B2 for high droop coefficients augments the total amount of asymmetrical current in the system, increasing the overload of lines, cables, and converters. Therefore, the configuration of the DC voltage droop control should also consider the asymmetrical operation of the DC network in order not to produce excessive overloading of a particular station or high voltage asymmetry.

On the other hand, if galvanic isolation is not considered in DC-DC converters, the distribution of current asymmetry and the value of the voltage asymmetry depend also on the grounding resistance of symmetrical monopolar HVDC stations, as was shown in the previous sections.

Figure 2.15 and Figure 2.16 shows the influence of the droop coefficient of bipolar stations in DCS3 when symmetrical monopolar stations in DCS2 are grounded through a zero and high resistance, respectively.

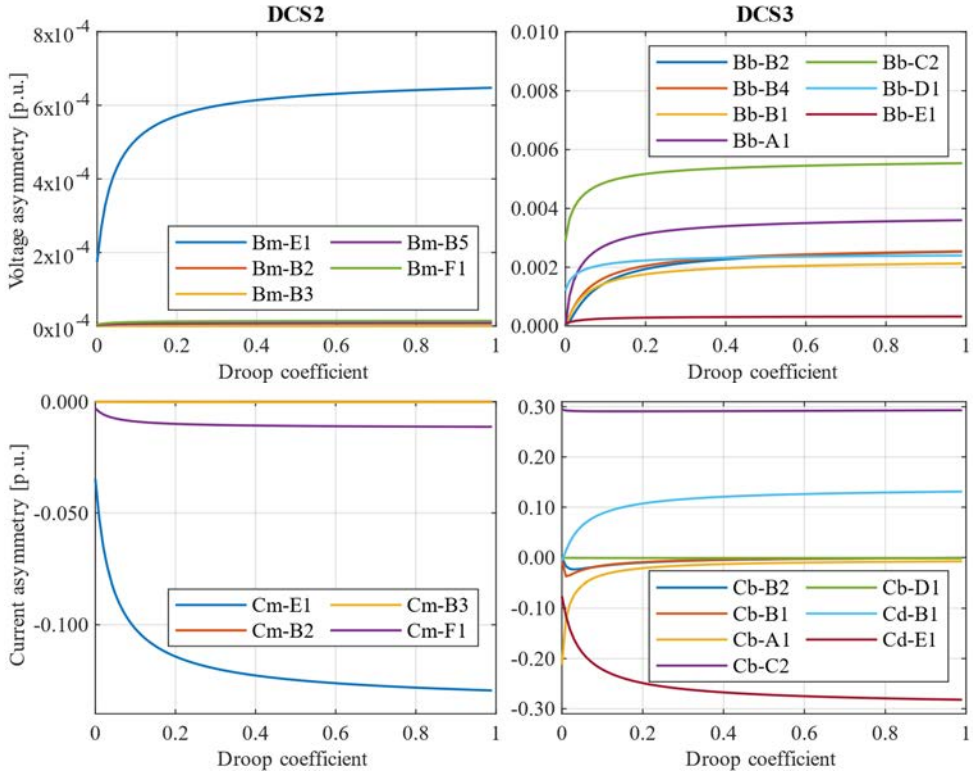

Figure 2.15. Current and voltage asymmetry as a function of the droop coefficient when DC-DC converters do not provide galvanic isolation and stations in DCS2 are solidly grounded.

Figure 2.15 shows that the voltage asymmetry does not reach values as higher as those shown in Figure 2.14 due to the small resistive path to ground that the symmetrical monopolar stations represent, regardless of the droop coefficient.

However, the lack of galvanic isolation causes the asymmetrical current to be distributed between stations according to the network resistance and their grounding resistance. Therefore, as the droop coefficient increases, the asymmetrical current flowing through DCS2 also does, specifically through station Cm-E1, representing the less resistive path to ground from station Cb-C2.

In contrast, Figure 2.16 shows that the behaviour of the DCS3 system is similar to that shown in Figure 2.14 since the voltage asymmetry increases almost linearly with the droop coefficient, and stations in DCS2 practically absorb the asymmetrical current. The main difference concerning the scenario with galvanic isolation is that the voltage asymmetry is also transmitted to the DCS2 system.

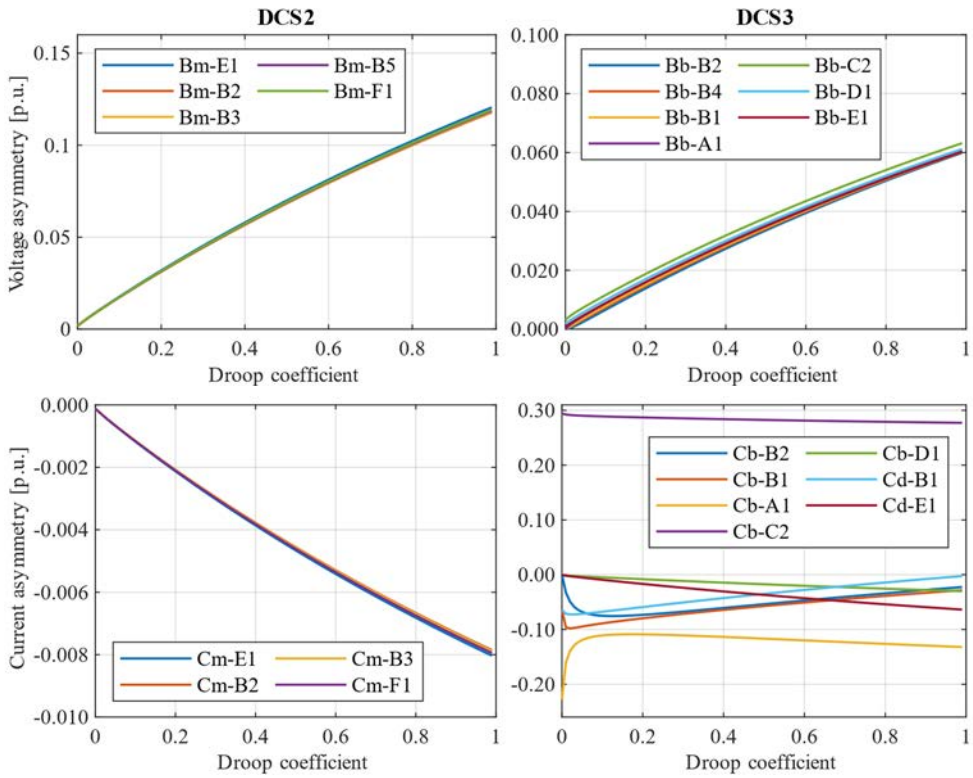

Figure 2.16. Current and voltage asymmetry as a function of the droop coefficient when DC-DC converters do not provide galvanic isolation and stations in DCS2 are grounded through a 100 Ω resistance.

Therefore, the droop coefficient in bipolar systems can have several implications in the case of asymmetrical contingencies. These consequences affect not only the bipolar system itself but also other systems to which it is connected via a DC-DC converter unless this converter provides galvanic isolation.

2.4.3.2. Influence of the location of the station controlling the DC voltage in case of centralised voltage control

When centralised voltage control is implemented in the bipolar system DCS3, the station responsible for the DC voltage control behaves as solidly grounded from the point of view of the asymmetrical operation. Therefore, the current and voltage asymmetry depend on the distance of that station to the point of the DC network where the asymmetrical contingency occurs.

Figure 2.17 shows the behaviour of the system facing the outage of the negative pole converter of station Cb-C2 when station Cb-A1 controls the DC voltage. The results are present for a range of grounding resistance in the station of the DCS2 system. As Cb-A1 is one of the stations electrically closest to station Cb-C2, the voltage asymmetry is significantly reduced regardless of the grounding resistance of the DCS2 system stations. In addition, station Cb-A1 is the main sink of the asymmetrical current, regardless of the grounding resistance in the stations of the system DCS2. Therefore, if the grounding resistance of the system DCS2 increases, the asymmetrical current absorbed by station Cb-A1 also grows up to fully compensate for the asymmetry created by the outage of the negative pole converter of station Cb-C2.

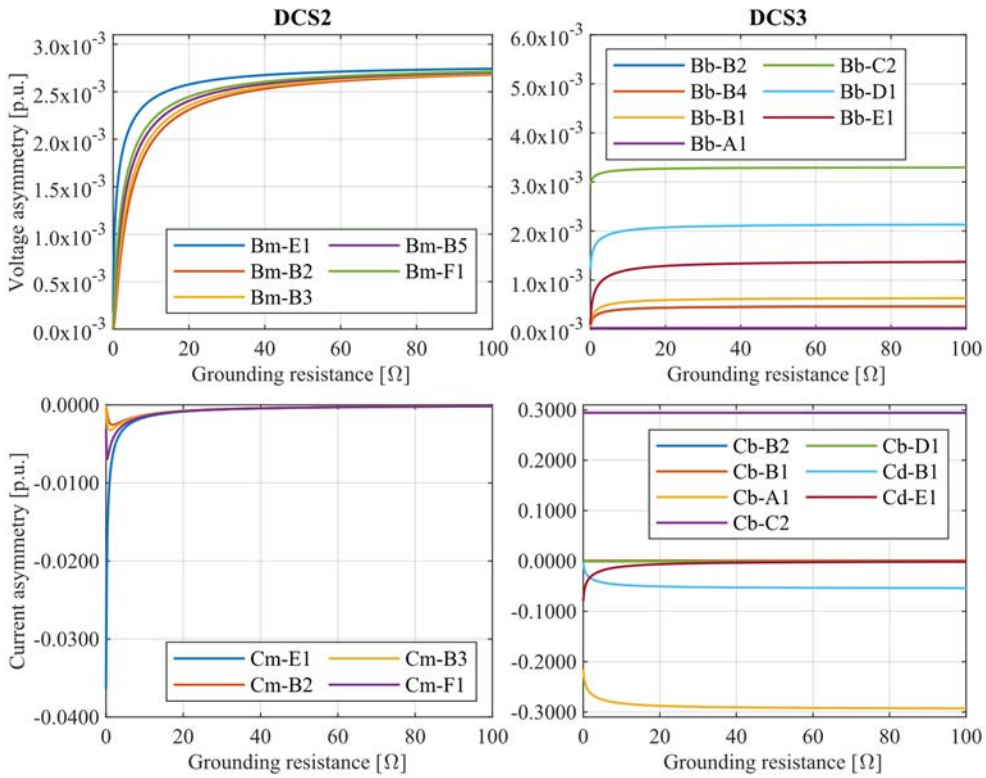

Figure 2.17. Current and voltage asymmetry when Cb-A1 implements a centralised DC voltage control as a function of the grounding resistance of stations in system DCS2.

If the station controlling the DC voltage in the system DCS3 is located further away the station Cb-C2, an increment of the asymmetrical voltage is expected after the same contingency happens. This scenario is represented in Figure 2.18, where station Cb-B2 controls the DC voltage.

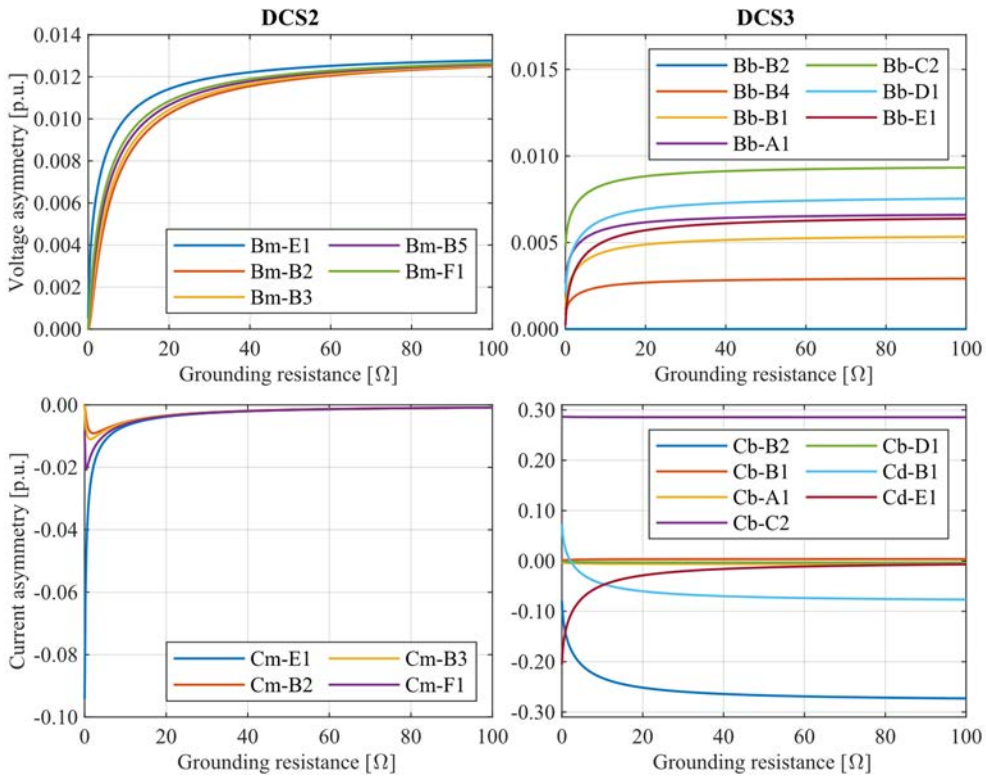

Figure 2.18. Current and voltage asymmetry when Cb-B2 implements a centralised DC voltage control as a function of the grounding resistance of stations in system DCS2.

As shown in Figure 2.18, the voltage asymmetry is much higher than that observed in Figure 2.17, considering the same grounding resistance value in DCS2 system stations. The amount of asymmetrical current transmitted to the system DCS2 also rises for the same grounding resistance. However, for high grounding resistances, it is station Cb-B2 that absorbs all the current asymmetry originated by the outage of the negative pole converter of station Cb-C2.

Also, regardless of the station that performs the centralised voltage control, it can be observed that the rest of the stations controlling the active power hardly absorb asymmetrical current. Therefore, the overloading of the stations absorbing asymmetrical current is higher than that obtained in the case of a distributed DC voltage control where different stations share the total current asymmetry in system DCS3. Therefore, in the case of centralised voltage control, the further away the contingency is from the station controlling the DC voltage, the higher the voltage asymmetry that appears in the DC system.

2.5. Conclusions

This chapter has studied the asymmetrical operation of a DC network composed of DC systems with different configurations interconnected through DC-DC converters.

The analysis developed has identified the different issues that can affect the post-contingency steady-state of a heterogeneous DC network after a contingency affecting a

single DC pole. The main aspects identified are related to the HVDC stations and DC-DC converters.

For DC-DC converters, the most critical factor is the ability to provide galvanic isolation. This capability allows a DC system to be completely isolated from the asymmetrical disturbance occurring in another DC system connected via a DC-DC converter.

The response of an HVDC station to an asymmetrical perturbation highly depends on its configuration: a) symmetrical monopolar or b) bipolar. In the case of symmetrical monopolar stations, their current and voltage asymmetry in the steady state depends on the grounding resistance. On the other hand, the steady-state response of the bipolar HVDC stations to an asymmetrical perturbation in the DC network depends on their control. This response can be defined as a function of a virtual grounding resistance.

However, DC networks are composed of several HVDC stations and DC-DC converters. Therefore, the steady-state scenario of the whole DC network after an asymmetrical perturbation depends on the response of each HVDC station and DC-DC converter according to its configuration.

The topology of the DC network and the location of each HVDC station and DC-DC converter, as well as the site of the contingency, also have a significant impact on the post-contingency scenario. Besides, the amount of active power that the element that suffers the contingency transfers is also important.

The main conclusion is that a detailed analysis of each DC network is necessary to assess all the possible contingencies in the worst operating scenario. This is necessary to avoid equipment overloading or excessive over/under-voltages that can cause the outage of more elements in the post-contingency scenario.

Therefore, both the grounding resistance design in the case of symmetrical monopolar stations and the control configuration of the bipolar stations should consider the asymmetrical operation.

CHAPTER 3. DYNAMIC ANALYSIS[1]

This chapter focuses on the influence of the earthing system impedance of symmetrical monopolar stations on the dynamic performance of a heterogeneous HVDC grid during asymmetrical operation. The analysis is carried out through EMT dynamic simulations considering several control strategies. The impact on the protection system is also investigated.

[1] This chapter reproduces the content published in J. Serrano-Sillero, M. Á. Moreno, and A. Morales, "HVDC grids with heterogeneous configuration stations under DC asymmetrical operation," Int. J. Electr. Power Energy Syst., vol. 113, 2019.

3.1. Introduction

Chapter 2 has demonstrated that there are numerous factors involved in the asymmetrical DC operation and that determine the post-contingency steady-state in a heterogeneous DC grid. However, the steady-state reached is only a part of the complete system response and valid steady-state results do not guarantee the absence of excessive over/under-voltages or overcurrents during the transient response. Therefore, the dynamic response of a heterogeneous DC grid under asymmetrical DC operation requires further investigation.

Results from Chapter 2 proved that the grounding resistance and the control strategy determine the behaviour of HVDC stations during asymmetrical DC operation. Therefore, this chapter focuses on studying the influence of the grounding impedance of the symmetrical monopolar station on the performance of a heterogeneous meshed DC grid during asymmetrical operation. Different scenarios are analysed from a dynamic approach via EMT simulations in PowerFactory to cover the possible control strategies of DC grids. Results from the simulations allow pointing out the problems that may arise. Furthermore, the impact of the grounding system on the protection system is also addressed.

For the shake of clarity, the dynamic analysis is carried out using as test system a symmetrical monopolar station that is connected to a point-to-point bipolar HVDC link without galvanic isolation between them. Consequently, the three HVDC stations form a three-terminal meshed DC grid. This simple system allows for a better understanding of the simulation results than a larger DC system where several control interactions can occult the dynamics related to the asymmetrical DC operation.

The chapter is organised as follows. Section 3.2 presents an overview of configurations and earthing options in HVDC links. Section 3.3 develops the converter equations and delves into the variables influencing the asymmetrical operation. Section 3.4 assesses selected case studies and scenarios. Finally, the conclusions obtained are gathered in Section 3.5.

3.2. HVDC converter station configuration and earthing system

Figure 3.1 shows a representation of three converter station configurations [33]. The symbol E refers to the most frequent locations for the earthing system. The dashed line represents the metallic return.

The way an HVDC station is grounded can be classified according to the grounding point (AC side vs DC side), the magnitude of the impedance (low or high), or the type of impedance (resistive, inductive, capacitive, or a combination) [33]. Low impedance leads to high short-circuit currents during pole-to-ground faults, whereas high impedance offers high voltage stress on station equipment [32], [34]. Furthermore, the nature of the impedance determines the dynamic behaviour: an inductive impedance limits the rising rate of the fault current and increases the transient overvoltage during a fault; a capacitive

impedance limits the rising rate of voltage while causing a higher transient fault current; a resistive impedance reduces steady-state earth current, increases steady-state DC voltage and damps current or voltage oscillations.

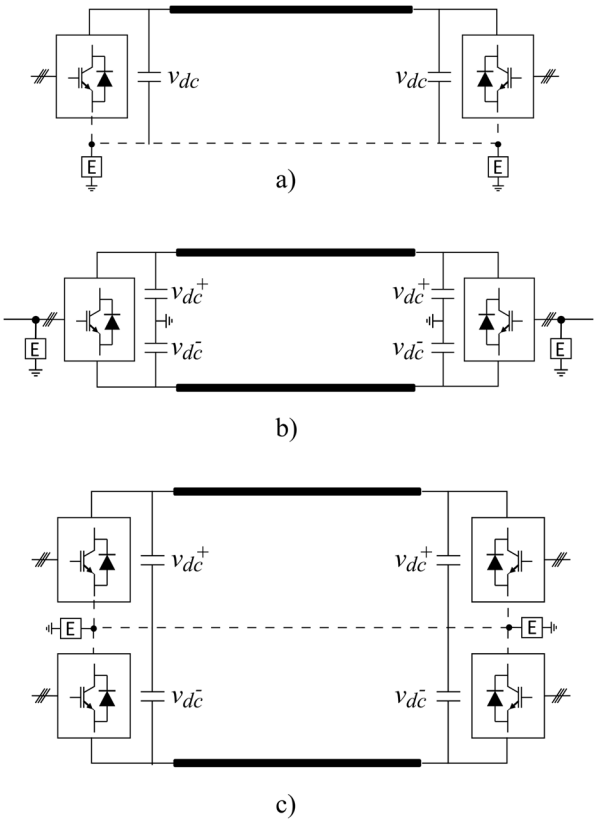

Figure 3.1. HVDC converter station configurations: a) asymmetrical monopole; b) symmetrical monopole; c) bipole.

Reference [33] presents alternatives to locate the earthing point in asymmetrical monopolar and bipolar MMC-HVDC stations, although the usual locations are shown in Figure 3.1 [32], [34]. The preferred choice in MMC-HVDC symmetrical monopolar stations is to ground the AC side [78] against the option of high DC resistances to connect both poles to the earth at the DC side.

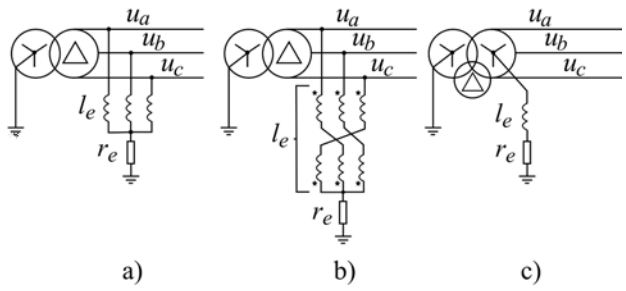

Figure 3.2. AC side grounding systems: a) star point reactor; b) zig-zag transformer; c) Yyd transformer with an earthing impedance.

The most frequent AC side grounding methods are shown in Figure 3.2. Their purpose is to provide a path for zero-sequence currents. They typically use a Yd transformer with

additional grounding equipment, such as a star point reactor, a zig-zag grounding transformer or a Yyd transformer with earthing impedance [77]. Further information about these AC side grounding methods can be consulted in [86]. The zig-zag transformer is more specifically addressed in [78].

3.2.1. Asymmetrical monopolar configuration

The asymmetrical monopole configuration in Figure 3.1 a) requires only one fully insulated high-voltage conductor since the earthed pole uses a metallic conductor or the ground as a return path.

In an MTDC system consisting entirely of asymmetrical monopolar stations, at least one must be grounded through a very low resistance electrode [33]. Alternatively, a reactance can be connected in series with the resistance to limit the rising rate of the current in case of faults. The rest of the stations in the MTDC system can be connected either to that electrode through a metallic return, or they can have their own grounding electrode. It is also recommendable to set more than one grounding point in an extensive system to keep the voltage in the metallic return low enough. Additionally, the AC side must be isolated from the earth to prevent a zero-frequency current component from flowing through the AC grounding point.

3.2.2. Symmetrical monopolar configuration

The symmetrical monopole configuration shown in Figure 3.1 b) needs a fully insulated high-voltage conductor per pole, increasing the cost per installed MW but avoiding issues related to ground currents [32]. In this case, the pole-to-pole DC voltage is the rated DC voltage; each pole has opposite polarity and half-rated DC voltage. The type of grounding system determines the system behaviour during pole-to-ground faults [32], [33].

Any options shown in Figure 3.2 are valid for the AC side grounding configuration [31]. In the case of the star point reactor, the reactance needs to be high enough to limit reactive power consumption and losses [78]. The zig-zag transformer offers advantages concerning the star point reactor [78]. It limits the zero-sequence current depending on the magnitude of the grounding resistance, like in the star point reactor. Still, it simultaneously provides a high impedance path for both positive and negative sequence currents, avoiding reactive power consumption during regular operation. Therefore, lower reactance values than those used for the star-point reactor can be used. The Yyd transformer with a grounding impedance uses the neutral point of the wye winding of the transformer to ground the system through an impedance without constraints regarding the magnitude of the resistance or the reactance.

3.2.3. Bipolar configuration

The bipolar configuration shown in Figure 3.1 c) can be viewed as two asymmetrical monopoles interconnected by sharing the pole connected to the ground. Although the cost increases, the redundancy justifies the higher investment. Both poles are subjected to the

rated DC voltage, with opposite polarity [32]. In a bipolar system, a metallic conductor or the ground can be used as a return path, like in the asymmetrical monopolar configuration. Each pole can continue working like an asymmetrical monopole if the other one is disconnected [33].

The behaviour during faults depends entirely on the type of grounding system [32], [34]. For example, the bipolar configuration can be isolated or grounded on the DC side. In case of zero grounding impedance, or when the return path is the earth itself, this system behaves like an asymmetrical monopole during pole-to-ground faults. On the other hand, when the system is isolated or grounded through a high impedance, the neutral conductor must be insulated, increasing the costs. Regarding the grounding of the AC side, the same concerns highlighted for the asymmetrical monopolar stations [33] can be considered for the bipolar stations.

3.3. Asymmetry in DC grids

Contingencies in heterogeneous meshed HVDC grids can eventually result in a DC grid asymmetry, which occurs when positive and negative poles do not carry the same current and/or do not have the same voltage (absolute value). The DC asymmetrical operation manifests as a zero-sequence component in the voltage and/or current on the converter AC side.

In Figure 3.3, phase-*j* of a three-phase MMC converter is represented, where i_{ac}^{j} is the AC current flowing into the converter, u_{ac}^{j} is the phase-*j* AC voltage, i_{dc}^{+} and i_{dc}^{-} are the positive and negative DC-pole currents, and v_{dc}^{+} and v_{dc}^{-} are the positive and negative DC-pole voltages respectively.

According to the references given in Figure 3.3, the following equations can be derived:

$$\begin{cases} i_{u}^{j} = i_{diff}^{j} + \dfrac{i_{ac}^{j}}{2} \\ i_{l}^{j} = i_{diff}^{j} - \dfrac{i_{ac}^{j}}{2} \end{cases} \tag{3.1}$$

where i_{u}^{j} and i_{l}^{j} are the upper and lower arm currents in phase-*j*, respectively, and i_{diff}^{j} is a current circulating through the phase-*j* leg and the DC link. Then:

$$i_{ac}^{j} = i_{u}^{j} - i_{l}^{j} \tag{3.2}$$

$$i_{diff}^{j} = \frac{i_{u}^{j} + i_{l}^{j}}{2} \tag{3.3}$$

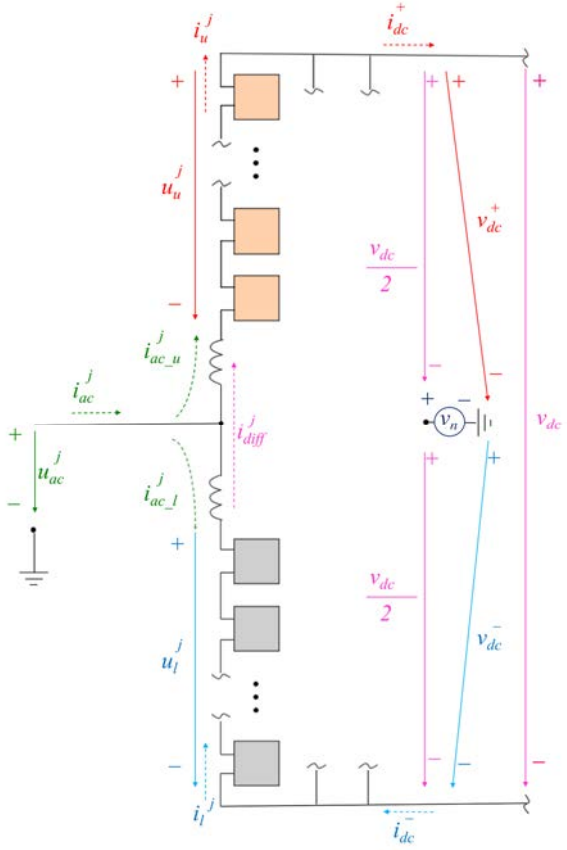

Figure 3.3. Schematic diagram of one phase of an MMC-HVDC converter. Voltages are represented with solid arrows, and currents with dashed arrows.

Considering the three phases, DC currents flowing through the positive and negative poles are calculated as follows:

$$i_{dc}^{+} = \sum_{j=1}^{3} i_u^j = \sum_{j=1}^{3} i_{diff}^j + \frac{1}{2}\sum_{j=1}^{3} i_{ac}^j \tag{3.4}$$

$$i_{dc}^{-} = \sum_{j=1}^{3} i_l^j = \sum_{j=1}^{3} i_{diff}^j - \frac{1}{2}\sum_{j=1}^{3} i_{ac}^j \tag{3.5}$$

Summing and subtracting (3.4) and (3.5):

$$i_{dc}^{+} + i_{dc}^{-} = 2\sum_{j=1}^{3} i_{diff}^j \tag{3.6}$$

$$i_{dc}^{+} - i_{dc}^{-} = \sum_{j=1}^{3} i_{ac}^j \tag{3.7}$$

From the previous equations, it can be deduced that:

- When no zero-sequence AC current exists, positive and negative DC-pole currents are equal:

$$i_{dc}^{+} = i_{dc}^{-} = i_{dc} = \sum_{j=1}^{3} i_{diff}^{j} \tag{3.8}$$

- When positive and negative DC-pole currents differ, then a zero-sequence current appears at the AC side:

$$i_{dc}^{+} - i_{dc}^{-} = 3i_{ac0} \tag{3.9}$$

Applying Kirchhoff's voltage law to the upper and lower converter arms of the phase-*j* in Figure 3.3 yields:

$$u_u^j = v_{dc}^{+} - u_{ac}^j + l_{arm}\frac{di_u^j}{dt} \tag{3.10}$$

$$u_l^j = v_{dc}^{-} + u_{ac}^j + l_{arm}\frac{di_l^j}{dt} \tag{3.11}$$

In Figure 3.3, a DC offset voltage (v_n) is included in the fictitious DC-side neutral point to account for asymmetries in the positive and negative DC-pole voltages:

$$\begin{cases} v_{dc}^{+} = \dfrac{v_{dc}}{2} + v_n \\ v_{dc}^{-} = \dfrac{v_{dc}}{2} - v_n \end{cases} \tag{3.12}$$

Accordingly, the pole-to-pole DC voltage and the DC offset voltage are given by:

$$v_{dc} = v_{dc}^{+} + v_{dc}^{-} \tag{3.13}$$

$$v_n = \frac{v_{dc}^{+} - v_{dc}^{-}}{2} \tag{3.14}$$

Subtracting (3.10) from (3.11) yields:

$$u_l^j - u_u^j = -2v_n + 2u_{ac}^j - l_{arm}\frac{di_{ac}^j}{dt} \tag{3.15}$$

A new variable can be introduced, which can be regarded as a virtual potential [72], [87]:

$$e^j = \frac{u_l^j - u_u^j}{2} \tag{3.16}$$

Then, (3.15) can be written as:

$$e^j = u_{ac}^j - \frac{1}{2} l_{arm} \frac{di_{ac}^j}{dt} \tag{3.17}$$

From (3.17), and considering the three phases, the zero-sequence equation is derived:

$$e_0 = u_{ac0} - \frac{1}{2} l_{arm} \frac{di_{ac0}}{dt} - v_n \tag{3.18}$$

From the previous equation, it can be deduced that:

- When the positive and negative DC-pole voltages are equal, the neutral point voltage is zero, and there is no zero-sequence AC voltage.

$$v_{dc}^+ = v_{dc}^- = \frac{1}{2} v_{dc} \tag{3.19}$$

- When the positive and negative DC-pole voltages differ, a zero-sequence AC voltage appears in the system:

$$u_{ac0} = e_0 + \frac{1}{2} l_{arm} \frac{di_{ac0}}{dt} + v_n \tag{3.20}$$

If the converter is grounded on its AC side, (3.20) can be rewritten by replacing u_{ac_0} with the voltage drop through the equivalent grounding impedance:

$$v_n = -e_0 - \left(\frac{1}{2} l_{arm} + l_e\right) \frac{di_{ac0}}{dt} - r_e i_{ac0} \tag{3.21}$$

Therefore, the DC asymmetric operation is related to the zero–sequence quantities on the AC side of the converter.

Under DC asymmetric operation, the power asymmetry (p_{asy}) between poles is defined by:

$$p_{asy} = \frac{1}{2}(p_{dc}^+ - p_{dc}^-) = \frac{1}{2}(v_{dc}^+ i_{dc}^+ - v_{dc}^- i_{dc}^-) \tag{3.22}$$

Considering (3.9) and (3.12), the power asymmetry can be expressed as follows:

$$p_{asy} = \frac{1}{2} v_n (i_{dc}^{+} + i_{dc}^{-}) + \frac{3}{4} i_{ac0} (v_{dc}^{+} + v_{dc}^{-}) \tag{3.23}$$

Equation (3.23) reveals the main variables that affect the DC power asymmetry, making easier the study of these quantities from the point of view of DC systems. In (3.23), the pole-to-pole DC voltage is unaffected by the DC offset voltage (see (3.13)) and, therefore, also by the zero-sequence. On the other hand, the sum of the positive and negative DC-pole currents is unaffected by the zero-sequence (see (3.6)). Thus, it can be said that the first term in (3.23) represents the power asymmetry due to voltage asymmetry, whereas the second term stands for the power asymmetry caused by a current asymmetry. Moreover, the second term only appears in symmetrical monopolar stations since they can be earthed on their AC side.

Therefore, from equations developed in this section, in case of asymmetrical operation in an HVDC system due to a contingency, the impact on the quantities of the system can be assessed based on the following:

- The magnitude of the power asymmetry. As (3.22) expresses, a contingency or fault affecting both DC poles will not produce any asymmetry. If it affects just one of them, the higher the power missing, the higher the asymmetry.
- The earthing system and topology of the HVDC station. When an asymmetry in DC-pole currents and/or voltages occurs, a zero-sequence voltage and/or current appears on the AC side of the converter. The contribution of all these quantities to the power asymmetry depends on the topology and the earthing system, as expressed by (3.23).

However, additional aspects will influence the dynamic behaviour of the entire system during asymmetrical operation. The earthing impedance of symmetrical monopolar stations transfers the perturbation from the affected grid pole to the healthy one through a DC current and/or voltage asymmetry. As a result, positive and negative pole converters will react to an asymmetrical perturbation according to (3.4), (3.5) and (3.12) in the opposite direction. Therefore, the control strategy of the HVDC grid and the stations involved are also crucial aspects during asymmetrical operation. A case study approach is used in the next section to obtain a general overview of the problems that may arise due to the asymmetrical operation of the grid under different possible circumstances. This comprehensive analysis allows for getting guidelines and recommendations to select an appropriate grounding impedance for each situation.

3.4. Study cases

The behaviour of an HVDC system during an asymmetrical operation is analysed in this chapter through EMT simulations performed in DIgSILENT PowerFactory. Several cases are examined to study the impact of the earthing impedance of symmetrical monopolar stations on the HVDC system under different circumstances. Cases 1-4 analyse the influence of the earthing resistance of symmetrical monopolar stations on the response of

an HVDC system during asymmetrical operation, considering the most usual control strategies of HVDC grids. Cases 5-6 evaluate the impact of the earthing impedance of symmetrical monopolar stations on the protection system of the HVDC grid. The purpose of this analysis is to provide guidelines for choosing a suitable earthing impedance for symmetrical monopolar stations in heterogeneous HVDC grids.

The heterogeneous three-terminal HVDC grid used in this demonstration is depicted in Figure 3.4. Two bipolar stations (Cb-A, Cb-B) and one symmetrical monopole station (Cm-C) are interconnected. All converters are considered to be MMC-VSC type. The asymmetrical operation is obtained with the outage of one of the converters of a bipolar station. The main parameters are gathered in Table 3.1. The converter controllers are extracted from [85].

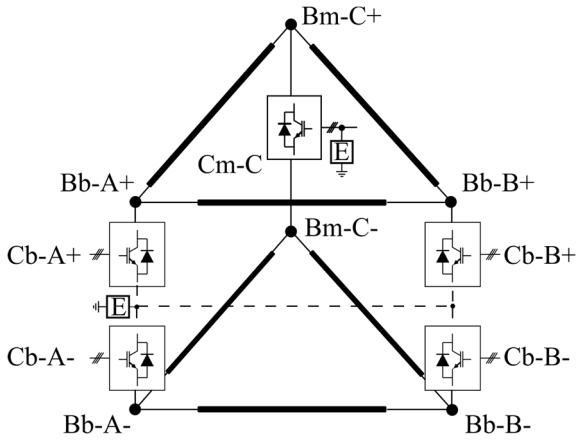

Figure 3.4. Three-terminal meshed heterogeneous HVDC system.

Table 3.1. Parameters of the system.

AC grid system voltage	220 kV RMS
Nominal frequency	50 Hz
DC grid system voltage	+/-350 kV
Rated active power of converters	800 MW
Number of SMs per arm	400
SM capacitor	10 mF
Arm inductor	28 mH
Line length	200 km
Line parameters (R, L, G, C) (for 0.001 Hz)	0.011 Ω/km, 0.9356 mH/km, 0 μS/km, 0.0123 μF/km

Regarding the grounding system, the dashed line in Figure 3.4 is used explicitly for the symmetrical monopolar station because the purpose is to obtain general conclusions without focusing on any predefined grounding topology. The three grounding systems shown in Figure 3.2 for symmetrical monopolar stations behave like a reactance in series with resistance from the zero-sequence point of view. Thus, in each case, three different values for the grounding resistance (r_e) in the AC side of the symmetrical monopolar HVDC station Cm-C are considered: a) 0 p.u., b) 0.5 p.u., c) ∞ p.u.

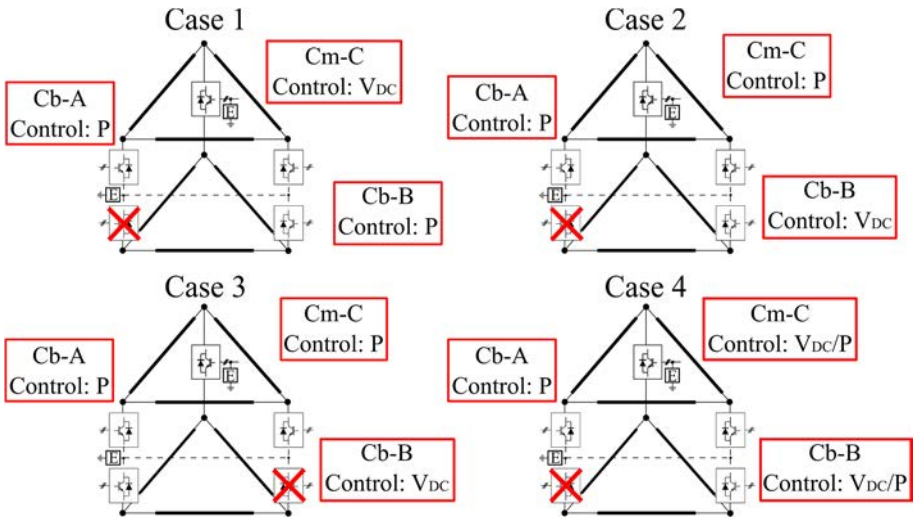

Figure 3.5. Negative pole outage in four different cases for asymmetrical operation analysis

Figure 3.5 briefly overviews the selected study cases 1-4, indicating the negative pole under outage (following a contingency) and the control mode in each HVDC station.

The dynamic behaviour of the grid in each case is analysed through the evolution of DC voltages and currents and zero-sequence quantities on the AC side of Cm-C. Moreover, the active power flow on both sides of HVDC stations is examined. Power is positive when flowing from the AC side to the DC side, according to the references in Figure 3.3.

3.4.1. Case 1. Centralised voltage control in Cm-C station. Outage of the negative pole converter of the Cb-A station.

In this first case, the monopolar converter assumes the voltage control of the DC grid. Both bipolar stations are operating in constant active power transfer mode. The loss of the negative pole at the Cb-A station is analysed. Current and voltage responses in the Cm-C converter are shown in Figure 3.6. In addition, Figure 3.7 shows the AC and DC active power flow in the three stations.

When the converter is grounded, the change in DC voltage results in the actuation of the Cm-C DC voltage controller to keep the pole-to-pole DC voltage at the setpoint value. Still, the system may become unstable in case of null grounding resistance, as the red curves show in Figure 3.6. This is due to two opposite effects: a) the Cm-C DC-pole voltages cannot change from their initial value to the new steady state since there is no zero-sequence voltage and the controller fixes the pole-to-pole DC voltage; b) the zero-sequence current injection resulting from the asymmetry tends to change the DC-pole voltages in the opposite direction, also involving the power controller of the other HVDC stations. Additionally, this instability is transferred as undamped oscillations of active power to the AC side of the Cm-C HVDC station, as seen in the three upper graphs in Figure 3.7. By contrast, if the value of the earthing resistance increases, the power oscillation damping also increases, and the system is stable after the disturbance.

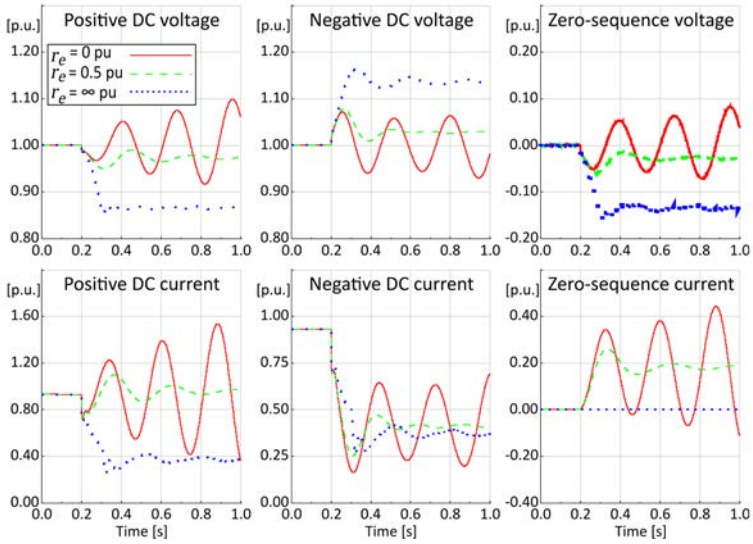

Figure 3.6. Case 1 – Cm-C currents (i_{dc}^{+}, i_{dc}^{-} and i_{ac0}) and voltages (v_{dc}^{+}, v_{dc}^{-} and u_{ac0}) under different values of the Cm-C earthing resistance.

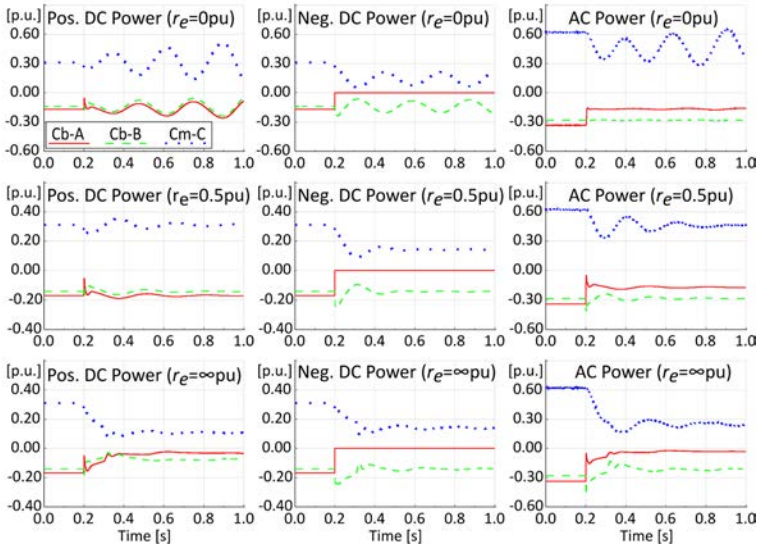

Figure 3.7. Case 1 - DC and AC active power flow in the three HVDC stations under different values of the Cm-C earthing resistance.

When the system is isolated from the ground ($r_e = \infty$), the DC voltage variation after the contingency results in a zero-sequence voltage on the AC side of the Cm-C HVDC station. This voltage leads the system to a new steady state at a higher voltage level at one pole (negative pole) and a lower voltage level at the other pole (positive pole) (Figure 3.6). The increase in the pole voltage will negatively affect the insulation level. The voltage drop of the other pole will saturate the converter and reduce its transmission capacity, resulting in an imbalance of power on the AC side (Figure 3.7). This impact can be reduced by decreasing the earthing resistance value of the Cm-C station.

3.4.2. Case 2. Centralised voltage control in Cb-B station. Outage of the negative pole converter of the Cb-A station.

In this case, the Cb-B bipolar station is responsible for the DC voltage control of the system, and the other stations work in power control mode (see Figure 3.5). Under these control conditions, the outage of the negative pole at the Cb-A station is analysed.

Figure 3.8 shows the voltage and current response of the Cm-C station, whereas the DC and AC power flows in each HVDC station are plotted in Figure 3.9. Only the negative pole in the Cb-B HVDC station changes its active power contribution after the contingency.

Looking at Figure 3.8, the system becomes unstable when the grounding resistance is zero, as in the previous case. From (3.21), it is clear that as long as the positive and negative DC voltages differ, the derivative of the zero-sequence current on the AC side is not null when the resistive part of the grounding impedance is zero. Therefore, the zero-sequence current increases continuously. In this case, the Cm-C HVDC station should be disconnected since the uncontrolled rise in the zero-sequence current results in an overcurrent in the three upper arms. Increasing the value of the earthing resistance improves the system stability.

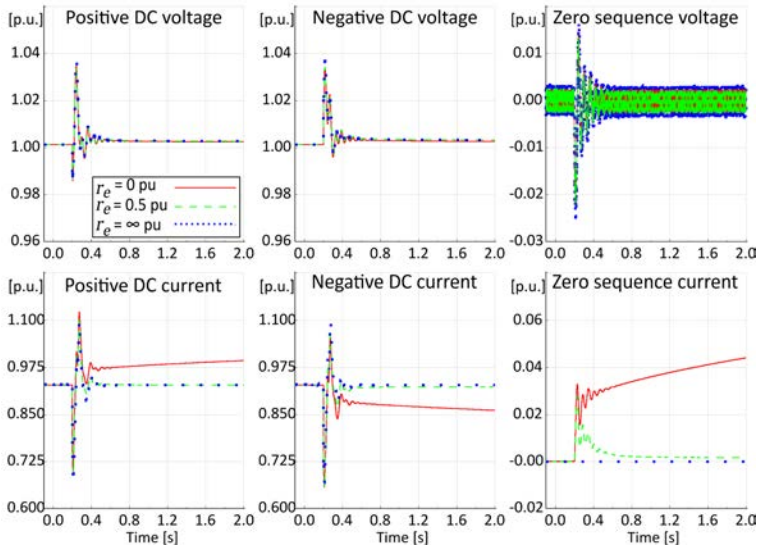

Figure 3.8. Case 2 – Cm-C currents (i_{dc}^{+}, i_{dc}^{-} and i_{ac0}) and voltages (v_{dc}^{+}, v_{dc}^{-} and u_{ac0}) under different values of the Cm-C earthing resistance.

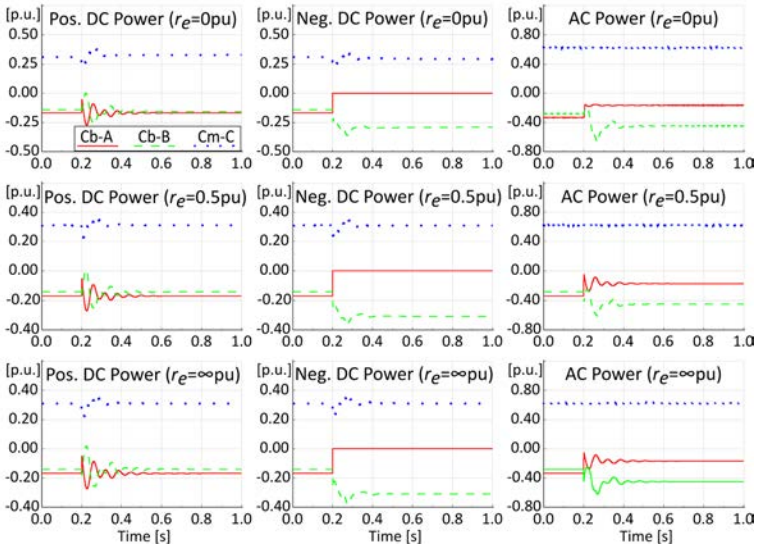

Figure 3.9. Case 2 - DC and AC active power flow in the three HVDC stations under different values of the Cm-C earthing resistance.

When the system is isolated from the ground, the pole outage causes a transient voltage at the DC poles, but the system is stable. In addition, the Cb-B DC voltage controller acts and drives voltage to its reference value in the three scenarios under analysis because each pole of the bipolar station Cb-B can control the positive and negative DC voltage independently. Nevertheless, a slight voltage asymmetry always exists in the system due to other losses in both poles of the DC grid. From Figure 3.9, it can be inferred that there is no apparent influence of the earthing resistance on the AC power injection.

3.4.3. Case 3. Centralised voltage control in Cb-B station. Outage of the negative pole converter of the Cb-B station.

The purpose of this case is to show the behaviour of the system when a pole is disconnected at the HVDC station that controls the DC voltage (Cb-B), being the remaining converters in active power control mode. It is worth mentioning that the control strategy of the grid is the same as in the previous case; what changes is the control mode of the converter suffering the outage.

Figure 3.10 displays the voltages and currents at the Cm-C HVDC station. Figure 3.11 shows the DC and AC active power flow in each station.

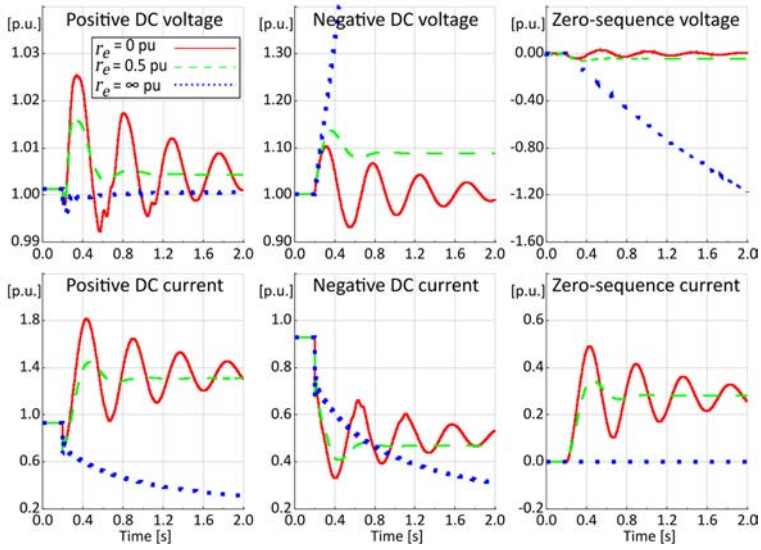

Figure 3.10. Case 3 – Cm-C currents (i_{dc}^{+}, i_{dc}^{-} and i_{ac0}) and voltages (v_{dc}^{+}, v_{dc}^{-} and u_{ac0}) under different values of the Cm-C earthing resistance.

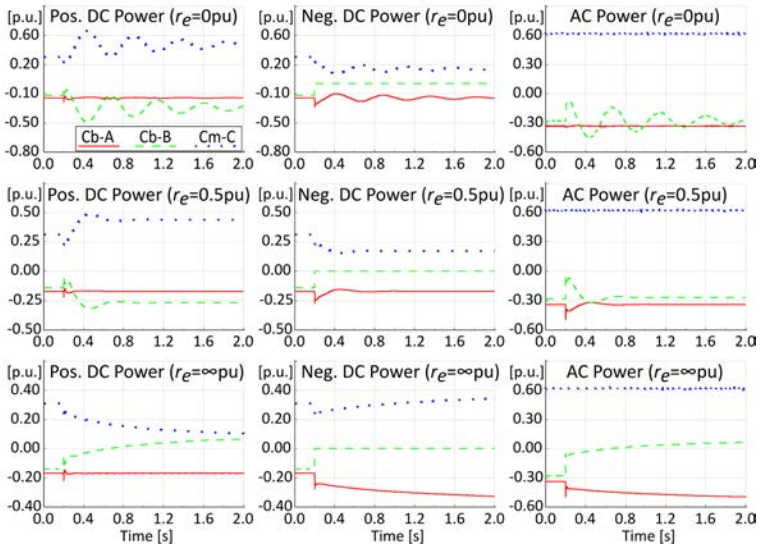

Figure 3.11. Case 3 - DC and AC active power flow in the three HVDC stations under different values of the Cm-C earthing resistance.

When the converter Cm-C is grounded, the appearance of the zero-sequence quantities due to the asymmetry transfers the disturbance to the healthy pole. It contributes to balancing the DC voltage in the affected one. Moreover, the positive Cb-B converter regulates its active power injection to keep the positive DC voltage setpoint, stabilising the negative pole. Although the system is stable, a resistive earthing value improves the damping of the oscillations on both the DC and the AC side, as observed in Figure 3.10 and Figure 3.11. However, because of the zero-sequence current, the positive DC current increases, and the negative one decreases (see Figure 3.10). Increasing the Cm-C earthing resistance will reduce the zero-sequence current and, thus, the overcurrent. However, it will produce a DC overvoltage.

Unlike the previous cases, the system becomes unstable when the Cm-C station is isolated from the ground. The DC current imbalance at the negative pole causes an increase in the

DC voltage at that pole. The positive DC voltage remains almost constant since the positive pole of the Cb-B converter controls the DC voltage. Since the control logic of the Cm-C converter tries to keep the active power constant, the DC current at both poles must progressively decrease. The negative DC voltage will continue to rise steadily until the currents at the negative pole of the grid reach a new balance. The negative DC voltage reaches about 3.40 p.u. after 2 seconds of simulation, but the scale in Figure 3.10 is adjusted to a lower value to improve the visualisation and analysis.

Notice that the network control strategies in cases 2 and 3 are identical before the contingency, but the results differ. Therefore, the control strategy of the HVDC grid and the grounding impedance of symmetrical monopolar stations are not the only aspects impacting the asymmetrical operation but also the control mode of the lost converter.

3.4.4. Case 4. Distributed voltage control in Cb-B y Cm-A stations.

The outage of a pole in an HVDC station that operates in active power control mode is simulated, with the rest of the converter stations in Vdc/P droop control mode. Two different droop gains (k_{droop}) have been considered in this case: a) 0.05 p.u. and b) 1 p.u.

Figure 3.12 and Figure 3.13 show that the system is unstable for any of the values of earthing resistance when k_{droop} is 0.05 p.u. This is due to the high level of sensitivity to voltage deviations rather than the resistance value. Therefore, the contingency makes the system unstable, affecting both DC and AC sides.

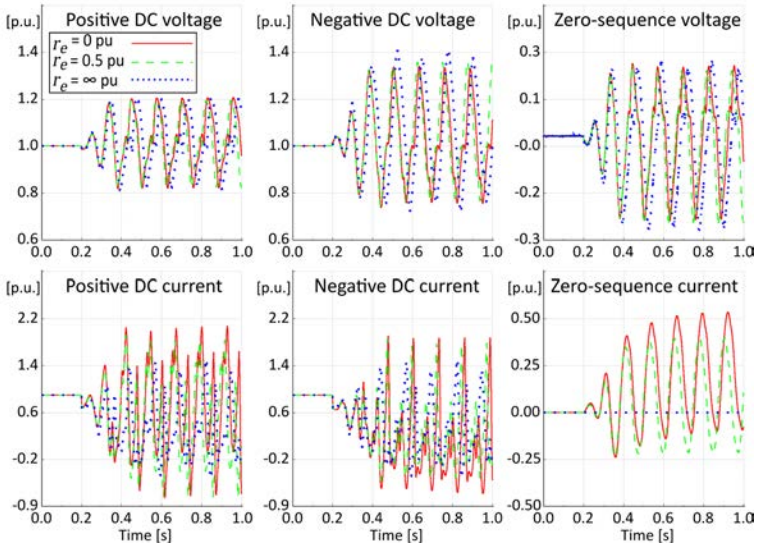

Figure 3.12. Case 4, k_{droop} = 0.05 p.u. – Cm-C currents (i_{dc}^{+}, i_{dc}^{-} and i_{ac0}) and voltages (v_{dc}^{+}, v_{dc}^{-} and u_{ac0}) under different values of the Cm-C earthing resistance.

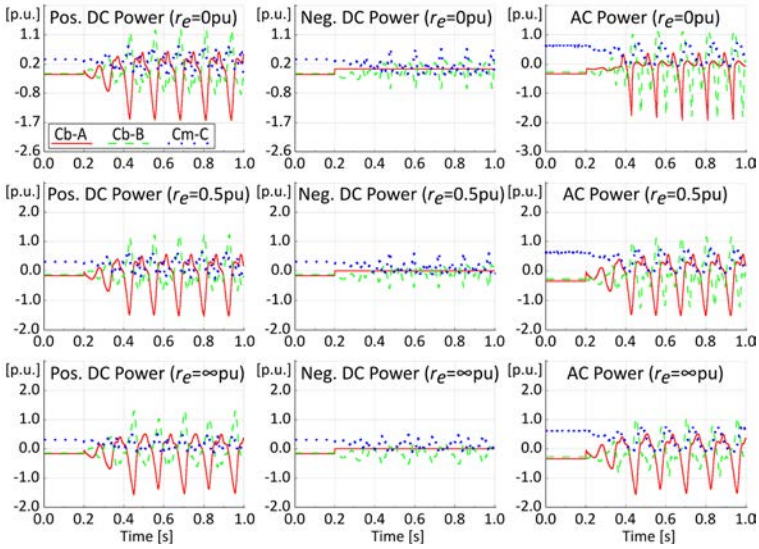

Figure 3.13. Case 4, k_{droop} = 0.05 p.u. - DC and AC active power flow in the three HVDC stations under different values of the Cm-C earthing resistance.

If k_{droop} = 1.00 p.u., the system maintains stability for all the scenarios evaluated, as shown in Figure 3.14 and Figure 3.15. The fact of using one of the grounding systems or another has a significant impact on overcurrents and voltage deviations produced in the system during the transient, as well as in the new steady state.

The voltage deviation increases with the increase in the Cm-C grounding resistance value while the overcurrent is reduced. Therefore, the most significant voltage deviation appears when the Cm-C station is not grounded, as seen in Figure 3.14. This can cause two problems depending on the sign of the variation: a high voltage level endangers all the equipment; an excessively low voltage can saturate converters and limit their transmission capacity.

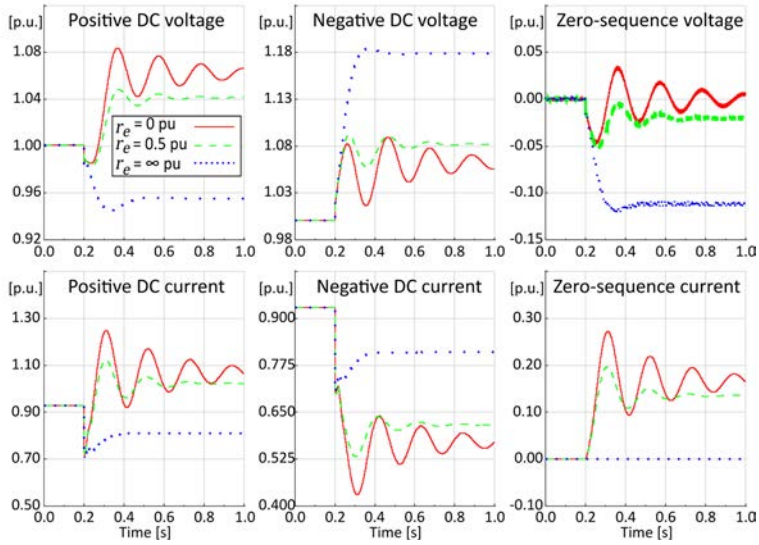

Figure 3.14. Case 4, k_{droop} = 1.00 p.u. – Cm-C currents (i_{dc}^{+}, i_{dc}^{-} and i_{ac0}) and voltages (v_{dc}^{+}, v_{dc}^{-} and u_{ac0}) under different values of the Cm-C earthing resistance.

However, Figure 3.14 shows that the highest current appears when the Cm-C station grounds through zero resistance. Therefore, all equipment is at risk of damage in this

scenario unless the protections act. Therefore, a compensation between the value of the highest current and the magnitude of the voltage deviation is necessary by selecting an adequate resistance value. As for the AC side, the earthing resistance does not affect the active power injected (see Figure 3.15) unless the converters saturate due to low DC voltage.

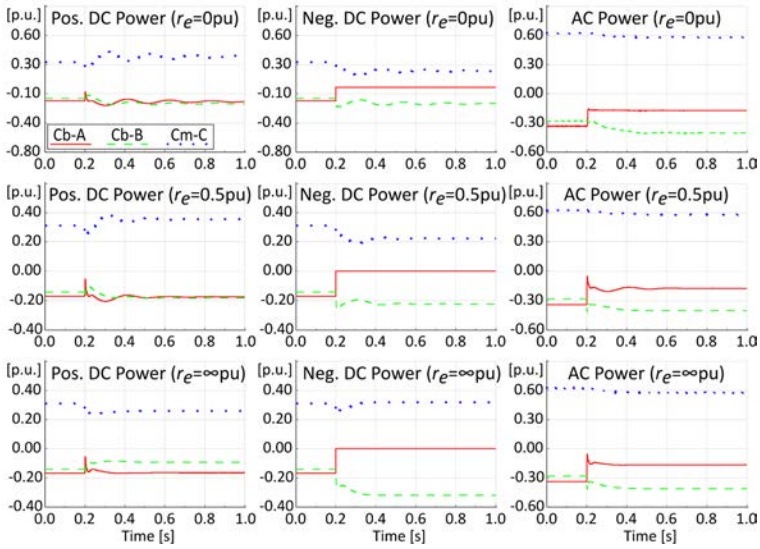

Figure 3.15. Case 4, k_{droop} = 1.00 p.u. - DC and AC active power flow in the three HVDC stations under different values of the Cm-C earthing resistance.

Table 3.2 summarises the critical situations during asymmetrical operation in each study case depending on the grounding resistance value of the symmetrical monopolar station. Although the 0.5 p.u. resistance value offers good behaviour in most cases, it is worth mentioning that a different resistance value could lead the system to overcurrent, overvoltage, a saturation of converters, power oscillation or even unstable situations.

Table 3.2. Summary of effects produced by the asymmetrical operation in the different cases.

	Grounding resistance		
Study Cases	**0 p.u.**	**0.5 p.u.**	**∞ p.u.**
Case 1	DC current instability AC power oscillations	-	DC overvoltage Converter saturation
Case 2	DC current instability DC overcurrent	-	-
Case 3	DC overcurrent AC power oscillations	DC overcurrent	DC overvoltage DC voltage instability
Case 4 (k_{droop} = 0.05)	General instability	General instability	General instability
Case 4 (k_{droop} = 1)	DC overcurrent	-	DC overvoltage Converter saturation

3.4.5. Cases 5 and 6. Effect of the short-circuit location.

Based on the analysis of cases 1-4, a suitable earthing impedance can be chosen for symmetrical monopolar stations to improve the dynamic response during asymmetrical operations. However, when a new HVDC station is connected to a DC system, the grounding impedance also affects short-circuit currents. That is why the primary purpose

of these cases is to assess the impact of the Cm-C grounding impedance on the short-circuit currents in the event of a pole-to-ground fault. It is assumed that the neutral point of the two bipolar HVDC stations is connected through a metallic return solidly earthed in the Cb-A station.

A pole-to-ground fault at the negative pole of the line connecting the Cm-C and Cb-A stations has been simulated in two different locations, as shown in Figure 3.16. In the first case, the fault is close to the Cb-A station, whereas in the second, it is close to the Cm-C station. Short-circuit currents flowing through the line to the fault are examined in both cases.

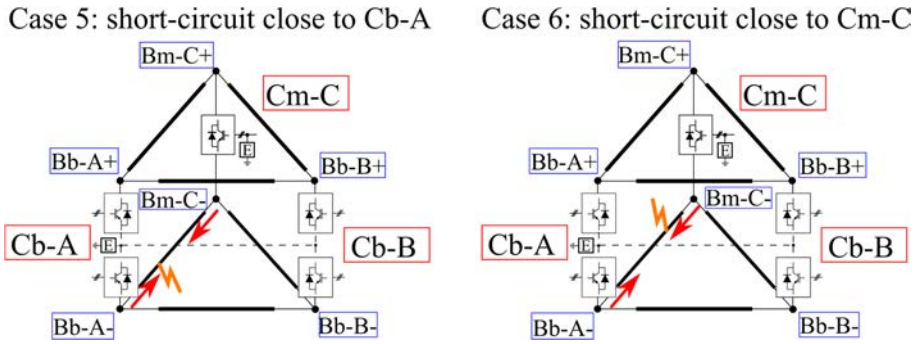

Figure 3.16. Short-circuit location in two different cases for asymmetric operation analysis.

Results are depicted in Figure 3.17 and Figure 3.18. The two upper graphs of each figure compare the currents obtained with a high reactance and three different magnitudes of resistance. The two lower graphs compare the currents with zero grounding resistance and two different inductance values. Besides, the graphs on the left show the currents flowing from terminal Bm-C towards the fault, and the right graphs show the currents flowing from terminal Bb-A.

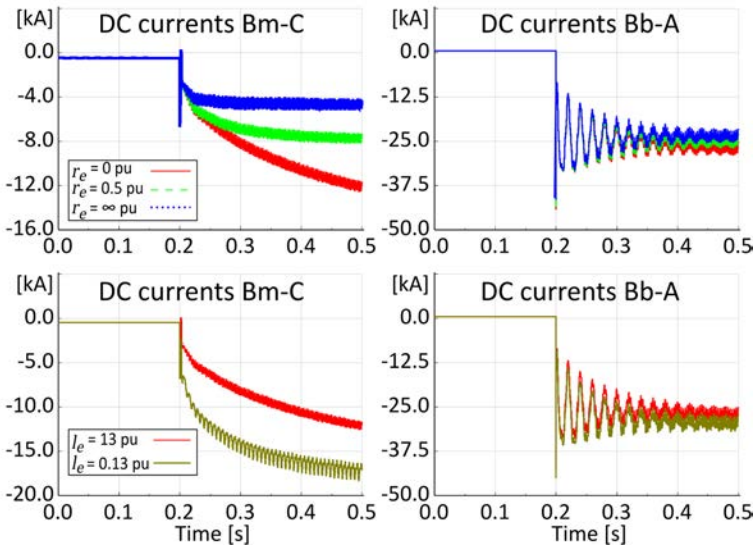

Figure 3.17. Case 5 - Short-circuit currents at both ends of the line under different Cm-C earthing systems when the fault is near the Cb-A station.

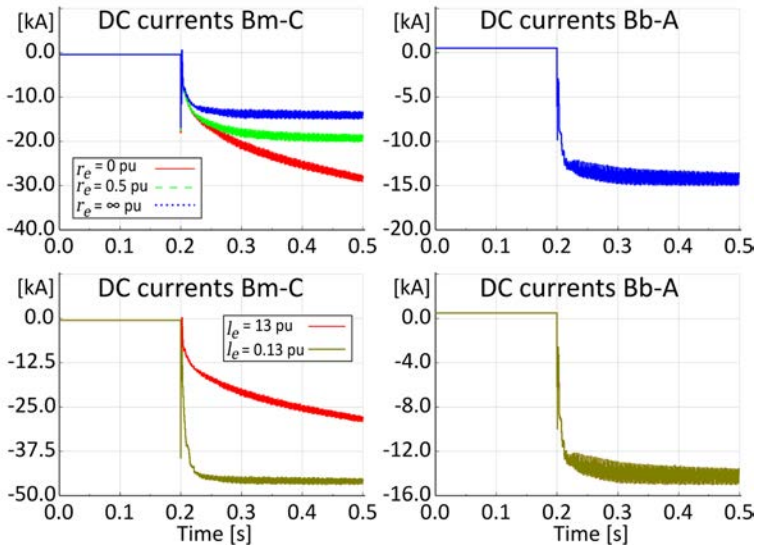

Figure 3.18. Case 6 - Short-circuit currents at both ends of the line under different Cm-C earthing systems when the fault is near the Cm-C station.

From the analysis of Figure 3.17 and Figure 3.18, it can be concluded that the grounding impedance significantly influences the short-circuit currents flowing from the Bm-C terminal (Cm-C station). The impact is less critical on short-circuit currents flowing from the Bb-A terminal (Cb-A station). However, it is still important as the short-circuit current grows gradually, achieving a difference of several kA after the first three hundred milliseconds of the fault.

Therefore, the grounding impedance of symmetrical monopolar stations barely modifies the contribution from the rest of the converter stations to the short-circuit current during the first moments after the fault. This suggests that the connection of a new symmetrical monopolar station to an HVDC system with bipolar stations will not affect the existing fast-acting protections in the system. Hence, the dimensioning of the symmetrical monopolar station grounding impedance should be selected considering two criteria: aiming for a proper operation of the grid during asymmetrical conditions and the contribution of this station to short-circuit currents.

3.5. Conclusions

In this work, as far as the authors know, the effect of the grounding impedance of symmetrical monopolar stations on heterogeneous meshed HVDC grids is analysed for the first time. One of the most significant findings is that the magnitude of the earthing resistance plays a crucial role in the asymmetrical operation of the HVDC grid. The results from this study indicate that the value of this resistance should be chosen according to the overall control strategy of the HVDC grid and the control mode of the lost converter. Otherwise, inappropriate values can lead to overcurrents, overvoltages, a saturation of converters, power oscillations or instability situations. Generally, using a grounding resistance offers a satisfactory performance in most cases, but specific analyses of the circumstances are recommended.

It is also shown that the grounding impedance of symmetrical monopolar stations barely modifies the short-circuit current contribution from the rest of the stations during the first tens of milliseconds after a pole-to-ground fault. Fast-acting protection systems will clear the short-circuit contribution from the rest of the converters before any impact can be observed. This suggests that the criteria to select the grounding impedance of symmetrical monopolar stations should focus on the performance during asymmetrical operations and their current contribution in case of pole-to-ground faults.

Additionally, this chapter highlights the complexity of defining a single methodology to be applied to all HVDC grids due to their different technology and specific grid planning development. Particular attention should be paid when designing and planning HVDC grids with heterogeneous configuration stations to guarantee viability and reliability even under asymmetrical operation. These findings provide insights for future research on the impact of the design parameters on the system dynamics, the implementation of zero-sequence controls in symmetrical monopolar stations to improve the dynamic response and the development of rules for the design of the grounding impedance under asymmetrical operation.

CHAPTER 4. SMALL-SIGNAL MODELLING[2]

This chapter provides a new small-signal stability model for analysing the asymmetrical DC operation. The model has been validated with EMT dynamic simulations considering several values for the grounding impedance and different control strategies in the system.

[2] This chapter reproduces part of the content published in J. Serrano-Sillero and M. Á. Moreno, "Small-signal stability analysis of the asymmetrical DC operation in HVDC networks," *Electr. Power Syst. Res.*, vol. 214, p. 108942, Jan. 2023.

4.1. Introduction

Chapter 3 has demonstrated that an asymmetrical DC operation can lead a heterogeneous DC system to instability. Control interactions and stability have been widely studied through dynamic EMT simulations and small-signal analysis approaches in the literature. Most of these works perform the analysis considering a homogeneous DC grid with a single HVDC station topology [88]–[90], although there are some exceptions where DC systems with MMC-VSC and LCC-based HVDC stations are examined [27], [91]–[93]. However, the stability analysis in heterogeneous DC systems still needs further research.

Furthermore, the study through time-consuming time-domain simulations is not feasible for that purpose, especially in the case of large HVDC systems. Therefore, the stability study through a small-signal analysis approach can provide further information and is a powerful tool to be applied in large DC systems.

The first step to perform such a small-signal analysis is to count with valid HVDC station models. However, small-signal models present in the literature focus on the small-signal research during symmetrical operation of the DC system [90], [94]–[96], so they do not model either explicitly both DC poles or the grounding system. Both factors are essential for analysing the asymmetrical DC operation, although.

For that reason, the primary purpose of this chapter is to develop suitable models for small-signal analysis of DC grids during asymmetrical DC operation. Thus, the main contributions of the chapter are a) the development of a small-signal stability model that is feasible for asymmetrical DC operation studies, grounding systems design and control tunning, and b) the validation of the small-signal model with electromagnetic transients (EMT) dynamic simulation in PowerFactory.

The chapter is organised as follows: section 4.2 describes the system used for the study and its small-signal model; section 4.3 presents the validation of the small-signal model with EMT dynamic simulation; and finally, the conclusions are gathered in section 4.4.

4.2. System modelling

To address the analysis of DC asymmetrical operation in an MTDC system, where symmetrical monopolar and bipolar topologies coexist without galvanic isolation between them, a simple model has been considered in PowerFactory. This model consists of a DC link connecting a bipolar station with a symmetrical monopolar one, as shown in Figure 4.1. The symmetrical monopolar HVDC station uses a zig-zag transformer as a grounding system, whereas the bipolar HVDC station is solidly earthed. For the MMC-VSCs, the Average Value Model (AVM) is adopted [85], [97]. Therefore, the valves are not explicitly modelled, and the AC side is represented through a controlled voltage source on each arm. The capacitor voltages of all submodules are assumed to be equal; thus, no circulating currents flow between the phase legs. The DC side is modelled as a current source with the equivalent capacitance of the submodules in parallel.

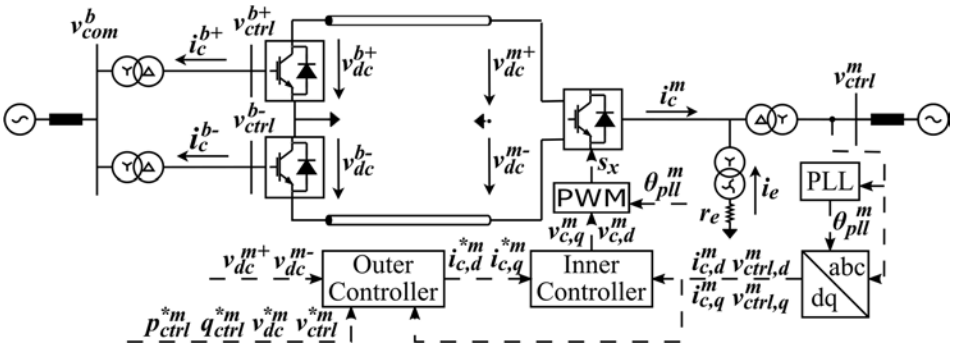

Figure 4.1. Connection of a symmetrical monopolar HVDC station with a bipolar one.

Figure 4.1 also represents the general control scheme for the symmetrical monopolar HVDC station. An analogous controller applies for each converter of the bipolar station. These controllers are based on those described in [85], and their gains are gathered in Table B.2 in Appendix B.

4.2.1. State–space representation

The system shown in Figure 4.1 can be modelled as a compound of three equivalent circuits, as depicted in Figure 4.2: the AC side of the bipolar station, in red colour; the AC side of the monopolar station, in blue paint; and the DC side, in green colour. Also, the control system for the monopolar station converter is represented in yellow. As mentioned, analogous controllers apply to the bipolar station converters. The Phase-Locked Loop (PLL) in Figure 4.1 is not considered in Figure 4.2 since the dynamics of the PLL hardly affect the DC asymmetrical operation.

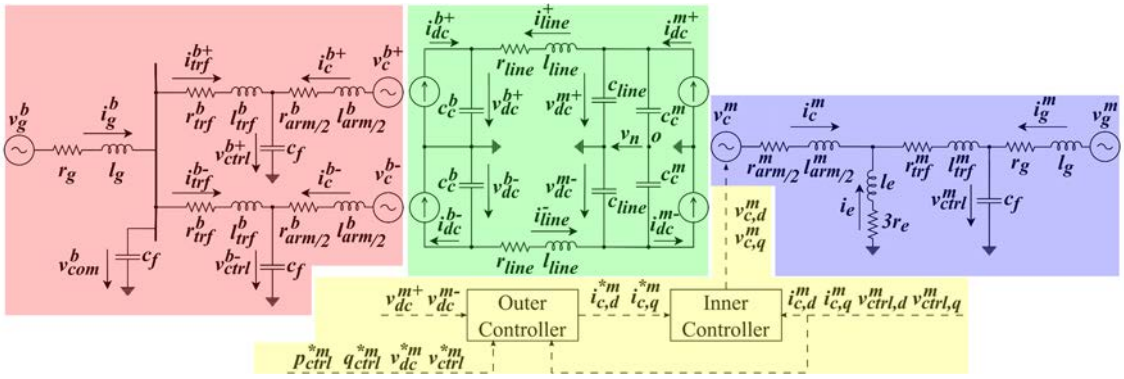

Figure 4.2. Per unit equivalent system for the AC side of the bipolar (red) and monopolar (blue) station, the DC side (green) and the control system (yellow).

The equivalent circuits in Figure 4.2 are explained below. Positive references for voltages and currents are shown.

The electrical equations are presented in a synchronous reference frame where the direct axis is aligned with the voltages v_{ctrl}^{m} and v_{ctrl}^{b+}, respectively. Considering that the bipolar station works symmetrically, the voltage v_{ctrl}^{b-} will be aligned with v_{ctrl}^{b+} and thus also with the direct axis of the synchronous reference frame.

Converters are represented as voltage sources at their AC side (v_c^m, v_c^{b+} and v_c^{b-}) in series with the equivalent impedance of a leg ($\frac{r_{arm}}{2}$ and $\frac{l_{arm}}{2}$). Each converter is connected to its respective AC grid through a transformer represented by its equivalent series impedance (r_{trf} and l_{trf}). The zig-zag transformer of the symmetrical monopolar HVDC station is modelled as an open circuit for the positive and negative sequences, but as an equivalent inductance per phase (l_e) and an equivalent resistance from the star point to ground (r_e) for the zero-sequence. The earth current circulating per each phase is represented by i_e. The external AC grids are modelled by Thévenin equivalent circuits. Furthermore, several capacitors (c_f) of small capacitance are located at some busbars of the AC systems for convenience, to make the voltage at that point a state variable.

Regarding the equivalent circuit of the DC system, the current sources at both ends represent the current injection from HVDC stations. The DC current injection from the symmetrical monopolar HVDC station is modelled as two current sources coupled by the expression $i_{dc}^{m+} - i_{dc}^{m-} = 3i_e$. Therefore, when there is no earth current, both sources can be simplified into a single current source injecting a current i_{dc}^m. The equivalent capacitor of the monopolar HVDC station (c_{eq}^m) is divided into two capacitors located between each DC pole and the middle point O ($c_c^m = 2c_{eq}^m$). For the DC line, a nominal π-model is used. At the terminals of the bipolar HVDC station, the corresponding half capacitance of the π-model of the line (c_{line}) is grouped with the equivalent capacitor of each converter of the bipolar HVDC station (c_{eq}^b), so that $c_c^b = c_{eq}^b + c_{line}$.

Finally, the coupling between the two AC areas and the DC link is the result of applying the active power balance equation to each converter:

$$v_{c,d}^m i_{c,d}^m + v_{c,q}^m i_{c,q}^m + 2v_{c,0}^m i_{c,0}^m = \frac{1}{2}(v_{dc}^{m+} i_{dc}^{m+} + v_{dc}^{m-} i_{dc}^{m-}) \tag{4.1}$$

$$v_{c,d}^{b\pm} i_{c,d}^{b\pm} + v_{c,q}^{b\pm} i_{c,q}^{b\pm} = \frac{1}{2}\left(v_{dc}^{b\pm} i_{dc}^{b\pm}\right) \tag{4.2}$$

The inner voltage dynamics of each converter are governed by its control system. As mentioned, Figure 4.2 shows the controller part considered for developing the linearised model in the monopolar station.

Besides, Figure 4.3 shows the block diagram of the outer loop (a-e) and inner loop (f) controllers. The outer controller of each converter consists of two independent control loops that generate the active current reference ($i_{c,d}^*$) and the reactive current reference ($i_{c,q}^*$). The inner controller computes the components of the converter inner voltage in the synchronous reference frame ($v_{c,d}$ and $v_{c,q}$).

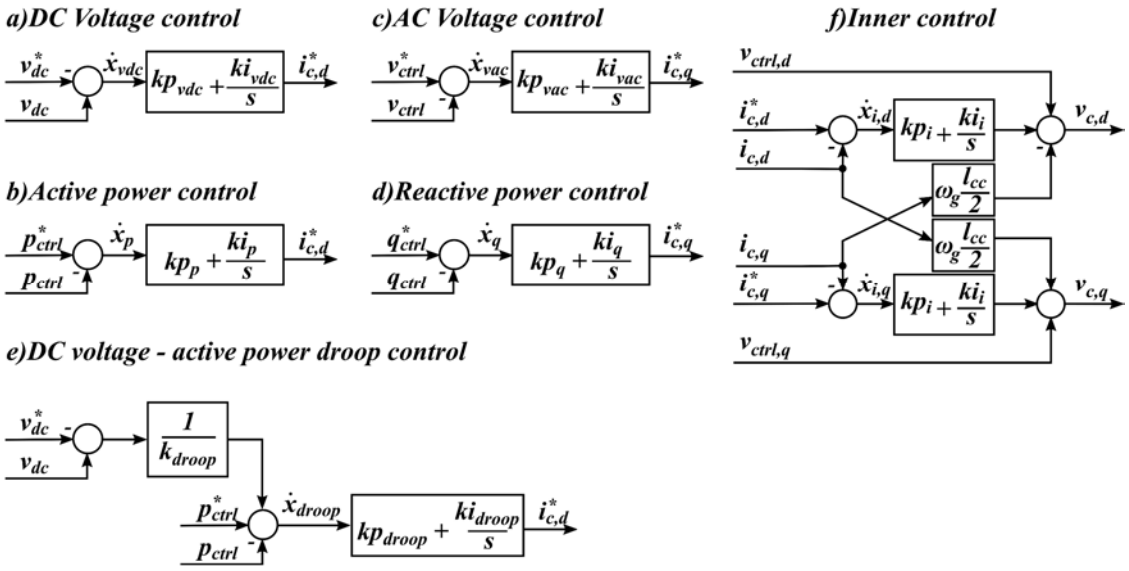

Figure 4.3. Outer Control Loops (a-e) and inner control loop (f).

The set of equations that describe the complete control of each converter, together with the electrical equations from Figure 4.2, constitute the state-space representation of the system. The values of the passive elements and the control parameters are gathered in Appendix B.

4.2.2. Small–signal modelling

The state-space model representation comprises a nonlinear system that can be linearised around an operating point to obtain a small-signal model, as in (4.3).

$$\Delta\dot{\mathbf{x}} = \mathbf{A} \cdot \Delta\mathbf{x} + \mathbf{B} \cdot \Delta\mathbf{u} \tag{4.3}$$

The state variables vector $\Delta\mathbf{x}$ consists of six sub-vectors that contain the states of the six subsystems that make up the complete system (AC side of the monopolar HVDC station, AC side of the bipolar HVDC station, DC electrical system, and control system of each converter):

$$\Delta\mathbf{x} = \left[\Delta\mathbf{x}_{\mathbf{ac}}^{\mathbf{m}}\ \Delta\mathbf{x}_{\mathbf{ac}}^{\mathbf{b}}\ \Delta\mathbf{x}_{\mathbf{dc}}\ \Delta\mathbf{x}_{\mathbf{ctrl}}^{\mathbf{m}}\ \Delta\mathbf{x}_{\mathbf{ctrl}}^{\mathbf{b+}}\ \Delta\mathbf{x}_{\mathbf{ctrl}}^{\mathbf{b-}}\right]^T \tag{4.4}$$

These state vectors are described in (4.5) - (4.10). Notice that the elements of the state vectors corresponding to the outer control can vary depending on the control strategy implemented. In this case, the change of the controllers related to the active power and DC voltage regulation is only considered for validation.

$$\Delta\mathbf{x}_{\mathbf{ac}}^{\mathbf{m}} = \left[\Delta i_{c,d}^{m}\ \Delta i_{c,q}^{m}\ \Delta i_{g,d}^{m}\ \Delta i_{g,q}^{m}\ \Delta v_{ctrl,d}^{m}\ \Delta v_{ctrl,q}^{m}\right] \tag{4.5}$$

$$\begin{aligned}\Delta\mathbf{x}_{\mathbf{ac}}^{\mathbf{b}} = [&\Delta i_{c,d}^{b+}\ \Delta i_{c,q}^{b+}\ \Delta i_{trf,d}^{b+}\ \Delta i_{trf,q}^{b+}\ \Delta v_{ctrl,d}^{b+}\ \Delta v_{ctrl,q}^{b-}\ \Delta i_{c,d}^{b-}\ \Delta i_{c,q}^{b-} \ldots \\ &\ldots \Delta i_{trf,d}^{b-}\ \Delta i_{trf,q}^{b-}\ \Delta v_{ctrl,d}^{b-}\ \Delta v_{ctrl,q}^{b-}\ \Delta i_{g,d}^{b}\ \Delta i_{g,q}^{b}\ \Delta v_{com,d}^{b}\ \Delta v_{com,q}^{b}]\end{aligned} \tag{4.6}$$

$$\Delta\mathbf{x_{dc}} = \left[\Delta v_{dc}^{m+}\ \Delta v_{dc}^{m-}\ \Delta v_{dc}^{b+}\ \Delta v_{dc}^{b-}\ \Delta i_{line}^{+}\ \Delta i_{line}^{-}\ \Delta i_e\right] \tag{4.7}$$

$$\Delta\mathbf{x_{ctrl}^{m}} = \begin{cases} \left[\Delta x_{i,d}^{m}\ \Delta x_{i,q}^{m}\ \Delta x_{vdc}^{m}\ \Delta x_{vac}^{m}\right], & \textbf{\textit{DC voltage control}} \\ \left[\Delta x_{i,d}^{m}\ \Delta x_{i,q}^{m}\ \Delta x_{p}^{m}\ \Delta x_{vac}^{m}\right], & \textbf{\textit{Active power control}} \\ \left[\Delta x_{i,d}^{m}\ \Delta x_{i,q}^{m}\ \Delta x_{droop}^{m}\ \Delta x_{vac}^{m}\right], & \textbf{\textit{DC voltage – active power control}} \end{cases} \tag{4.8}$$

$$\Delta\mathbf{x_{ctrl}^{b+}} = \begin{cases} \left[\Delta x_{i,q}^{b+}\ \Delta x_{i,q}^{b+}\ \Delta x_{vdc}^{b+}\ \Delta x_{q}^{b+}\right], & \textbf{\textit{DC voltage control}} \\ \left[\Delta x_{i,q}^{b+}\ \Delta x_{i,q}^{b+}\ \Delta x_{p}^{b+}\ \Delta x_{q}^{b+}\right], & \textbf{\textit{Active power control}} \\ \left[\Delta x_{i,q}^{b+}\ \Delta x_{i,q}^{b+}\ \Delta x_{droop}^{b+}\ \Delta x_{q}^{b+}\right], & \textbf{\textit{DC voltage – active power control}} \end{cases} \tag{4.9}$$

$$\Delta\mathbf{x_{ctrl}^{b-}} = \begin{cases} \left[\Delta x_{i,d}^{b-}\ \Delta x_{i,q}^{b-}\ \Delta x_{vdc}^{b-}\ \Delta x_{q}^{b-}\right], & \textbf{\textit{DC voltage control}} \\ \left[\Delta x_{i,d}^{b-}\ \Delta x_{i,q}^{b-}\ \Delta x_{p}^{b-}\ \Delta x_{q}^{b-}\right], & \textbf{\textit{Active power control}} \\ \left[\Delta x_{i,d}^{b-}\ \Delta x_{i,q}^{b-}\ \Delta x_{droop}^{b-}\ \Delta x_{q}^{b-}\right], & \textbf{\textit{DC voltage – active power control}} \end{cases} \tag{4.10}$$

In summary, the small-signal model of the system includes 41 state variables.

Regarding the states Δx_{vac}^{m}, Δx_{q}^{b+}, Δx_{q}^{b-}, Δx_{p}^{m}, Δx_{p}^{b+}, Δx_{p}^{b-}, Δv_{dc}^{m+}, Δv_{dc}^{m-}, Δv_{dc}^{b+} and Δv_{dc}^{b-}, the linearization is done by taking into account the equivalent circuits in Figure 4.2 and the block diagrams in Figure 4.3. The bipolar HVDC station is assumed to operate symmetrically in the initial operating point and, therefore, no zero-sequence current/voltage is considered. Subscript *o* indicates the value of a variable in the initial operating point. These considerations yield the next expressions:

$$\Delta\dot{x}_{vac}^{m} \approx -\Delta v_{ctrl,d}^{m} + \Delta v_{ctrl}^{*m} \tag{4.11}$$

$$\Delta\dot{x}_{p}^{m} \approx -v_{ctrl,do}^{m}\Delta i_{c,d}^{m} - i_{c,do}^{m}\Delta v_{ctrl,d}^{m} - i_{c,qo}^{m}\Delta v_{ctrl,q}^{m} + \Delta p_{ctrl}^{*m} \tag{4.12}$$

$$\Delta\dot{x}_{p}^{b\pm} \approx -v_{ctrl,do}^{b\pm}\Delta i_{c,d}^{b\pm} - i_{c,do}^{b\pm}\Delta v_{ctrl,d}^{b\pm} - i_{c,qo}^{b\pm}\Delta v_{ctrl,q}^{b\pm} + \Delta p_{ctrl}^{*b\pm} \tag{4.13}$$

$$\Delta\dot{x}_{q}^{b\pm} \approx -i_{c,do}^{b\pm}\Delta v_{ctrl,q}^{b\pm} + v_{ctrl,do}^{b\pm}\Delta i_{c,q}^{b\pm} + i_{c,qo}^{b\pm}\Delta v_{ctrl,d}^{b\pm} + \Delta q_{ctrl}^{*b\pm} \tag{4.14}$$

$$\begin{aligned}\Delta\dot{v}_{dc}^{m+} = \Bigg[&\Delta i_{dc}^{m+}\left(1 - \frac{c_c^m}{2(c_c^m + c_{line})}\right) - \Delta i_{line}^{+}\left(1 - \frac{c_c^m}{2(c_c^m + c_{line})}\right) \\ &- \Delta i_{dc}^{m-}\frac{c_c^m}{2(c_c^m + c_{line})} + \Delta i_{line}^{-}\frac{c_c^m}{2(c_c^m + c_{line})}\Bigg]\frac{\omega_b}{c_{line}}\end{aligned} \tag{4.15}$$

$$\begin{aligned}\Delta\dot{v}_{dc}^{m-} = \Bigg[&\Delta i_{dc}^{m-}\left(1 - \frac{c_c^m}{2(c_c^m + c_{line})}\right) - \Delta i_{line}^{-}\left(1 - \frac{c_c^m}{2(c_c^m + c_{line})}\right) \\ &- \Delta i_{dc}^{m+}\frac{c_c^m}{2(c_c^m + c_{line})} + \Delta i_{line}^{+}\frac{c_c^m}{2(c_c^m + c_{line})}\Bigg]\frac{\omega_b}{c_{line}}\end{aligned} \tag{4.16}$$

$$\Delta v_{dc}^{b\pm} = \left(\Delta i_{dc}^{b\pm} + \Delta i_{line}^{\pm}\right)\frac{\omega_b}{c_c^b} \tag{4.17}$$

where the linear expressions that describe the DC currents Δi_{dc}^{m+} and Δi_{dc}^{m-} are presented in (4.18) and the linear expression for Δi_{dc}^{b+} and Δi_{dc}^{b-} is obtained in (4.19).

$$\begin{aligned}\Delta i_{dc}^{m\pm} \approx 2\frac{\left(v_{c,do}^{m} i_{c,do}^{m} + v_{c,qo}^{m} i_{c,qo}^{m}\right)}{\left(v_{dc,o}^{m+} + v_{dc,o}^{m-}\right)^2}\left(\Delta v_{dc}^{m+} + \Delta v_{dc}^{m-}\right) \\ - 2\frac{v_{c,do}^{m}\Delta i_{c,d}^{m} + i_{c,do}^{m}\Delta v_{c,d}^{m} + v_{c,qo}^{m}\Delta i_{c,q}^{m} + i_{c,qo}^{m}\Delta v_{c,q}^{m}}{\left(v_{dc,o}^{m+} + v_{dc,o}^{m-}\right)} \pm \frac{3}{2}\Delta i_e\end{aligned} \tag{4.18}$$

$$\begin{aligned}\Delta i_{dc}^{b\pm} \approx 2\frac{\left(v_{c,do}^{b\pm} i_{c,do}^{b\pm} + v_{c,qo}^{b\pm} i_{c,qo}^{b\pm}\right)}{\left(v_{dc,o}^{b\pm}\right)^2}\Delta v_{dc}^{b\pm} \\ - 2\frac{v_{c,do}^{b\pm}\Delta i_{c,d}^{b\pm} + i_{c,do}^{b\pm}\Delta v_{c,d}^{b\pm} + v_{c,qo}^{b\pm}\Delta i_{c,q}^{b\pm} + i_{c,qo}^{b\pm}\Delta v_{c,q}^{b\pm}}{v_{dc,o}^{b\pm}}\end{aligned} \tag{4.19}$$

The expressions defining the remaining states of the vector **Δx** are first-order linear equations drawn directly from Figure 4.2 and Figure 4.3 and can be consulted in Appendix B.

4.3. Validation of the small–signal model

Once the equations and assumptions that define the proposed small-signal model have been introduced, this section gathers a validation of the model against EMT dynamic simulations in PowerFactory.

An asymmetrical perturbation is simulated by applying a slight step in the setpoint of one of the converters in the bipolar HVDC station. The response of both models is then compared.

Figure 4.4 shows the power flow results for the initial operating point considered. Red values represent the active power flow in MW, and blue values the reactive power flow in Mvar. The black arrows indicate the positive direction of the power flow. Finally, the voltage magnitude, in p.u., and phase angle, in degrees, are represented inside a box.

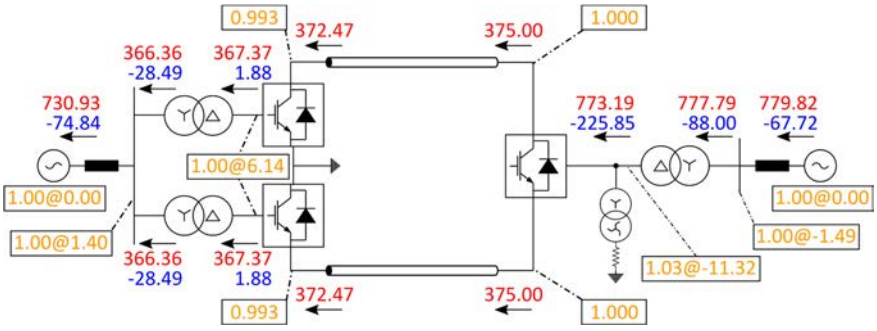

Figure 4.4. Initial conditions of the system for the base case.

The operating point shown in Figure 4.4 represents a high active power transfer from the monopolar to the bipolar HVDC station. This scenario is convenient for the analysis because, as explained later in Chapter 5, it is under these circumstances that stability is

most compromised from the perspective of the asymmetrical DC operation. However, other operating conditions will also be discussed in Chapter 5.

The validation encompasses different control strategies and different grounding impedance values. In addition, the effect of the controller parameters is also assessed.

4.3.1. Centralised voltage control in the symmetrical monopolar station

This section gathers the validation of the small-signal model of the system when the symmetrical monopolar station controls the DC voltage, and the bipolar station controls the active power flow. Furthermore, the symmetrical monopolar stations control the AC voltage, whereas the bipolar one controls the reactive power flow.

In this case, the asymmetrical disturbance used for the validation consists of a small step (0.01 p.u.) in the active power reference of the negative pole converter of the bipolar station.

Figure 4.5 and Figure 4.6 show the comparison of the time-domain responses for several grounding resistance values. The consistency in the time-domain responses of both models allows us to validate the new small-signal model.

Different dynamic behaviours can be identified: an unstable and oscillatory for a zero-resistance value, an underdamped response for 0.05 p.u. resistance value, an overdamped response for 0.25 p.u. resistance value and an unstable non-oscillatory response for 0.6 p.u. resistance value (this response is shown partially to represent the curves on a proper scale). Note that positive and negative DC quantities present an opposite response to one another.

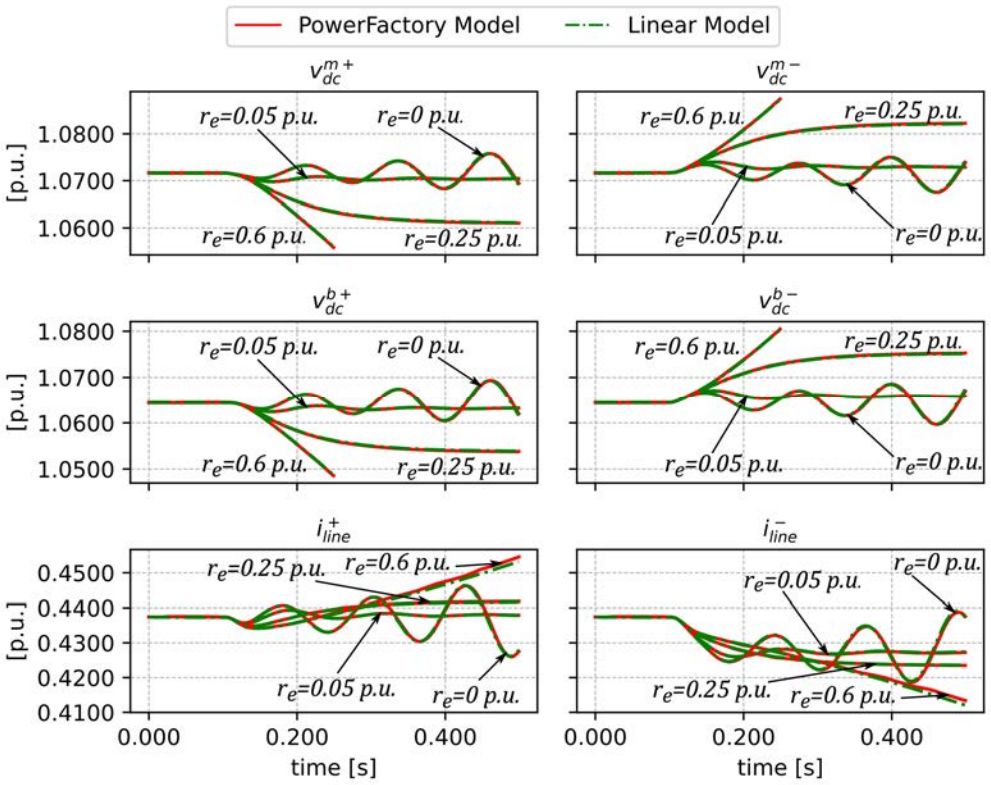

Figure 4.5. DC quantities response to a DC asymmetry for several grounding resistances.

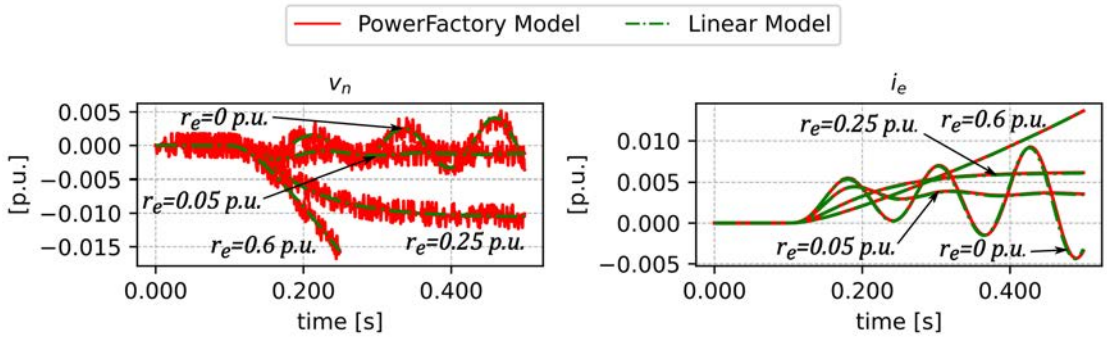

Figure 4.6. Zero-sequence voltage and earth current response to a DC asymmetry for several grounding resistances.

4.3.2. Centralised voltage control in the bipolar HVDC station

This section deals with validating the small-signal model of the system when the symmetrical monopolar station controls the active power and the bipolar station controls the DC voltage. In addition, as in the previous case, the symmetrical monopolar stations control the AC voltage, while the bipolar station controls the reactive power flow.

The asymmetrical disturbance provoked in this case consists of a small step (-0.0005 p.u.) in the DC voltage reference of the negative pole converter of the bipolar station. The comparison comprises different values of grounding resistance (r_e) and proportional gain of the DC voltage controller (kp_{vdc}). The inductance of the grounding system remains constant at 1.63 p.u. (1.59 H). The initial conditions of the simulation are those represented in Figure 4.4.

Figure 4.7 and Figure 4.8 show the time-domain responses of the PowerFactory model and the small-signal model for zero grounding resistance and two different values of kp_{vdc} (0.1 and 8 p.u.). As can be observed, the system is stable for $kp_{vdc} = 8$, but not for $kp_{vdc} = 0.1$.

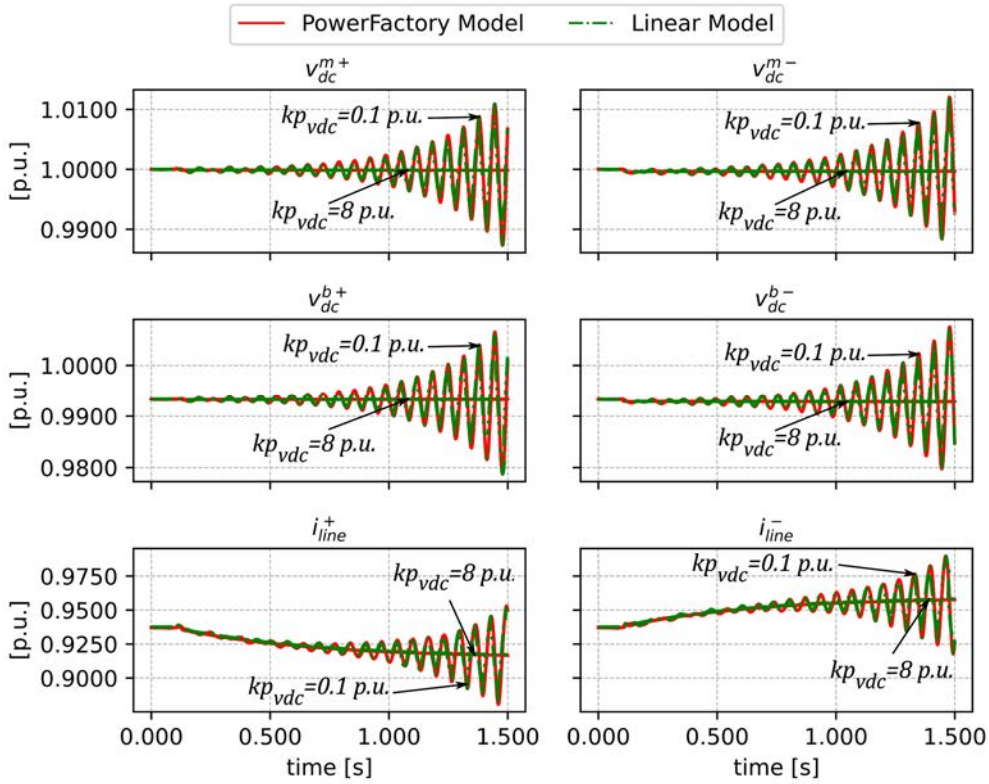

Figure 4.7. DC voltages and currents response to a DC power asymmetry for two values of kp_{vdc} with r_e = 0 p.u.

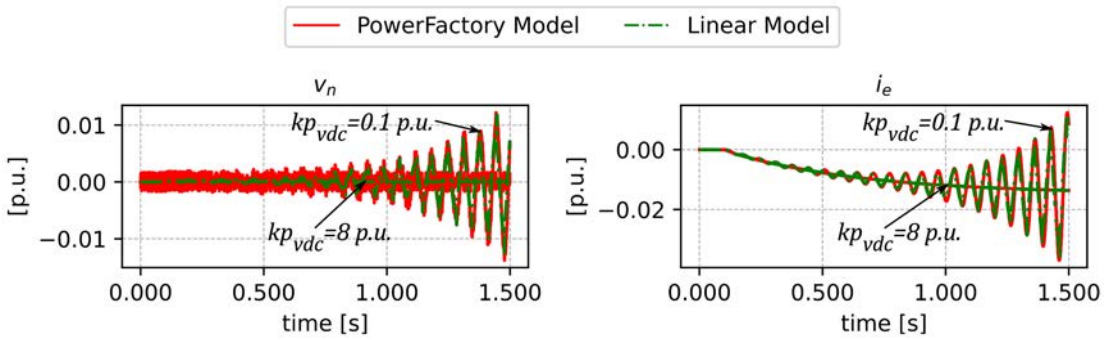

Figure 4.8. Zero-sequence voltage and earth current response to a DC power asymmetry for two values of kp_{vdc} with r_e = 0 p.u.

To compare the effect of the grounding resistance, the same simulation is performed considering a 0.6 p.u. resistance. Results in Figure 4.9 and Figure 4.10 show that the response presents a faster transient, and the system is no longer unstable. However, there is still a poorly damped irregular oscillation for $kp_{vdc} = 0.1$, which indicates several poorly damped oscillatory modes that do not depend on the grounding resistance.

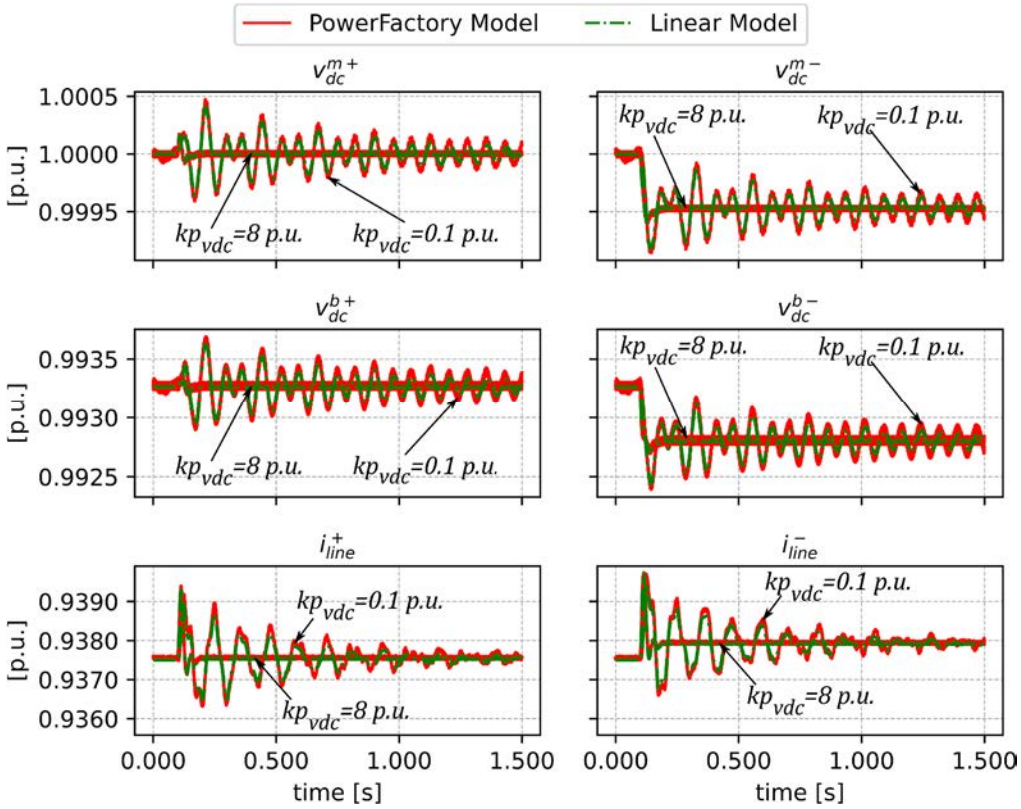

Figure 4.9. DC voltages and currents response to a DC power asymmetry for two values of kp_{vdc} with r_e = 0.6 p.u.

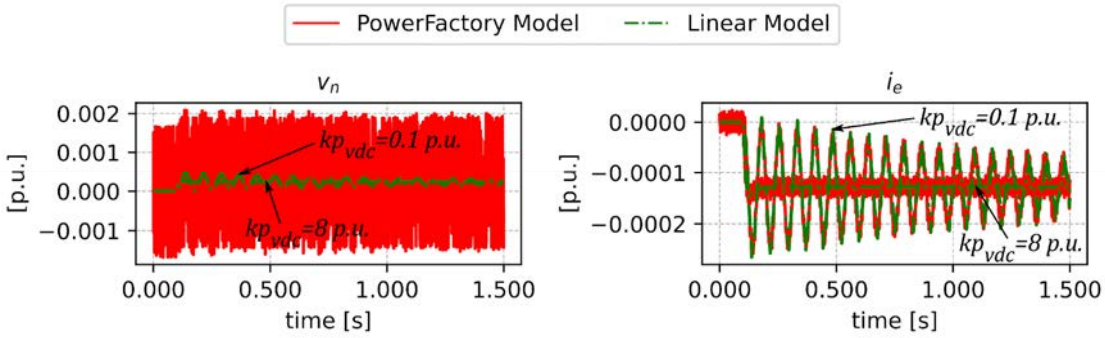

Figure 4.10. Zero-sequence voltage and earth current response to a DC power asymmetry for two values of kp_{vdc} with r_e = 0.6 p.u.

Note that in all cases, the positive and negative DC variables present an opposite response to each other.

The figures above prove that the small-signal model faithfully reflects the dynamic behaviour of the EMT simulation in PowerFactory.

4.3.3. Distributed DC voltage – active power droop control

This section aims to validate the linear model of the system implementing the distributed DC voltage droop control with the EMT model in PowerFactory. As in the previous cases, the symmetrical monopolar stations control the AC voltage, while the bipolar station controls the reactive power flow.

The asymmetrical disturbance for the comparison consists of a small step (-0.01 p.u.) in the active power reference of the negative pole converter of the bipolar station. Different values of grounding resistance (r_e) and DC voltage droop coefficients (k_{droop}) have been considered. The inductance of the grounding system remains constant at 1.63 p.u. (1.59 H). The initial conditions of the simulation are those represented in Figure 4.4.

Figure 4.11 and Figure 4.12 show the time-domain responses of the PowerFactory model and the small-signal model for zero grounding resistance and two different values of droop coefficient k_{droop} (0.1 and 1 p.u.). The droop coefficient is configured to the same value in both stations. As can be observed, the system is stable for $k_{droop} = 0.1$, but not for $k_{droop} = 1$.

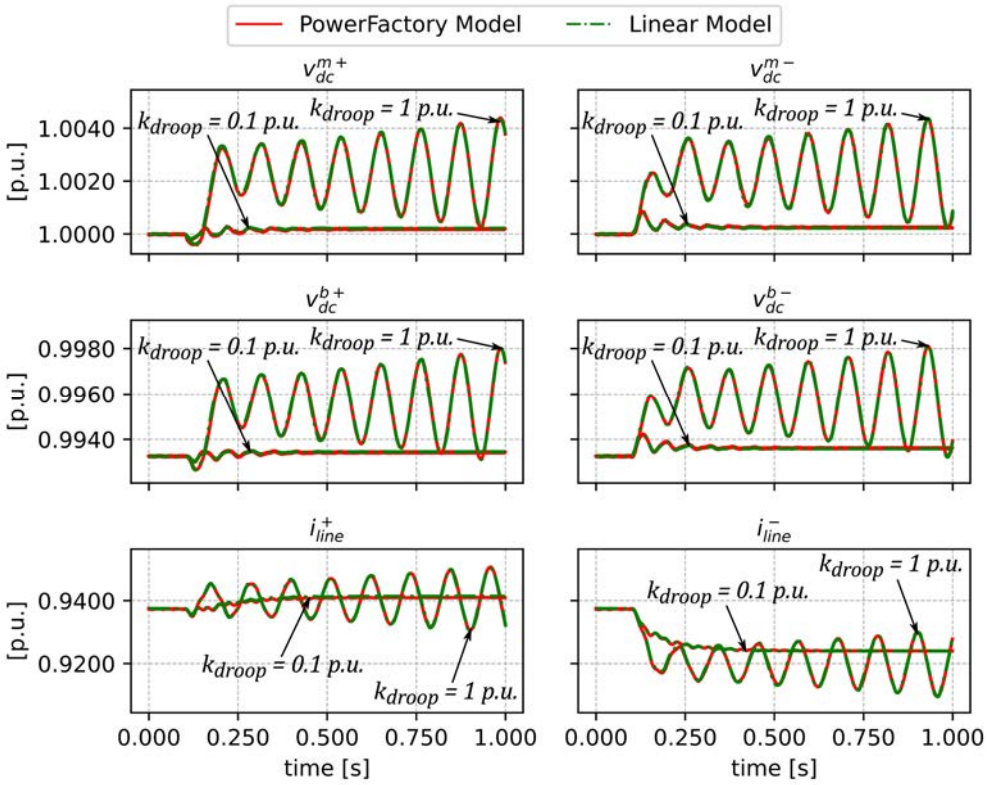

Figure 4.11. DC voltages and currents response to a DC power asymmetry for two values of k_{droop} with r_e = 0 p.u.

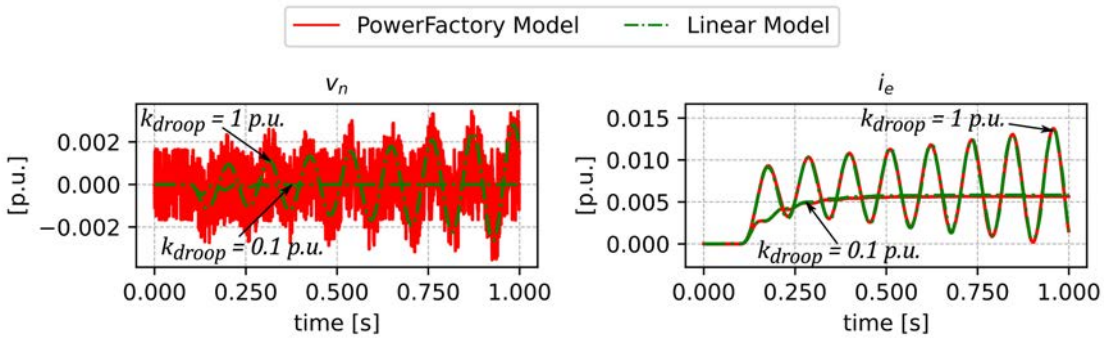

Figure 4.12. Zero-sequence voltage and earth current response to a DC power asymmetry for two values of k_{droop} with r_e = 0 p.u.

To compare the effect of the grounding resistance, the same simulation is performed by considering a resistance of 0.6 p.u. Results in Figure 4.13 and Figure 4.14 show that the response presents a faster transient for $r_e = 0.6$ compared to the previous case. In addition, the system is no longer unstable.

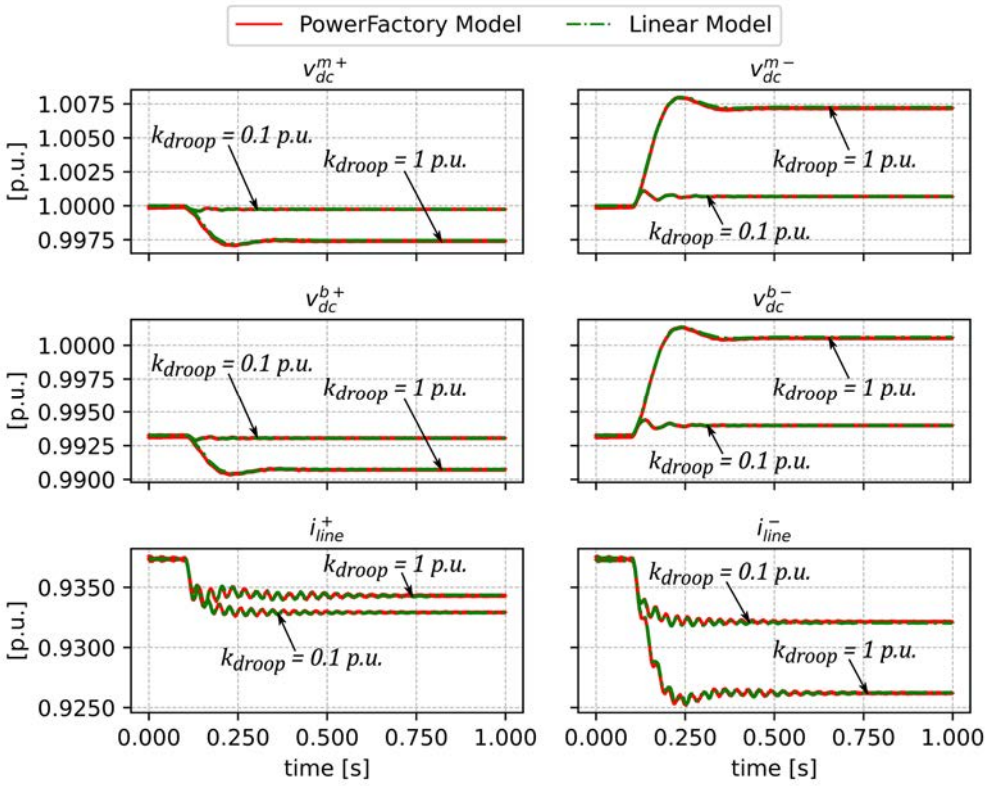

Figure 4.13. DC voltages and currents response to a DC power asymmetry for two values of k_{droop} with r_e = 0.6 p.u.

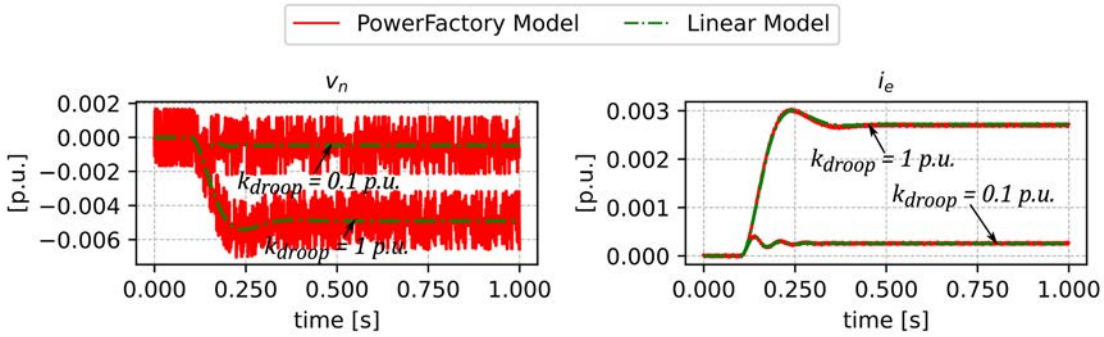

Figure 4.14. Zero-sequence voltage and earth current response to a DC power asymmetry for two values of k_{droop} with r_e = 0.6 p.u.

Note that positive and negative DC quantities present an opposite response to one another. Furthermore, the steady-state reached after the disturbance and the degree of DC voltage and DC current asymmetry depend on the droop coefficient. More importantly, the figures above prove that the small-signal model faithfully reflects the dynamic behaviour of the EMT simulation in PowerFactory.

4.4. Conclusions

This chapter has presented a new small-signal stability model for analysing the asymmetrical DC operation in HVDC systems with different HVDC station topologies and without galvanic isolation between them. In addition, the small-signal model includes the grounding system and equations for each pole separately; these considerations differentiate it from existing models and constitute a novelty. Finally, the new model has been validated against EMT simulations considering different control strategies.

The advantages of this model are: 1) it allows the identification of stability issues related to the asymmetrical DC operation that cannot be detected with other small-signal models, and 2) it can be applied to larger HVDC systems. Although time-domain simulations can represent this type of instability, they are inefficient for performing stability studies on large systems. Besides, they do not provide an easy method to recognise the main parameters and variables involved in a specific oscillation of the system.

CHAPTER 5. SMALL-SIGNAL STABILITY ANALYSIS[3]

The small-signal stability during asymmetrical operation considering different topologies, grounding impedances, or control strategies is yet to be addressed in the literature. For that reason, this chapter further investigates the role of the grounding impedance, controllers, and operating point in the small-signal stability of the system. Additionally, a new controller to enhance the system stability is proposed.

[3] This chapter reproduces part of the content published in J. Serrano-Sillero and M. Á. Moreno, "Small-signal stability analysis of the asymmetrical DC operation in HVDC networks," *Electr. Power Syst. Res.*, vol. 214, p. 108942, Jan. 2023.

5.1. Introduction

This chapter analyses how the asymmetrical DC operation affects the stability of a heterogeneous DC system. Accordingly, the new small-signal model described in Chapter 4 is utilised in this chapter to carry out the study. Most research papers assess stability from a symmetrical DC operation perspective. For example, the control interactions and their design were analysed in [90], [98]; the effect of a new connection of an HVDC station on DC voltage stability was studied in [94]; references [95], [99] examined the influence of the DC power flow direction on stability; power and DC voltage oscillations were investigated in [100], [101]. Even the stability of systems with LCCs and VSCs has been evaluated [91], [101]. Nonetheless, all the mentioned works neglected relevant aspects to analyse asymmetrical DC operation, such as representing the quantities of the positive and negative poles separately or including the grounding system in the analysis.

Furthermore, the small-signal analysis allows the identification of which system parameters are involved in the dynamics related to the asymmetrical DC operation and to define its appropriate values, both for controllers and equipment.

The main contributions of this chapter are summarised as follows: a) the analysis of the main aspects to be considered for the system operation considering different control strategies; b) the effect that the design of the grounding impedance has on the stability of the system in different conditions; c) the main parameters of the system control that intervene in the small-signal stability during asymmetrical operation are identified, and their effect is examined; and d) the design of a controller that enhances system stability during asymmetrical DC operation when existing controllers cannot improve stability is proposed.

The chapter is organised as follows: section 5.2 explains the main results derived from the small-signal analysis when the symmetrical monopolar station implements a centralised DC voltage control and introduces a new controller to enhance the system stability; section 5.3 focuses on the small-signal analysis of the system considering that the bipolar station implements a centralised DC voltage; section 5.4 carries out the small-signal research evaluating a distributed DC voltage control as control strategy of the system; and finally, the conclusions are gathered in section 5.5.

5.2. Small–signal stability analysis with centralised DC voltage control in the symmetrical monopolar station

This section analyses the small signal analysis of the system in Figure 4.1 when the symmetrical monopolar station controls the DC voltage and the AC voltage, whereas the bipolar station controls the active and the reactive power flow.

The small-signal stability of the system is assessed from different perspectives that cover the following aspects: a) influence of the grounding impedance, b) influence of the DC current, and c) sensitivity to the system parameters.

5.2.1. Influence of the grounding system resistance

The grounding resistance plays a key role in the asymmetrical DC operation since it determines the behaviour of the earth current (i_e) and the zero-sequence voltage (v_n).

The impact of its value on the small-signal stability is analysed through the root locus of the system in Figure 5.1 under the initial conditions described in Figure 4.4.

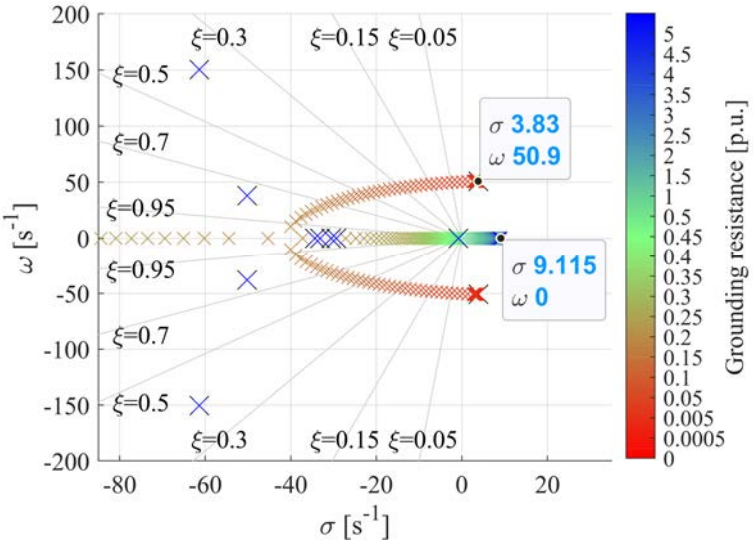

Figure 5.1. Root locus of the system for a grounding resistance sweep.

Figure 5.1 shows that a single mode is affected by the grounding resistance near the imaginary axis. This mode is critically damped for a resistance value of 0.19 p.u. and can be underdamped or even non-stable and oscillatory for lower resistance values, as well as overdamped or non-stable aperiodic for larger values.

The normalised participation of the states in the mode as a function of the resistance is depicted in Figure 5.2. Again, only states with participation greater than 0.01 are shown.

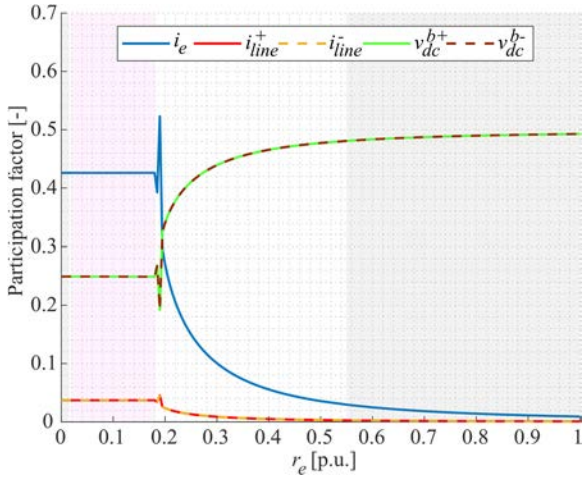

Figure 5.2. Participation factor for a range of grounding resistance. The grey, red and white areas represent unstable, underdamped, and overdamped modes.

As shown in Figure 5.2, the main variables participating in the mode are the earth current, the DC current, and the DC voltages at the bipolar station terminals. Around the resistance

value matching the critically damped mode, the participation factors change significantly due to the division of the mode into two aperiodic ones [102], representing an interaction between the earth current and the DC currents with the DC voltages.

The dynamic pattern of the mode can be observed in the DC voltages, DC currents, and earth current, according to Figure 5.3, so it does not spread to the rest of the AC system. Notice that in the overdamped region, as the resistance rises, the observability is hindered for the currents while it is enhanced for the voltages.

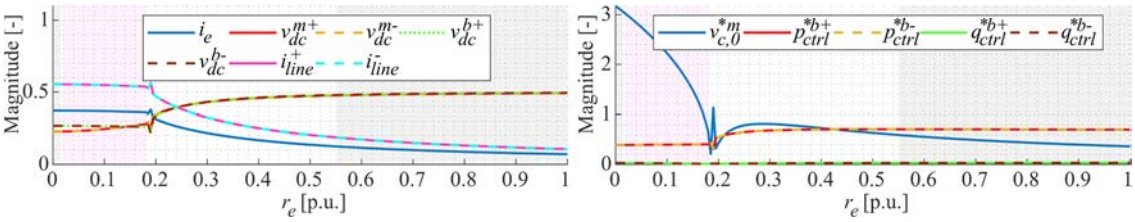

Figure 5.3. Mode observability (left) and controllability (right) as a function of grounding resistance. The grey, red and white areas represent unstable, underdamped, and overdamped modes.

According to Figure 5.3, the mode can be controlled by the zero-sequence reference voltage of the monopolar HVDC station and the active power references of the bipolar HVDC station. In particular, the zero-sequence voltage shows high controllability for low grounding resistances where the mode is oscillatory.

It is worth noting that the present controllers do not influence this specific mode since their states do not participate in it, nor is the mode observable in the controller measurements as feedback.

5.2.2. Influence of the grounding system inductance

The grounding inductance is also decisive for the asymmetrical DC operation since it impacts the transient response of the system. From the small-signal stability perspective, its influence on the eigenvalues is proved in Figure 5.4 for a constant grounding resistance (30.625 Ω - 0.1 p.u.). The initial conditions are those shown in Figure 4.4.

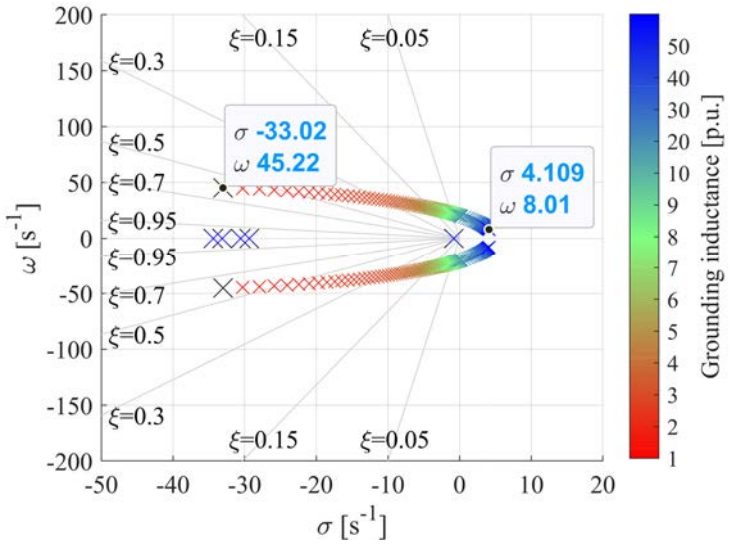

Figure 5.4. Root locus of the system for a grounding inductance sweep.

There is a single mode affected by the grounding inductance. The damping and the frequency of the mode decrease as inductance increases, leading to system instability if the grounding inductance reaches large enough values (around 9 p.u. – 3067 H), typical of a star point reactor used as a grounding method.

Figure 5.5 indicates that this mode is the same as in the case of the grounding resistance since the same states participate in the mode. Observe that the grounding inductance does not affect the participation of DC voltages. However, its increment raises the participation of earth current and reduces the participation of DC currents.

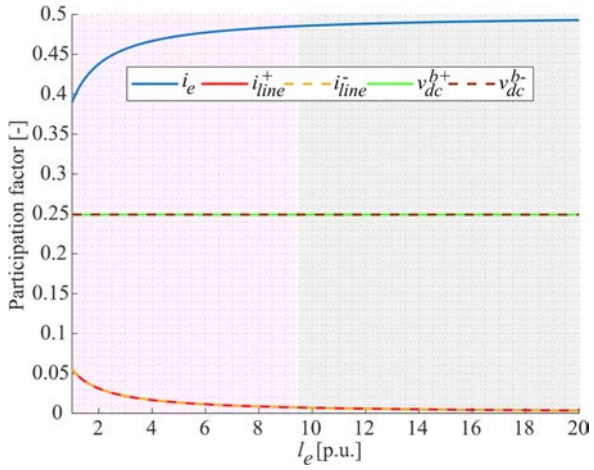

Figure 5.5. Participation factors for a grounding inductance range. The grey and red areas represent unstable and overdamped modes, respectively.

The observability of the mode against the inductance value of the grounding system is presented in Figure 5.6 (left). The mode is observable in DC voltages and currents and earth current. Still, as inductance rises, the observability increases in DC voltages and decreases in earth current and DC currents. Regarding the AC system, as the mode is only observable in the zero-sequence variables for any value of grounding impedance, it does

not spread beyond the delta-winding of the transformer. Thus, it does not affect the stability of the remaining AC system.

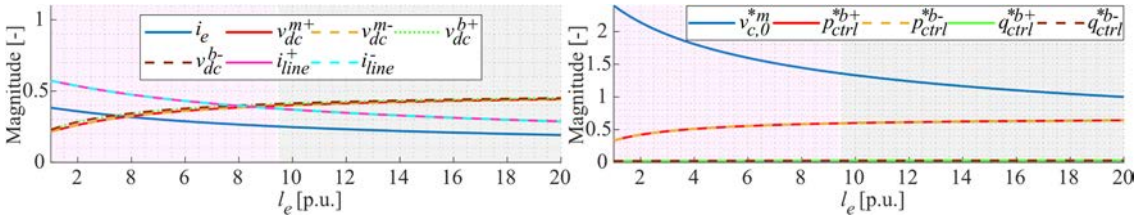

Figure 5.6. Mode observability (left) and controllability (right) as a function of the grounding system inductance. The grey and red areas represent unstable and underdamped modes, respectively.

Figure 5.6 (right) indicates that the main inputs that can control the mode continue to be the zero-sequence voltage reference of the monopolar station ($v_{c,0}^{*m}$) and the active power references of the bipolar station (p_{ctrl}^{*b+} and p_{ctrl}^{*b-}), regardless of the inductance.

5.2.3. Influence of the initial DC current before disturbance

This section delves into the impact of the DC current on the small-signal stability, specifically in the mode related to DC asymmetrical operation. For this analysis, the grounding resistance and inductance are 0 p.u. and 1.63 p.u., respectively.

To perform the DC current sweep, the active power references of the bipolar HVDC station are changed from those of the load flow shown in Figure 4.4 so that the complete DC current range is evaluated. The movement of the eigenvalues against the initial DC current is displayed in Figure 5.7.

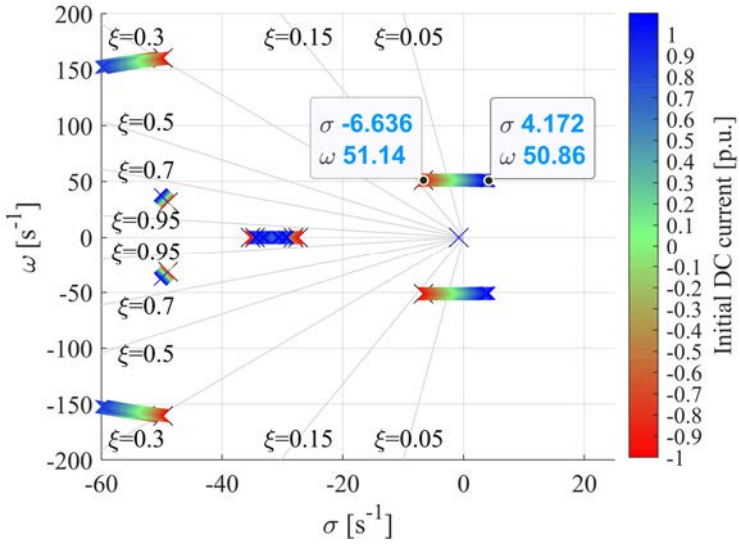

Figure 5.7. Root locus of the system as a function of the initial DC current.

Figure 5.7 shows that several modes are affected by DC current, but the least damped and potentially unstable is the one related to DC asymmetrical operation. Indeed, it is worth noting that DC current directly affects the damping of this mode whilst hardly modifying its frequency. Furthermore, the mode is stable for a negative DC current direction, even

considering a zero grounding resistance value. Thus, this fact confirms that the direction of the DC current determines system stability.

For the sake of simplicity, the participation factors, observability, and mode controllability are not shown since they remain unchanged for any value of the DC current, maintaining the values shown in Figure 5.2 and Figure 5.3 for a zero-grounding resistance.

5.2.4. Influence of other system parameters

Figure 5.8 shows the sensitivity of the mode related to the asymmetrical DC operation, where the sensitivity of the mode λ to the element a_{kj} of the state matrix A is defined as follows:

$$s = \frac{d\lambda}{da_{kj}} = \frac{d\sigma}{da_{kj}} + j\frac{d\omega}{da_{kj}} \tag{5.1}$$

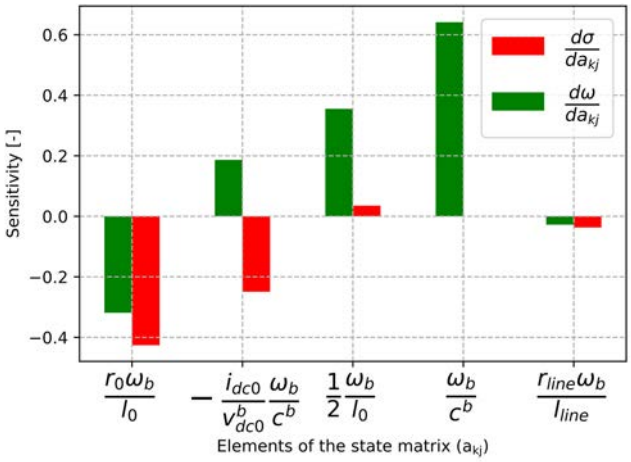

Figure 5.8. Sensitivity of the real and imaginary parts of the mode.

Observe that the main parameters affecting the mode are the zero-sequence impedance ratio, the DC voltage and DC current, the line impedance ratio, and the equivalent capacitance of the bipolar HVDC station.

The zero-sequence resistance $\left(r_0 = \frac{1}{2}r^m_{arm} + 3r_e\right)$ to inductance $\left(l_0 = \frac{1}{2}l^m_{arm} + l_e\right)$ ratio represents the highest impact on the real part of the mode and an important weight in its frequency. Both the real and imaginary parts of the mode diminish as this ratio rises. The resistance to inductance ratio of the DC line has the same trend but its weight is much smaller.

The parameter composed of the initial DC current and DC voltage of the bipolar station, together with its equivalent capacitance (c^b), also modifies the real and imaginary parts of the mode. Observe that this element represents an equivalent conductance to capacitance ratio. This equivalent conductance is negative when the DC current is positive, reducing the system damping.

The element of the state matrix that depends on the equivalent capacitance of the bipolar HVDC station, together with another that depends on the zero-sequence inductance, represent the main elements that affect the frequency of the mode.

Since the mode shows no noticeable sensitivity to the parameters of the controllers, it cannot be controlled by the typical control loops shown in Figure 4.3.

5.2.5. Zero–sequence controller design

The results suggest that it is possible to design a controller to dampen the mode related to DC asymmetric operation. Given the impact of the grounding impedance on the mode, the controller will be implemented in the monopolar station.

From a protection design perspective, a low grounding resistance allows for easy fault detection and faster tripping of relays. Still, it can lead to the development of an unstable or poorly damped mode. Therefore, the proposed controller is designed to improve the stability for low grounding resistance scenarios, regulating the zero-sequence voltage according to the measurement of the earth current. The controller is shown in Figure 5.9 and has two main control actions, provided by the upper and the lower path, which may or may not be combined.

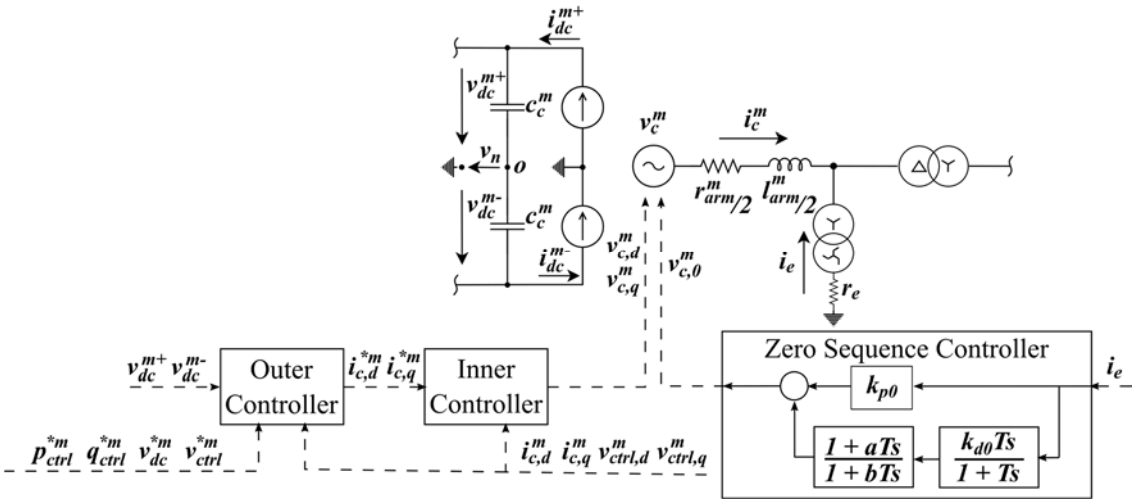

Figure 5.9. Controller to enhance system stability during asymmetrical operation.

In the upper path, the gain k_{p0} acts as a virtual grounding resistance so that it can be used to enhance the stability for any resistance value. Therefore, the movement of the mode as a function of this gain is similar to the movement presented in Figure 5.1 for a grounding resistance sweep, as displayed in the left graph in Figure 5.10. Therefore, the steady-state operating point after the disturbance changes depending on its value.

The lower path of the controller in Figure 5.9 has the advantage of working only during the transient without affecting the steady state. The right graph in Figure 5.10 displays the mode change with the rise of k_{d0} for a zero-grounding resistance when $k_{p0} = 0$. The damping of the unstable mode greatly enhances, even becoming an overdamped mode. Since the controller only acts during the transient and does not modify the effective grounding resistance in case of faults, it hardly affects the performance of protections.

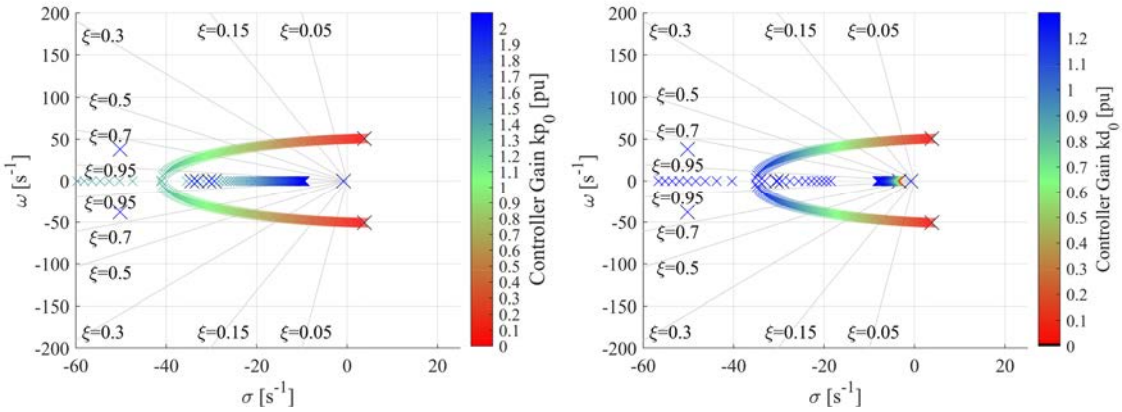

Figure 5.10. Root locus of the system for different values of k_{p0} (left) and k_{d0} (right).

The tuning of the proposed controller must be done considering the grounding impedance and the entire operating range of the HVDC system to achieve an appropriate response under all circumstances.

5.3. Small–signal stability analysis with centralised DC voltage control in the bipolar station

The analysis in 5.3 demonstrated that an asymmetrical DC operation could lead to instability or provoke undesired oscillations in the DC system. Specifically, the zero-sequence voltage and current resulting from that asymmetrical operation, and their interaction with the DC voltage and currents of the system, were the origin of the instability. That is why a zero-sequence controller was developed to improve the small-signal stability of the system.

This section analyses the same system (see Figure 4.1) under a different control strategy. The bipolar HVDC station controls the DC voltage, and the symmetrical monopolar HVDC station regulates the active power flow. This control scheme implies that the bipolar HVDC station can hold the active power of each pole separately to keep the pole-to-ground DC voltage at a specific value, which will strongly affect the response of the system during asymmetrical operation.

To begin with the small signal stability analysis of the system in these circumstances, the influence of the grounding impedance is studied. This first analysis also identifies which modes are involved in the asymmetrical DC operation. As a second step, a sensitivity analysis is carried out on the identified modes to find the most critical system parameters affecting them. Finally, the influence of these parameters on the small-signal stability of the system is examined.

The operating point chosen for the small-signal stability analysis is shown in Figure 4.4. It allows for comparing the small-signal stability of this case with the control strategy used in section 5.2 in similar circumstances. Nonetheless, other operation points will be considered later in this section. The parameters of the system and controllers are gathered in Appendix B.

5.3.1. Influence of the grounding system resistance

In section 5.2, it was proved that the grounding resistance plays a key role in the asymmetrical DC operation since it determines system stability. However, for the case analysed in this chapter, the root locus for a grounding resistance sweep is depicted in It points out that the system is stable regardless of the grounding resistance value. Therefore, the change of control strategy of the DC grid has considerably impacted the asymmetrical DC operation from the point of view of stability. The value of the grounding inductance is kept constant at 1.63 p.u. to obtain the results depicted in Figure 5.11.

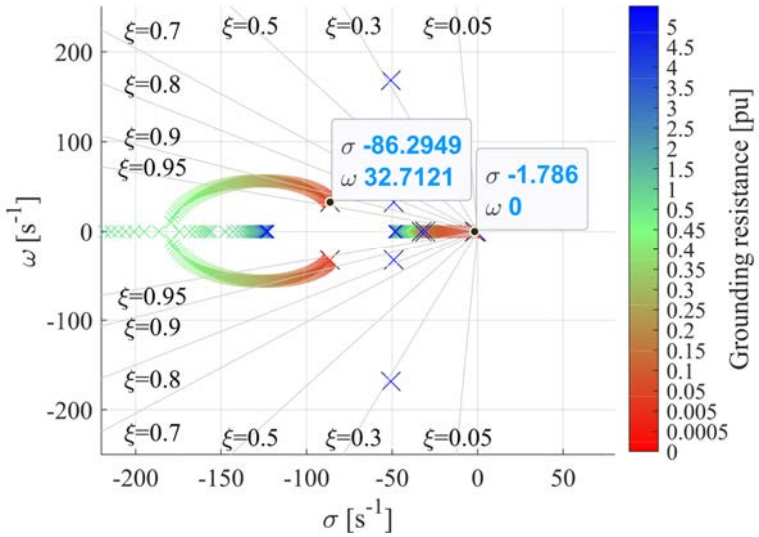

Figure 5.11. Root locus of the system for a grounding resistance sweep.

Figure 5.11 shows that the grounding resistance affects both a real mode and an oscillatory mode. The oscillatory mode turns into two real modes as the grounding resistance rises, but its decay rate is so high that it hardly impacts the dynamic behaviour of the system. On the other hand, the real mode represents the dominant dynamics for low values of the grounding resistance due to the proximity to the origin, thus affecting the settling time after a disturbance.

The participation of the states of the system in the real and the oscillatory mode, as a function of the grounding resistance, is represented in Figure 5.12.

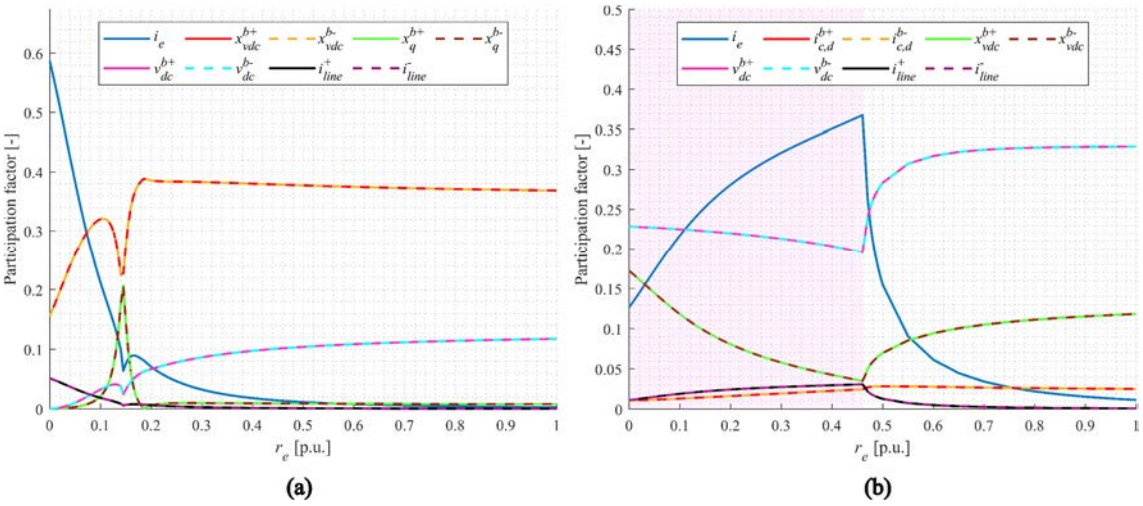

Figure 5.12. System variables with the highest participation factor in the real (a) and the oscillatory (b) mode for a grounding resistance sweep. The white zone represents a real and stable mode; the red zone represents an underdamped mode.

Figure 5.12 reveals that among the states with the highest participation in each mode are the earth current, the DC voltages, and the DC currents. These states also participated in the mode analysed in the last chapter. However, because of the new control strategy, the states of the DC voltage controller also present a noticeable participation in both modes.

Additionally, the real mode shows an interaction with the reactive power controller for a specific range of values of the grounding resistance due to the approach of this mode to the modes related to the reactive power controllers. Although this mode has a high decay rate for such a range of values, this interaction should also be considered during the design because it can negatively affect stability in other circumstances with lower decay rates. Finally, the oscillatory mode also shows appreciable participation of the AC active currents of the bipolar station.

The observability graphs of both modes, displayed in Figure 5.13, prove that the dynamics of these two modes appear in the DC system, the earth current, and the active current of the AC side of the bipolar HVDC station.

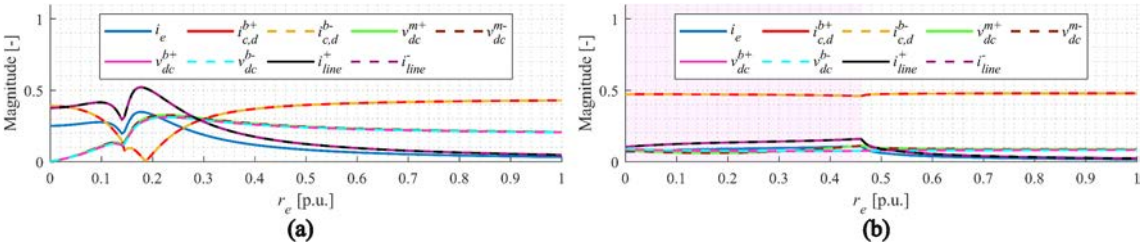

Figure 5.13. Observability of the real (a) and the oscillatory (b) mode for a grounding resistance sweep. The white zone stands for a real and stable mode; the red zone represents an underdamped mode.

However, note that the modes appear in counter-phase in both AC active currents, as Figure 5.14 shows. Therefore, the modes are cancelled beyond the common point of both converters forming the bipolar HVDC station and do not affect the rest of the AC system. Furthermore, there is a 180-degree difference between the phases of the observed positive

and negative DC variables. That is, these modes tend to cause a divergence between the DC positive and negative pole quantities, which is a characteristic of the asymmetrical DC operation.

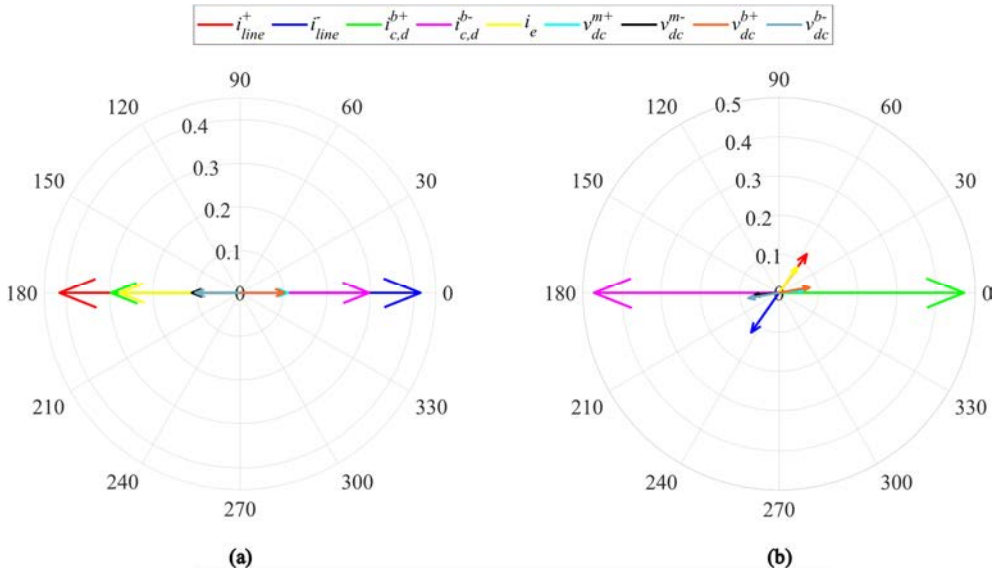

Figure 5.14. Observability polar plot for the real (a) and the oscillatory mode (b) for a grounding resistance value of 0.1 p.u.

The controllability of both modes is shown in Figure 5.15 as a function of the grounding resistance. These modes can be controlled mainly through the zero-sequence voltage reference of the monopolar station or the DC voltages references of the bipolar one. Since both modes are stable, implementing any particular controller may not be necessary.

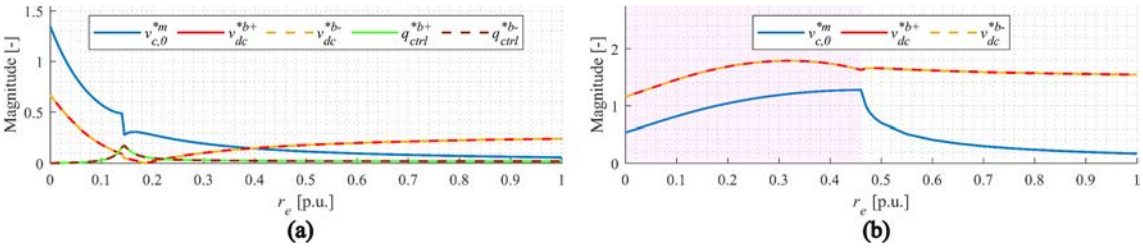

Figure 5.15. Controllability of the real (a) and the oscillatory (b) mode for a grounding resistance sweep. The white zone stands for a real and stable mode; the red zone represents an underdamped mode.

Therefore, the results indicate that very low values of grounding resistance do not cause instability but instead give rise to a slow transient response due to the proximity of the real mode to the origin, while larger values improve the dynamics.

5.3.2. Influence of the grounding system inductance

The grounding inductance does not affect the steady state of the asymmetrical DC operation. Still, it contributes to the transient response and stability of the system facing an asymmetrical DC operation. Its effect on the system stability is proved by tracking the trajectory of the system modes for a grounding inductance sweep, as depicted in Figure 5.16 (the grounding resistance is kept constant at 0.1 p.u).

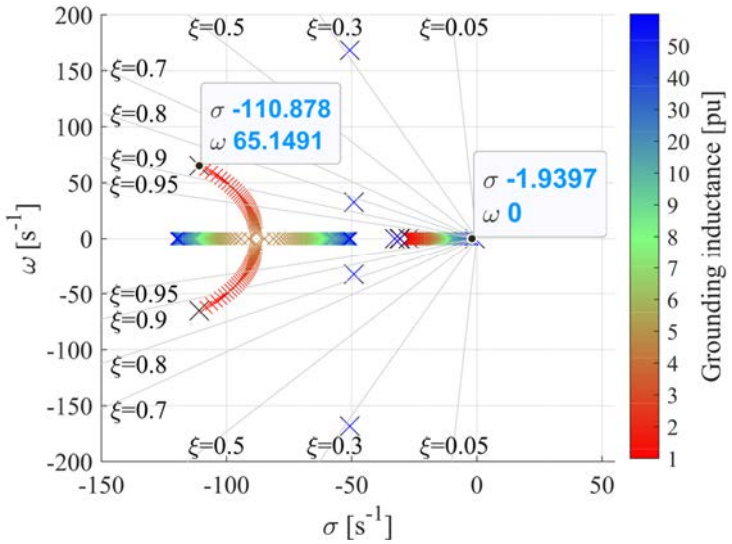

Figure 5.16. Root locus of the system for a grounding inductance sweep.

According to Figure 5.16, the grounding inductance value affects both a real mode and an oscillatory mode. These modes are the same as for the case of the grounding resistance sweep, as shown by the participation factors in Figure 5.17.

A high grounding inductance value improves the damping ratio of the oscillatory mode, although this mode still has little impact on system stability due to its fast time constant. Regarding the real mode, the increment of the inductance decreases its decay rate, provoking a slow transient response in extreme cases, which should be avoided. Therefore, large grounding resistances and low grounding inductances improve system stability.

Regarding the real mode participation factors depicted in Figure 5.17, the increment of the inductance increases the participation of the earth current and reduces that of the DC voltage controller. As for the oscillatory mode, the DC voltages of the bipolar station show the highest participation for low inductance values, whereas, for larger values, the participation of the DC voltage controller is the highest.

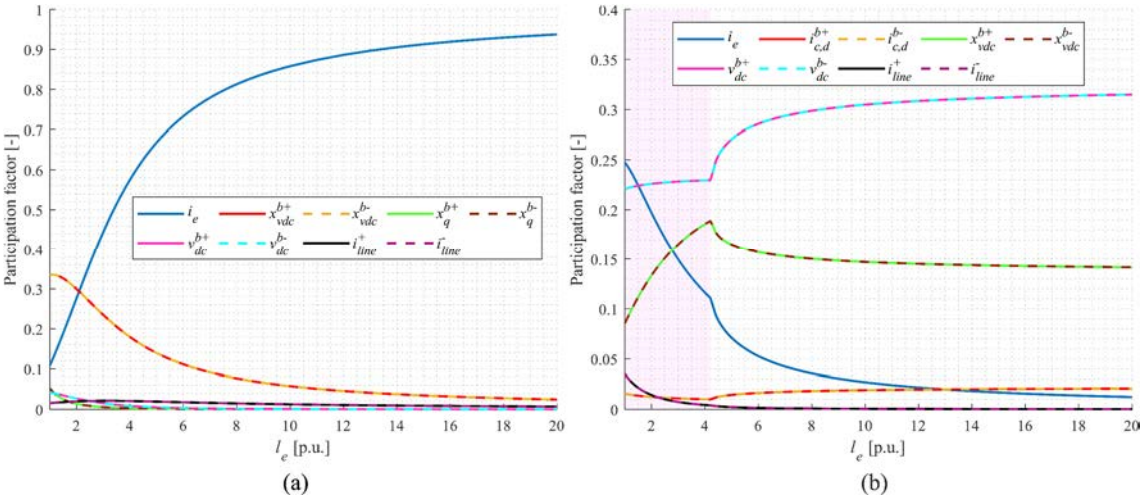

Figure 5.17. System variables with the highest participation factor in the real (a) and the oscillatory (b) mode for a grounding inductance sweep. The white zone stands for a real and stable mode; the red zone represents an underdamped mode.

Figure 5.18 shows that both modes are also observable in the same variables as in the grounding resistance case. However, the real mode is mainly observed in the DC currents, the earth current, and the active AC current of the bipolar station. In contrast, the oscillatory mode appears predominantly in the active AC current of the bipolar HVDC station.

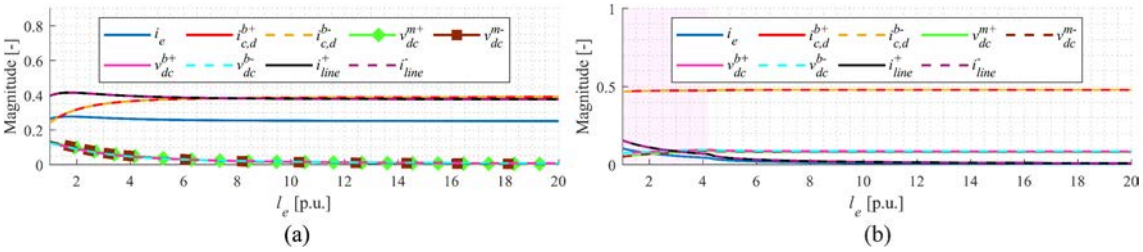

Figure 5.18. Observability of the real (a) and the oscillatory (b) mode for a grounding inductance sweep. The white zone stands for a real and stable mode; the red zone represents an underdamped mode.

As for controllability (Figure 5.19), the zero-sequence voltage and DC voltage references are the main input of the system controlling both modes. The controllability of the real mode enhances with the inductance value, but a higher inductance diminishes the controllability of the oscillatory one through the zero-sequence voltage.

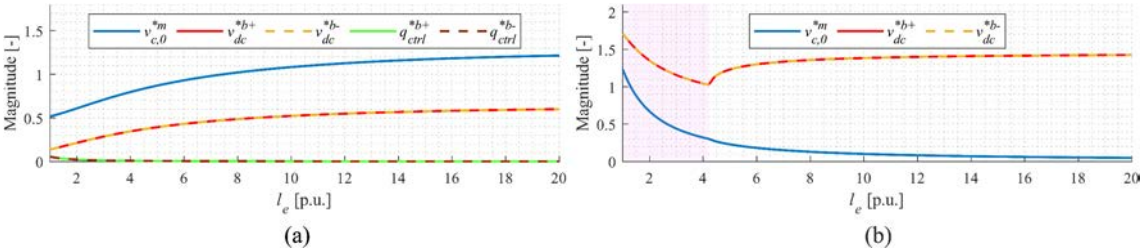

Figure 5.19. Controllability of the real (a) and the oscillatory (b) mode for a grounding inductance sweep. The white zone stands for a real and stable mode; the red zone represents an underdamped mode.

5.3.3. Sensitivity analysis

According to the participation factors for the different grounding resistance and inductance values, both modes represent an interaction of the DC voltage with the earth current. However, their different decay rate indicates that each mode represents an interaction of a different nature. Therefore, the system parameters influencing these two modes are analysed through a sensitivity analysis according to Equation (5.1).

Figure 5.20 shows the elements of the state matrix for which the real mode presents greater sensitivity. The results indicate that the real mode is mainly influenced by two factors: a) the system impedance in the path of the earth current and b) the dynamics of the DC voltage of the bipolar HVDC station. The impedances forming part of the earth current path are the grounding impedance, the arm impedance of the monopolar HVDC station, and the impedance of the DC system. On the other hand, the DC voltage dynamics of the bipolar HVDC station are related to the DC current balance and are represented by the terms of the state matrix containing the factor $\frac{\omega_b}{c_c^b}$. Specifically, the terms related to DC voltage dynamics for which the mode is most sensitive are the equivalent capacitance at the DC side of the bipolar HVDC station and the modulation factor, which approximates the relationship between the AC active current and the DC current of each converter in the bipolar station.

This suggests that this mode essentially depends on the topology and impedance of the system rather than the tuning of the existing controllers or the operation point. Other parameters different from those in Figure 5.20 may affect the mode but to a lesser extent.

In summary, the resistance-to-inductance ratio of the zero-sequence impedance of the system is the main factor affecting this mode. An increase in this ratio or the equivalent capacitance of the bipolar HVDC station increases the decay rate of the mode. Regarding the operating point, working with a lower modulation factor also increases the decay rate of the mode.

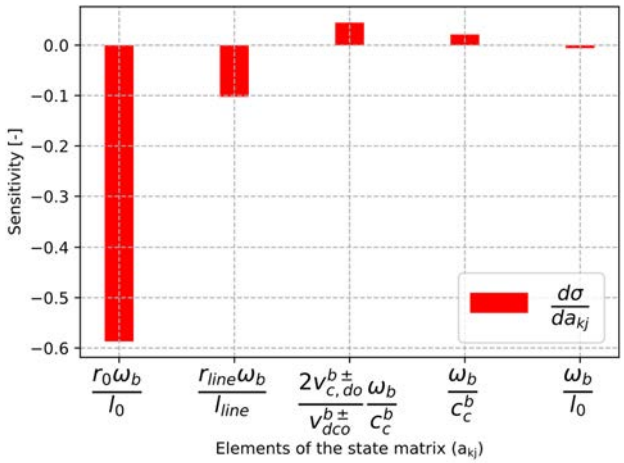

Figure 5.20. Sensitivity of the real mode.

Regarding the oscillatory mode, Figure 5.21 shows that it is affected by three dynamics: a) the DC voltage controller dynamics, b) the DC voltage dynamics of the bipolar station,

and c) the earth current dynamics. Among them, the dynamics of the DC voltage controller have the most significant impact, overall, the proportional gain kp_{vdc}. The integral gain ki_{vdc} also affects the mode, but the sensitivity is much smaller. The dynamics of the DC voltage are represented by the terms containing the factor $\frac{\omega_b}{c_c^b}$ and, for this mode, apart from the equivalent capacitance of the bipolar station itself, is very dependent on the operating point in terms of modulation factor and current direction. Finally, the earth current dynamics also influence the mode, as the terms containing the factor $\frac{\omega_b}{l_0}$ reveal.

In summary, incrementing the proportional gain of the DC voltage controller improves the damping ratio of the mode since it reduces its frequency and increases its decay rate. From the point of view of the operating point, a higher modulation factor improves the damping ratio of the mode together with an active power flowing from the bipolar to the monopolar station. Furthermore, the increase of the zero-sequence resistance to inductance ratio also improves the decay rate of the mode.

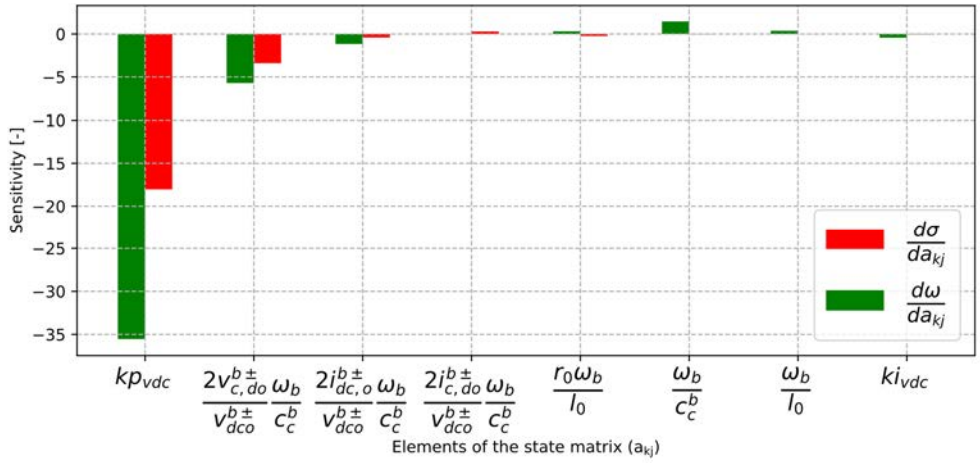

Figure 5.21. Sensitivity of the oscillatory mode.

Therefore, based on the previous analysis, the real mode represents the response of the earth current and its effect on the quantities of the system as a function of the system impedance. In contrast, the oscillatory mode is more related to the response of the DC voltage controller to that asymmetry in the DC system. Therefore, apart from the grounding impedance, the most critical factors for which the modes have shown great sensitivity are the initial operating point and the DC voltage controller gains. These aspects will be analysed in the following sections with further detail, although they are expected to have much more impact on the oscillatory mode than the real one.

5.3.4. Influence of the operating point

This section addresses the impact of the operating point on small-signal stability, specifically in the modes related to the asymmetrical DC operation. The sensitivity analysis showed that the real mode is hardly affected by this factor but not the oscillatory mode. Since a large grounding resistance improves the decay rate of both modes, it is set

to zero for worst-case conditions. The analysis focuses on the DC current and the DC voltage, while the grounding resistance and inductance are kept constant at 0 and 1.63 p.u., respectively.

Figure 5.22 shows that the magnitude and direction of the DC current influence more than two modes. The real and the oscillatory modes related to the asymmetrical DC operation are among them, according to the participation factors shown in Figure 5.23. Nonetheless, the real mode is barely influenced by the DC current. In contrast, the oscillatory one changes from real to oscillatory as the DC current changes from negative to positive values, i.e., as the active power flows from the monopolar to the bipolar station to a greater extent. However, this oscillatory mode keeps a fast time constant and damping ratio regardless of the DC current; thus, it less impacts the system stability.

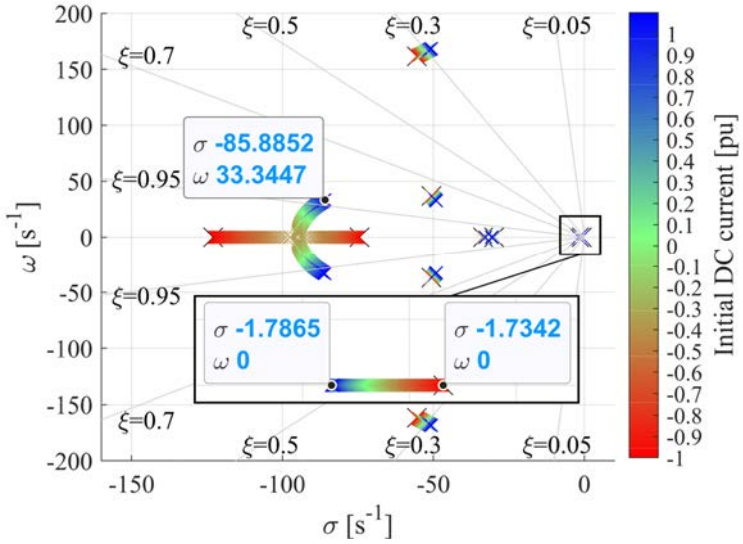

Figure 5.22. Root locus of the system for a DC current sweep.

Figure 5.23 shows that the magnitude and direction of the initial DC current hardly modify the participation of the states in the real mode. However, in the case of the oscillatory mode, the participation of the DC voltage of the bipolar station increases as the magnitude of the initial DC current flowing from the bipolar to the monopolar station does.

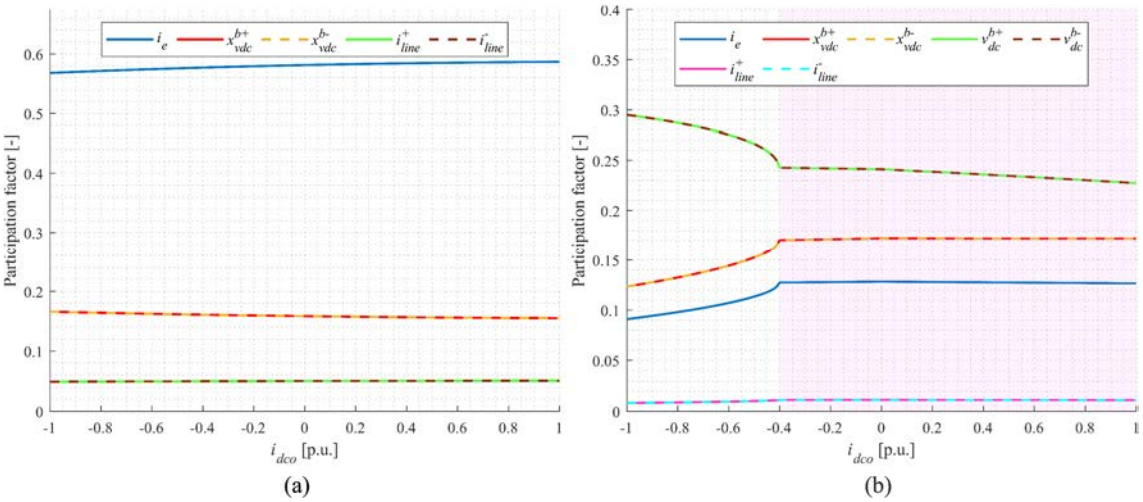

Figure 5.23. System variables with the highest participation factor in the real (a) and the oscillatory (b) mode for a DC current sweep. The white zone stands for a real and stable mode; the red zone represents an underdamped mode.

Concerning the initial DC voltage, Figure 5.24 shows the trajectories of the eigenvalues for a DC voltage sweep considering the negative and positive direction of the DC current. According to Figure 5.24, the DC voltage does not impact the real mode, only in the oscillatory one. Even though the oscillatory mode worsens its damping ratio, it is still damped enough for both DC current directions. The participation factors, observability, and controllability are not shown since they are similar to those shown previously.

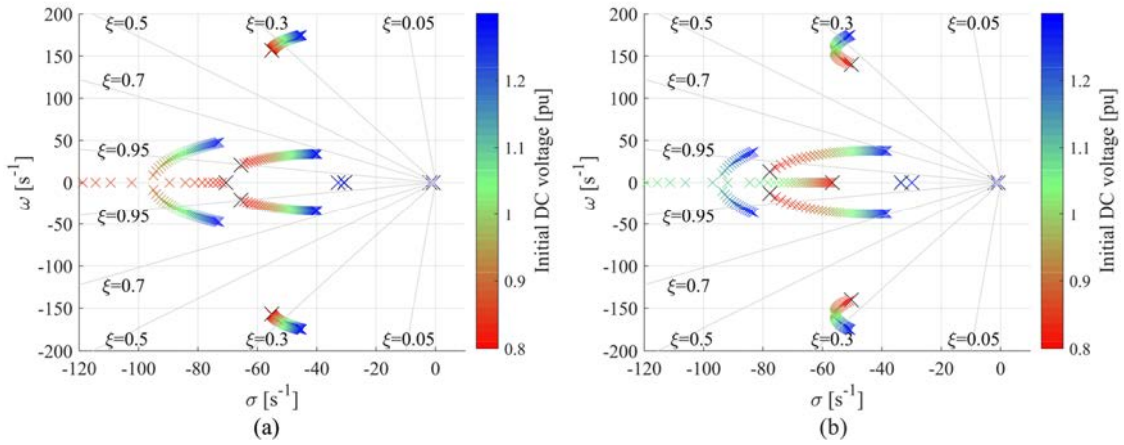

Figure 5.24. Root locus of the system for an initial DC voltage sweep for both directions of the DC current: a) positive DC current direction and b) negative DC current direction.

Therefore, the initial DC voltage or current hardly affects stability during asymmetrical DC operation. They are less decisive than in the case presented in section 5.2, where the monopolar station controlled the DC voltage. The main mode participating in the asymmetrical operation affected by these variables is the oscillatory mode. Its decay rate and damping ratio are large enough not to compromise the small-signal stability.

5.3.5. Influence of the DC voltage controller

Unlike in section 5.2, where the symmetrical monopolar HVDC station controls the DC voltage, the DC voltage controller is expected to influence the asymmetrical DC

operation. Specifically, the sensitivity results depicted in Figure 5.21 proved that the oscillatory mode related to the asymmetrical DC operation is affected by the tuning of the DC voltage controller. Therefore, the impact of the proportional and integral gains is explored below.

The effect of the proportional gain is shown in Figure 5.25, which demonstrates that several modes are affected by this gain.

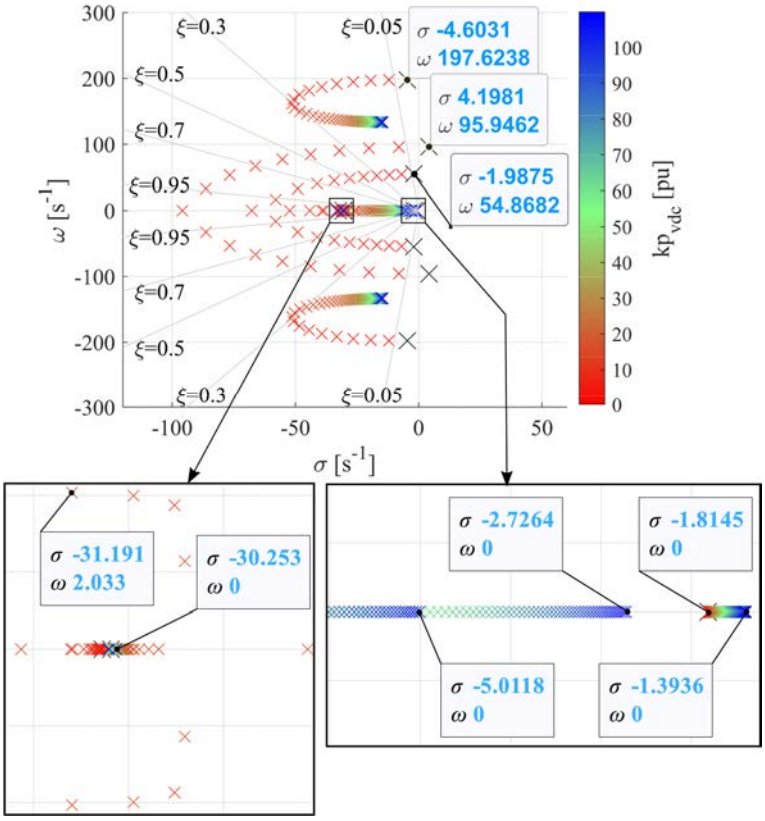

Figure 5.25. Root locus of the system for a sweep of the proportional gain of the DC voltage controller.

Observe that, for small gain values, there are three oscillatory modes close to the imaginary axis. One is unstable, and the other modes have a damping ratio lower than 5 per cent. As the proportional gain increases, two become aperiodic modes that approach the imaginary axis again. In addition, a real mode is affected to a lesser extent by this gain, which is also close to the imaginary axis and diminishes its decay rate as the proportional gain increases. The real and non-stable oscillatory modes are the two modes related to the asymmetrical DC operation, as inferred from the participation factors shown in Figure 5.26.

Therefore, Figure 5.25 proves that a small or zero proportional gain of the DC voltage controller worsens system stability from the asymmetrical DC operation perspective, but also in a broader sense since other modes are considerably affected that are not related to the asymmetrical operation. In turn, higher gain values prevent instability, but a value around 9 p.u. achieves the greatest damping of these three oscillatory modes.

The participation factors of the real and the oscillatory mode related to the asymmetrical DC operation are depicted in Figure 5.26. In the case of the real mode, as the proportional

gain of the DC voltage controller increases, the participation of the DC voltage controller states also rises and diminishes that of the earth current. As for the oscillatory mode, the participation of the different states varies considerably depending on the proportional gain value. Note that when the mode is overdamped, the mode turns oscillatory again and appears as an interaction with these reactive power controllers.

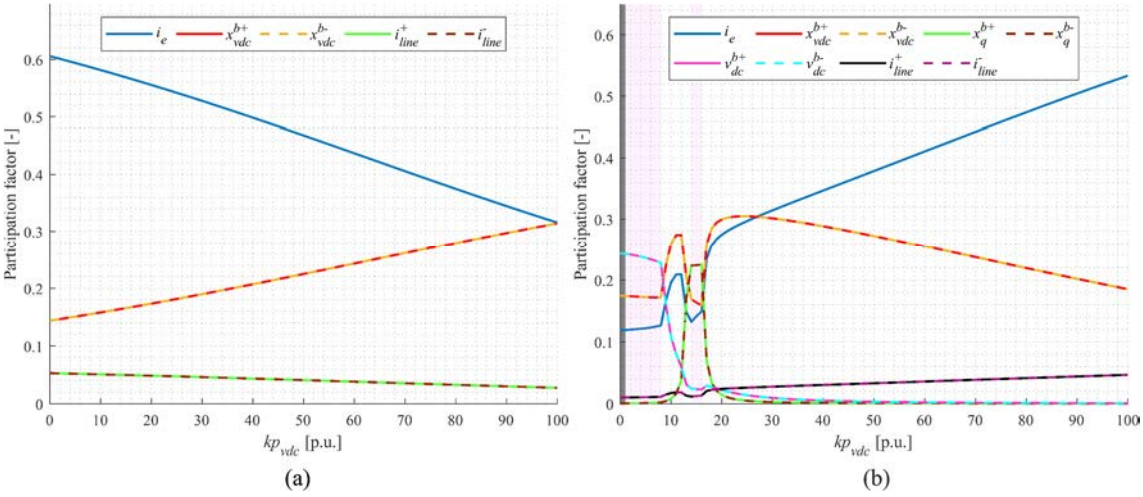

Figure 5.26. System variables with the highest participation factor in the real (a) and the oscillatory (b) mode for a proportional gain of the DC voltage controller sweep. The white zone stands for a real and stable mode; the red zone represents an underdamped mode, and the grey indicates an unstable mode.

Figure 5.27 shows the variables where these two modes are observable as a function of the proportional gain of the DC voltage controller. As previously mentioned, the real mode is not very sensitive to the variation of the kp_{vdc} gain. Therefore, its observability does not present any change. By contrast, the observability of the oscillatory mode suffers a higher variation as the proportional gain changes. For small proportional gain values, where this mode is more significant from the point of view of stability, this mode is underdamped and even unstable. It is mainly observable in the AC active currents, earth current, DC currents, and DC voltages. Although this underdamped or unstable oscillation appears in the AC active currents of the bipolar station, it does not affect the rest of the AC system because the oscillation in the AC active current is in counter-phase between poles, as shown in Figure 5.14.

In addition, note that the abrupt change in the observability of the oscillatory mode occurs due to an interaction when this mode approaches the modes related to that controller.

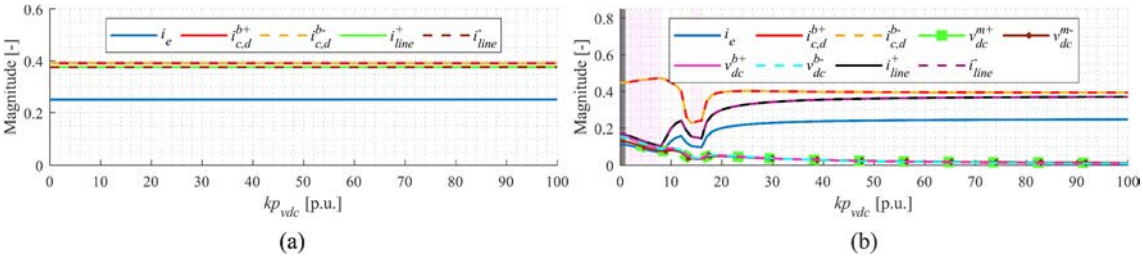

Figure 5.27. Observability of the real (a) and the oscillatory (b) mode for a sweep of the proportional gain of the DC voltage controller. The white zone stands for a real and stable mode, the red zone represents an underdamped mode, and the grey indicates an unstable mode.

Therefore, according to the results, the proportional gain of the DC voltage controller is a critical parameter that influences the asymmetrical DC operation and other system dynamics. Therefore, this gain should be tuned aiming for the proper dynamic behaviour of the system in different circumstances, including the asymmetrical DC operation.

Similarly, the integral gain of the DC voltage controller (ki_{vdc}) also affects several modes in the system, as can be observed in Figure 5.28, including those related to the asymmetrical DC operation. Notice that for a zero integral gain value, there are two real eigenvalues in the origin due to eliminating the two states of the DC voltage controller.

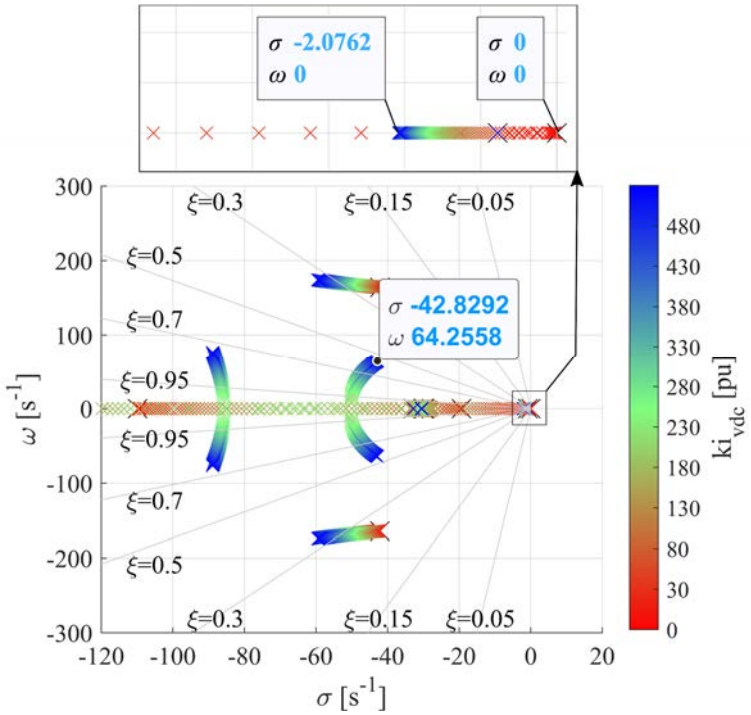

Figure 5.28. Root locus of the system for an integral gain of the DC voltage controller sweep.

The participation factors shown in Figure 5.29 demonstrate that the real mode and one of the oscillatory modes affected by the integral gain of the DC voltage controller are the two modes related to the asymmetrical DC operation. According to Figure 5.28, the oscillatory mode associated with the asymmetrical operation can be tuned to be underdamped, critically damped, or overdamped. Hence, the integral gain should be chosen in such a way as to ensure proper dynamic behaviour. As for the real mode, despite varying its decay rate with the integral gain, its variation is limited, and it still has a low decay rate regardless of the integral gain value.

Again, Figure 5.29 reflects the interaction between the DC voltage and reactive power controllers. Although this interaction does not present any issue from a stability perspective in these circumstances, due to the fast time constant of the modes, it should be considered for tuning the DC voltage and the reactive power controller.

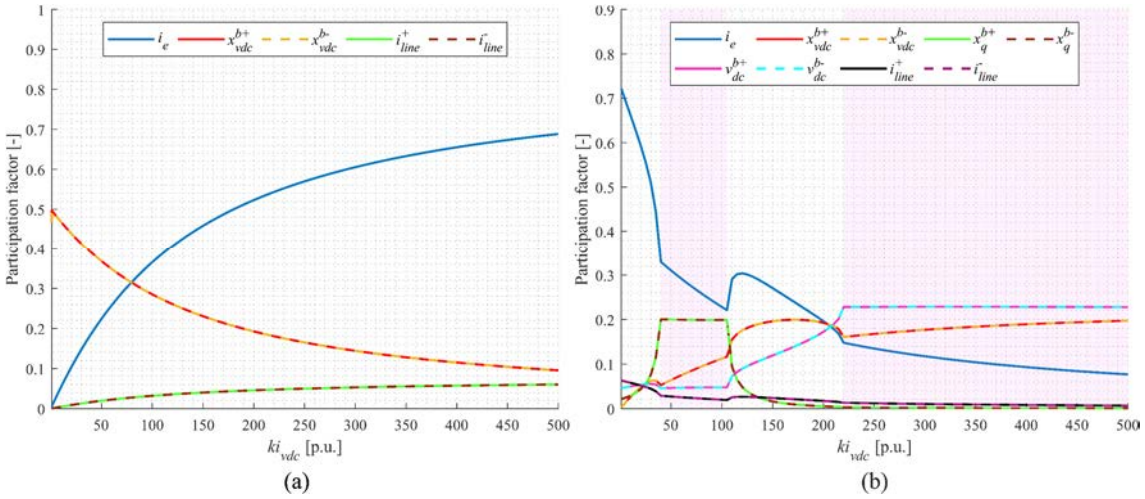

Figure 5.29. System variables with the highest participation factor in the real (a) and the oscillatory (b) mode for a sweep of the integral gain of the DC voltage controller. The white zone stands for a real and stable mode.

Figure 5.30 shows that the integral gain does not influence the observability of the real mode. Both are mainly observable in the AC active currents of the bipolar station, the earth current, the DC currents, and the DC voltages.

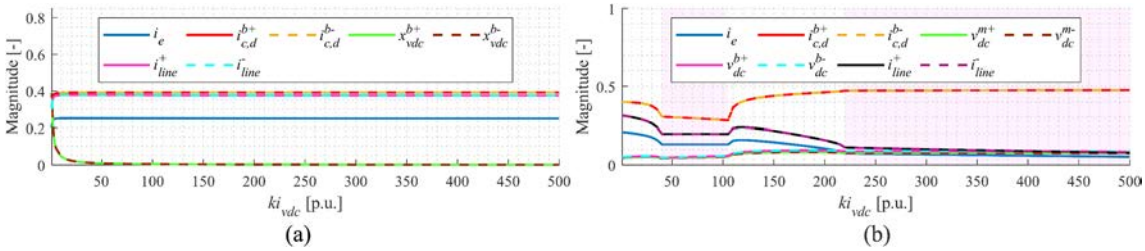

Figure 5.30. Observability of the real (a) and the oscillatory (b) mode for a sweep of the integral gain of the DC voltage controller. The white zone stands for a real and stable mode; the red zone represents an underdamped mode.

The analysis of this section demonstrates that the DC voltage controller settings affect significatively to the stability of the system, not only from the point of view of the asymmetrical DC operation. Several modes are influenced by the DC voltage controller gains, including the two modes related to the asymmetrical operation. Nonetheless, the effect on the real mode associated with the asymmetrical operation is limited. The proportional gain value mainly affects the oscillatory mode, which can be unstable for low values. Regarding the integral gain, low values make the two modes related to the asymmetrical operation become aperiodic modes close to the origin, causing a very slow transient. Therefore, in this case, and unlike the case discussed in the last section, the correct tuning of the DC voltage controllers is essential to achieve stability during asymmetrical DC operations.

5.3.6. Impact of the zero–sequence controller

The previous section introduced a zero-sequence controller to enhance system stability during an asymmetrical DC operation. However, this controller is unnecessary in the present case since correctly tuning the DC voltage controller is enough to keep the system

stable. Nonetheless, the controllability and observability of the two modes related to the asymmetrical DC operation have demonstrated that this zero-sequence controller can control them. Therefore, it is worth assessing whether the existence of this controller in the symmetrical monopolar HVDC station improves or degrades the stability and dynamic response when the DC grid is regulated by the control strategy studied in this section. Therefore, the effect of the zero-sequence controller in the monopolar station and its gain values are considered below.

The effect of the gain k_{d0} is shown in Figure 5.31 (a). On the one hand, the controller introduces a new real mode that moves from $\sigma = -3.3333\ s^{-1}$ to the left in the complex plane as the gain increases. On the other hand, the two modes affected by the asymmetrical DC operation are also affected by this controller gain. The oscillatory mode increases its decay rate, whereas the real mode decreases it. Therefore, the effect of this gain is a longer stabilisation time after a disturbance in the DC voltages, DC currents, the earth current, and the active currents of the bipolar HVDC station.

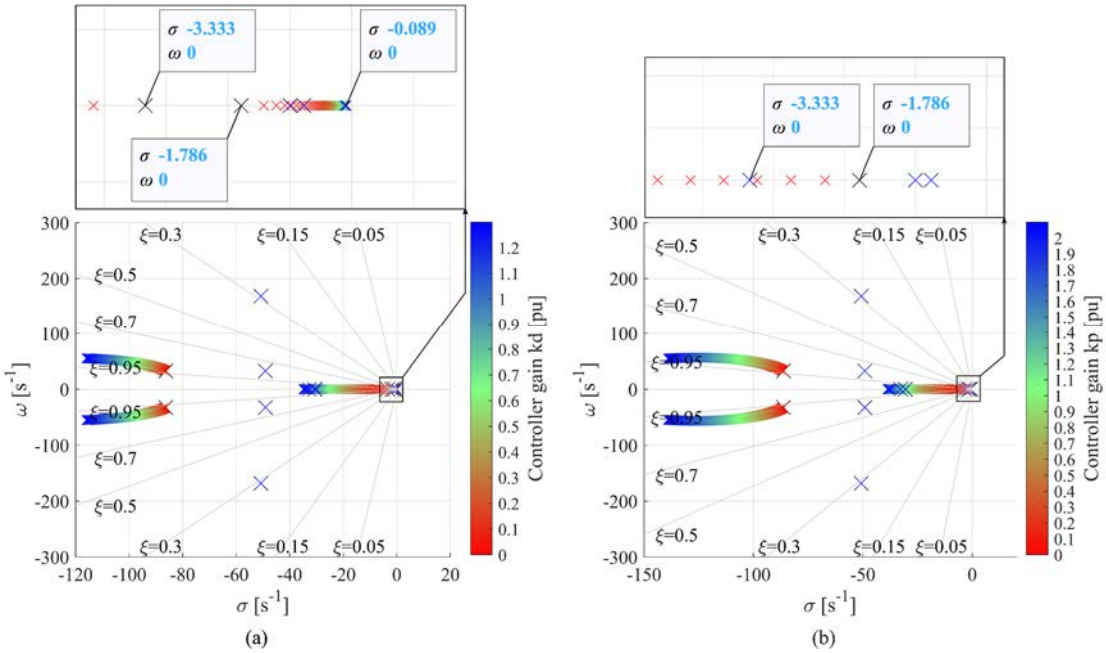

Figure 5.31. Root locus of the system for a sweep of the gain k_{d0} (a) and k_{p0} (b) of the zero-sequence voltage controller.

On the other hand, the proportional gain k_{p0} of the zero-sequence controller moves the modes related to the asymmetrical operation similarly to the grounding resistance, as shown in Figure 5.31 (b). This improves the decay rate of the real and the oscillatory mode but modifies the steady state during a permanent asymmetrical DC operation.

5.4. Small–signal stability analysis with distributed DC voltage – active power droop control

Sections 5.2 and 5.3 have demonstrated that the asymmetrical DC operation can lead to instability under certain conditions. In addition, the control strategy of the system has

proved to have a profound impact on these conditions and the dynamic behaviour during asymmetrical DC operation.

In this section, the system in Figure 4.1 is analysed by implementing a distributed DC voltage droop control as a control strategy. This control scheme implies that both stations regulate the DC voltage according to their droop coefficients. Therefore, due to the relationship between asymmetrical DC operation and how the system DC voltage is controlled, this control strategy is expected to affect the system response during asymmetrical operation strongly.

Following a similar procedure as in the previous sections, the influence of the grounding impedance on system stability is studied as a first step in identifying the modes related to the asymmetrical DC operation. Then, the main system parameters that affect these modes are identified through a sensitivity analysis that allows a deeper understanding of their impact on the system stability during asymmetrical DC operation.

The initial operating point of the previous chapters is chosen for the analysis (see Figure 4.4). This operating point allows comparing the small-signal stability of the system implementing the distributed DC voltage droop control with the control strategy used in sections 5.2 and 5.3 in similar circumstances. Nonetheless, other points of operation will be considered across the section and indicated where appropriate. The parameters of the system and controllers are gathered in Appendix B.

5.4.1. Influence of the grounding system resistance

First, the small-signal stability of the system is analysed for a range of grounding resistance values. The value of the grounding inductance is kept constant at 1.63 p.u. The root locus obtained is depicted in Figure 5.32. It shows that two modes are affected by the grounding resistance and, thus, are involved in the asymmetrical DC operation of the system. Figure 5.32 also reveals that the system remains stable for the entire range of grounding resistance values analysed and the study conditions.

In addition, implementing the DC voltage droop control strategy has caused the appearance of an additional poorly damped oscillatory mode in the vicinity of the imaginary axis unaffected by the grounding resistance ($-5.441 \pm j210.020$).

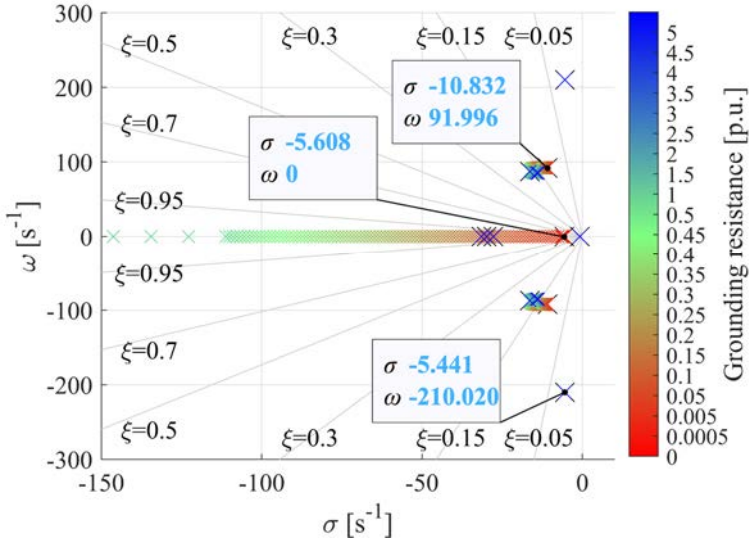

Figure 5.32. Root locus of the system for a grounding resistance sweep.

Regarding the two modes affected by the change in the grounding resistance, Figure 5.32 shows that they are a real mode and an oscillatory mode. The oscillatory mode has a low damping ratio for small grounding resistance values, and it is generally insensitive to changes in the grounding resistance.

The real mode has a slow decay rate for small grounding resistance values but gradually increases with grounding resistance. Therefore, for a considerable grounding resistance, the real mode hardly affects the dynamic response during asymmetrical DC operation.

To identify the states involved in each mode, Figure 5.33 represents the participation of the system states in the real and the oscillatory mode as a function of the grounding resistance.

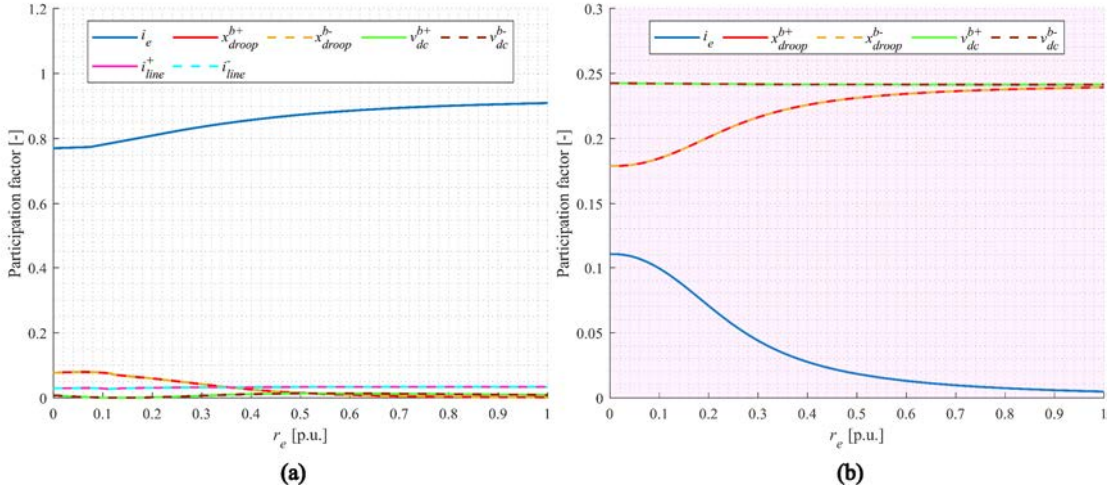

Figure 5.33. System variables with the highest participation factor in the real (a) and the oscillatory (b) mode as a function of the grounding resistance. The white zone stands for a real and stable mode; the red zone represents an underdamped mode.

Figure 5.33 reveals that the states with the highest participation in each mode are similar to those shown in the previous case, where the monopolar station controlled the active

power flow. However, because of the change of the control strategy, the controller states that participate in the modes for this case are those related to the DC voltage droop controller of each converter of the bipolar station. Note that the state of the DC voltage droop controller of the monopolar station does not participate in any of these two modes.

Regarding the real mode, although the DC voltage droop controller states of the bipolar station participate in it, their participation is small compared to the earth current, which presents the highest participation. On the other hand, the main states that participate in the oscillatory mode are the DC voltage droop controller of each converter of the bipolar station and the DC voltages of the bipolar station. In contrast, the participation of the earth current is not as significant. This indicates that the real mode is mainly related to the dynamics of the earth current and its interaction with the DC variables, and the oscillatory mode primarily represents the dynamics of the DC voltage and the response of the DC voltage droop controllers of the bipolar station.

As in section 5.3, where the monopolar station controls the active power flow, the observability graphs of both modes, displayed in Figure 5.34, prove that the dynamics of these two modes appear in the DC system, the earth current, and the active current at the AC side of the bipolar HVDC station.

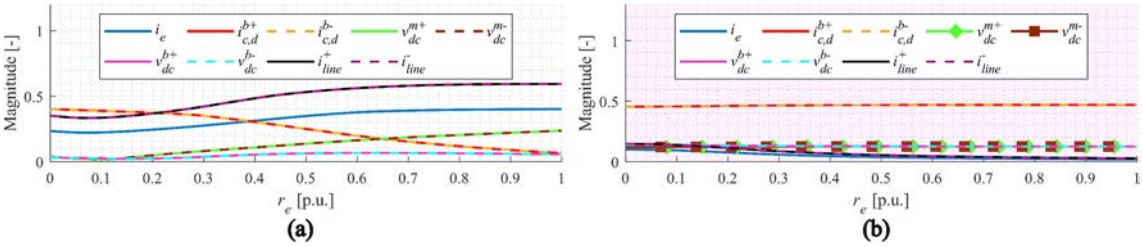

Figure 5.34. Observability of the real (a) and the oscillatory (b) mode as a function of the grounding resistance. The white zone stands for a real and stable mode; the red zone represents an underdamped mode.

Since both modes are related to the asymmetrical DC operation, which involves a different active power flow transmitted by each pole of the DC link, the dynamics of the asymmetrical behaviour appear in the AC active current of each converter in the bipolar station. From Figure 5.35, note, however, that there is a 180-degree phase difference in the observability of the DC variables of the positive and negative poles. This also applies to the AC active currents of the positive and negative pole converter of the bipolar station. Therefore, the modes cancel beyond the common point in the bipolar HVDC station and do not affect the rest of the AC system. The 180-degree phase difference between the observed positive and negative DC variables indicates that these modes tend to cause a divergence between the DC variables of both poles, a characteristic of the asymmetrical DC operation.

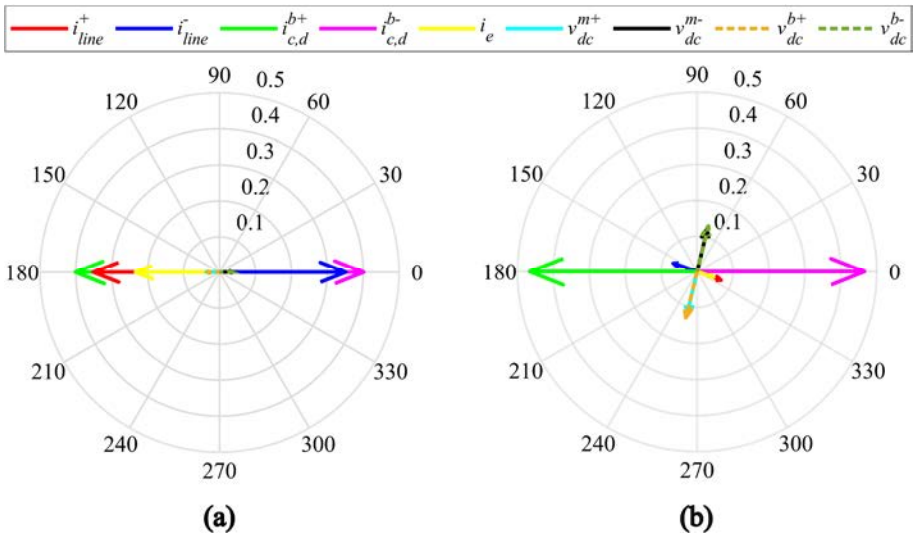

Figure 5.35. Observability polar plot for the real (a) and the oscillatory (b) mode for a grounding resistance of 0.1 p.u.

The controllability of both modes is shown in Figure 5.36 as a function of the grounding resistance. Both modes exhibit high controllability for small grounding resistance values through the zero-sequence voltage references of the monopolar station and the DC voltage references of the bipolar station.

Therefore, as both modes are observable at the DC voltages of the bipolar station, they can be controlled by the DC voltage droop controllers of the converters of the bipolar station. However, the controllability via DC voltage references decreases considerably for the real mode in case of higher grounding resistances, although it has a fast decay rate under these conditions.

The controllability through the zero-sequence controller discussed in the previous cases is also possible for both modes. However, the oscillatory mode presents lower controllability through this method for larger grounding resistances.

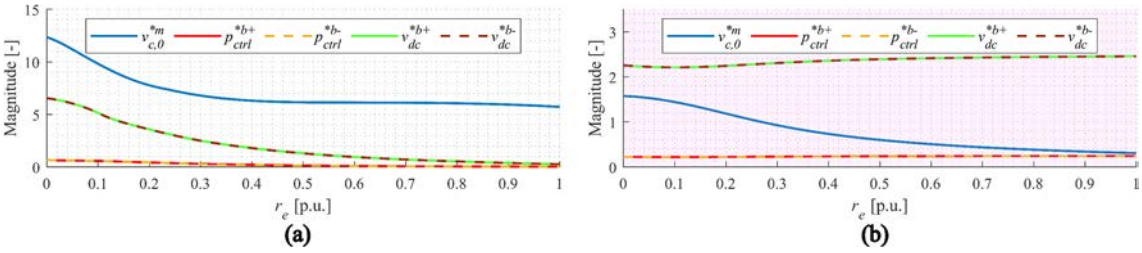

Figure 5.36. Controllability of the real (a) and the oscillatory (b) mode as a function of the grounding resistance. The white zone stands for a real and stable mode; the red zone represents an underdamped mode.

Therefore, the results evidence that very low values of grounding resistance do not cause instability, but more significant values improve the dynamics during asymmetrical operation by increasing the decay rate of the real mode and the damping ratio of the oscillatory one.

Although the analysis focuses on modes related to asymmetrical DC operation, it is important to note that the mode with the worst damping in Figure 5.32 ($-5.441 \pm j210.020$) is not involved in this type of operation. Even so, the cause of this poorly

damped mode is worth looking into, and its participation factors are depicted in Figure 5.37.

Observe that the main variables that participate in the mode are the DC currents, the DC voltages, the AC active current of the monopolar station, and the states of the DC voltage droop controllers of both the bipolar and the monopolar station. These participation factors suggest that the mode represents the interaction between the DC voltage droop control of the monopolar and the bipolar station via the system DC variables.

Therefore, it is likely that the $-5.441 \pm j210.020$ mode can be further damped by proper adjustment of the DC voltage droop regulators.

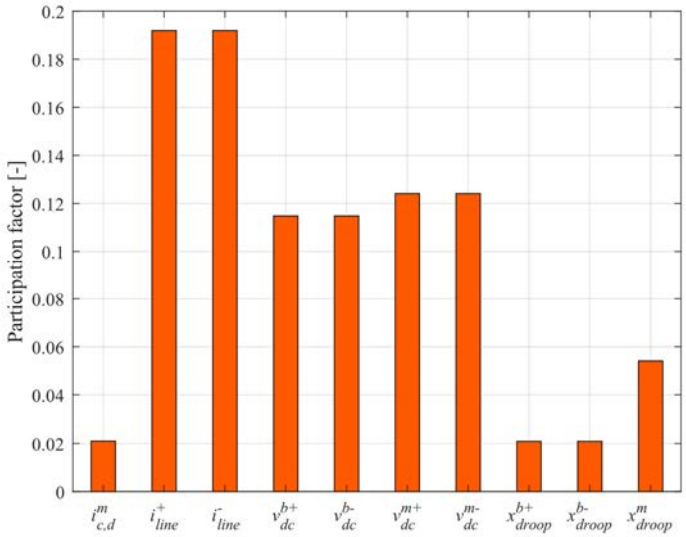

Figure 5.37. Participation factors of the -5.441±j210.020 mode.

5.4.2. Influence of the grounding system inductance

In this section, the study of the asymmetrical operation when the system implements a distributed DC voltage droop control strategy continues by analysing the effect of the grounding inductance on the small-signal stability.

Figure 5.38 shows the trajectory of the modes for a range of grounding inductance values while the grounding resistance is kept constant at 0.1 p.u.

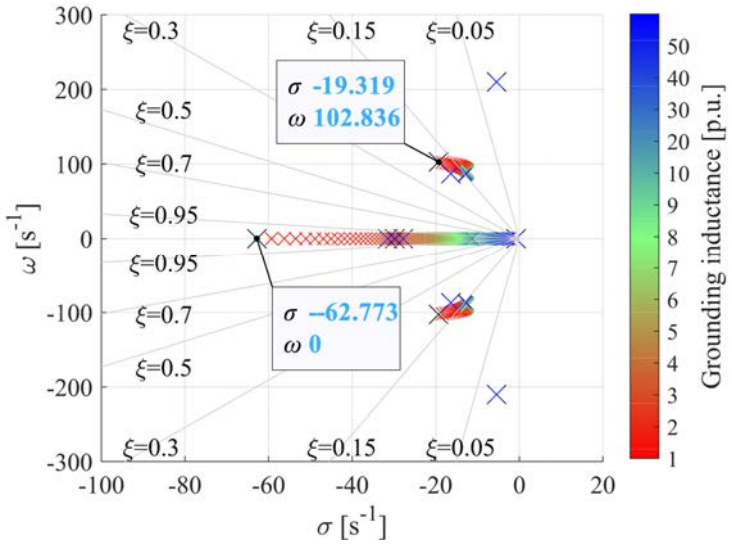

Figure 5.38. Root locus of the system for a grounding inductance sweep.

Figure 5.38 shows that the grounding inductance value affects a real mode and an oscillatory mode. These modes are the same as for the case of the grounding resistance sweep, as shown by the participation factors in Figure 5.39.

Compared with the root locus in Figure 5.32, these two modes worsen their damping ratio and reduce their decay rate as grounding inductance increases. For small values of grounding inductance, the system response during asymmetrical DC operation is governed mainly by the oscillatory mode due to the rapid decay rate of the real mode. Nonetheless, for high values of grounding inductance, the real mode progressively approaches the imaginary axis becoming a slow mode that dominates the response during asymmetrical DC operation. The change in the grounding inductance does not affect the worst damped mode. Therefore, large grounding resistances and low grounding inductances improve system stability.

The participation factors in Figure 5.39 show that the earth current is the main participating state in the real mode, whereas the DC voltage of the bipolar station and the DC voltage droop controller state of each converter in the bipolar station are the main states that participate in the oscillatory mode.

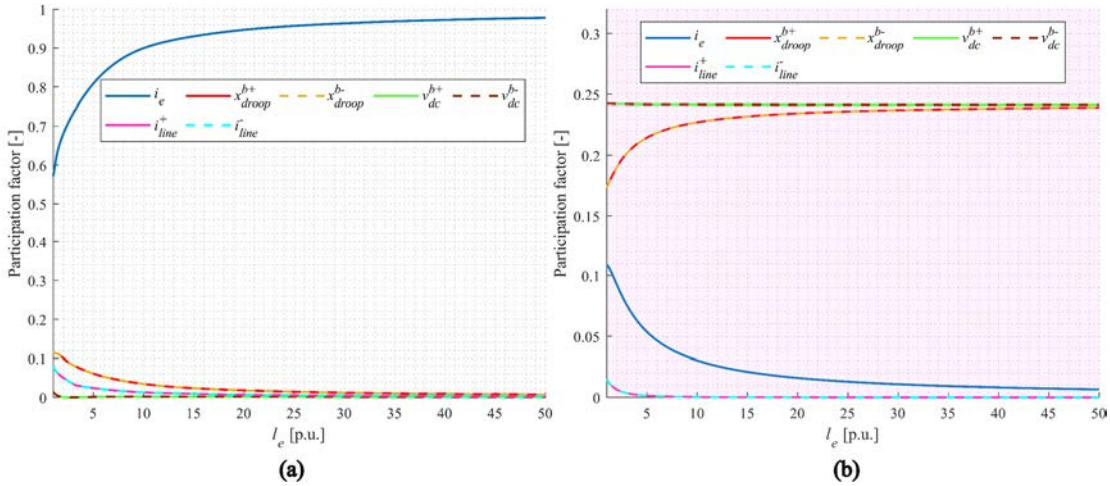

Figure 5.39. System variables with the highest participation factor in the real (a) and the oscillatory (b) mode as a function of the grounding inductance. The white zone stands for a real and stable mode; the red zone represents an underdamped mode.

Figure 5.40 shows that both modes are also observable in the same variables as in the grounding resistance case. The real mode is mainly observed in the active AC currents of the bipolar station, the DC currents, and the earth current, whereas the oscillatory mode appears predominantly in the active AC current of the bipolar HVDC station and the DC voltages.

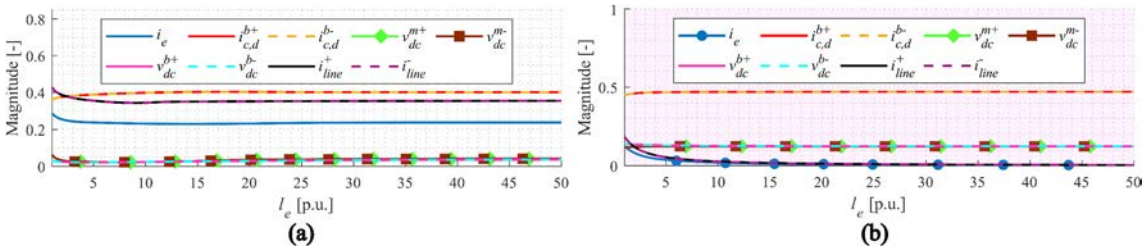

Figure 5.40. Observability of the real (a) and the oscillatory (b) mode as a function of the grounding inductance. The white zone stands for a real and stable mode; the red zone represents an underdamped mode.

As for controllability (Figure 5.41), the zero-sequence voltage and DC voltage references are the main inputs controlling both modes. The controllability of the real mode through the zero-sequence voltage of the monopolar station or the DC voltage references of the bipolar station is affected by the value of the grounding inductance. Still, the mode is controllable by these inputs for the entire inductance range. Regarding the oscillatory mode, its controllability by the DC voltage references of the bipolar station is hardly affected by the grounding inductance. By contrast, the controllability of the oscillatory mode through the zero-sequence voltage reduces considerably as the grounding inductance rises.

Since both modes are observable in the DC voltages of the bipolar station and are controllable through the DC voltage references of the bipolar station, they can be controlled by adjusting these DC voltage droop regulators. However, the effect of the DC voltage droop controller can be more limited in the real mode since the observability of this mode in the DC voltages is smaller.

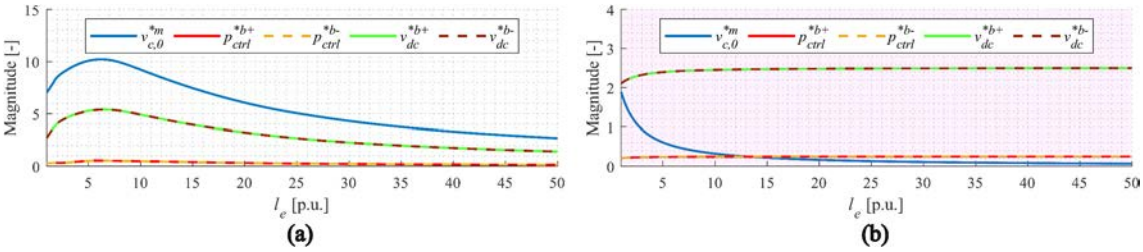

Figure 5.41. Controllability of the real (a) and the oscillatory (b) mode as a function of the grounding inductance. The white zone stands for a real and stable mode; the red zone represents an underdamped mode.

Although both the real and the oscillatory modes keep stable for the different values of grounding resistance and inductance assessed, a more detailed analysis is necessary to explore how these modes evolve depending on other system parameters or operating points.

5.4.3. Sensitivity analysis

Having identified the two modes related to the asymmetrical DC operation, it is worth analysing what other factors may influence them and, thus, the small-signal stability of the system during asymmetrical DC operation. Therefore, a sensitivity analysis is performed according to Equation (5.1).

Figure 5.42 and Figure 5.43 show the elements of the state matrix for which the real mode and the oscillatory mode present greater sensitivity. The results indicate that almost the same elements of the state matrix affect both modes, although the weight of each component is different for each of them. Therefore, these elements can be grouped into four categories: a) the dynamics of the earth current through the zero-sequence impedance, b) the initial operating point on the AC side of the bipolar station, c) the dynamics of the DC voltage droop controllers of the bipolar station and, d) the dynamics of the DC voltage of the bipolar station.

According to Figure 5.42 and Figure 5.43, as the ratio of resistance to the inductance of this impedance increases, the decay rate in both modes also increases, and the frequency of the oscillatory mode decreases. Note that the zero-sequence impedance on the AC side of the symmetrical monopolar station comprises the grounding impedance and the arm impedance of the monopolar station.

However, the sensitivity of the real mode to the zero-sequence impedance is higher than the sensitivity of the oscillatory mode. These conclusions are aligned with the results obtained in the previous sections.

Regarding the operating point on the AC side of the bipolar station, the magnitude of the controlled AC voltage of each converter of the bipolar station is the main variable that affects the modes. To a lesser extent, the reactive current also has a certain impact on them.

Increasing the AC voltage magnitude increases the decay rate and reduces the frequency of the oscillatory mode. Regarding the real mode, the influence of the AC voltage

magnitude depends on the proportional gain of the DC voltage droop controllers of the bipolar station $\left(kp^b_{droop}\right)$: for small gains, the increase of the controlled AC voltage increases the decay rate of the mode. In contrast, for higher gains, the effect is the opposite. As for the reactive current, the absorption of reactive current also improves the dynamic behaviour of both modes.

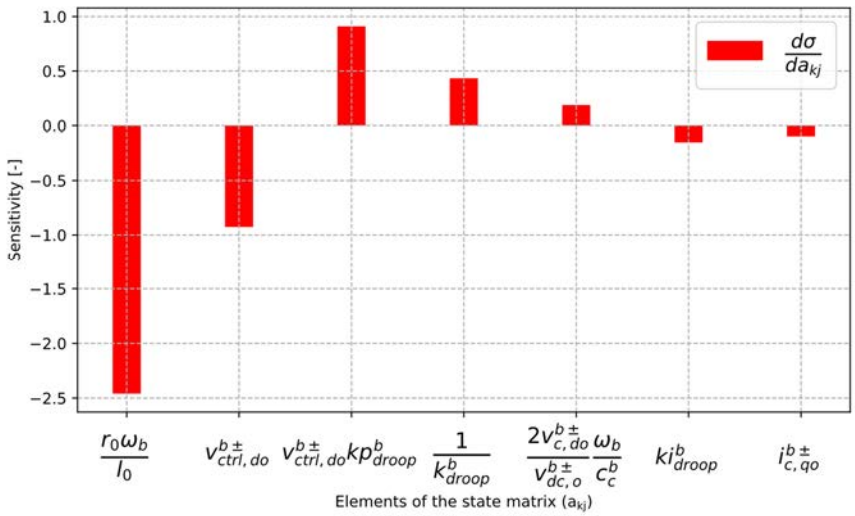

Figure 5.42. Sensitivity of the real mode

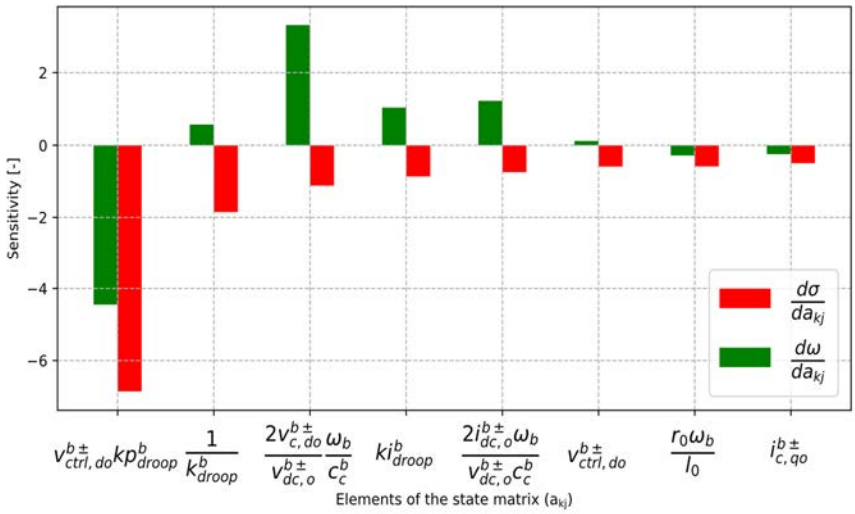

Figure 5.43. Sensitivity of the oscillatory mode.

The proportional $\left(kp^b_{droop}\right)$ and integral $\left(ki^b_{droop}\right)$ gains of the PI regulator composing the DC voltage droop controller of each converter of the bipolar station together with the droop coefficient $\left(k^b_{droop}\right)$ have also a considerable impact on both modes.

The increases of the proportional gain kp^b_{droop} tends to make the real mode slower, increasing the decay rate and reducing the frequency of the oscillatory one. On the other hand, regarding the integral gain ki^b_{droop}, its increment reduces the decay rate of both modes and augments the frequency of the oscillatory one. As for the droop coefficient

k_{droop}^{b}, higher values increase the decay rate of the real mode but reduce the decay rate and the frequency of the oscillatory one.

Note that neither the gains of the PI regulator nor the droop coefficient of the DC voltage droop controller of the monopolar station impact the real and oscillatory modes involved in the asymmetrical DC operation.

The dynamics of the DC voltage of the bipolar HVDC station are related to the DC current balance, and it is represented by the terms of the state matrix containing the factor $\frac{\omega_b}{c_c^b}$. Specifically, the terms related to the DC voltage dynamics for which both modes are more sensitive are the equivalent capacitance at the DC side of the bipolar HVDC station and the modulation factor, which approximates the relationship between the AC active current and the DC current of each converter of the bipolar station.

Increasing the modulation factor or reducing the equivalent capacitance c_c^b tends to reduce the decay rate of the real mode but increases the one of the oscillatory modes.

Additionally, the oscillatory mode is also affected by another term related to the dynamic of the DC voltage $\left(\frac{2i_{dc,o}^{b\pm}}{v_{dc,o}^{b\pm}}\frac{\omega_b}{c_c^b}\right)$ that can be considered as an equivalent resistance to capacitance ratio that approaches part of the response of the bipolar converter as an equivalent impedance. In this sense, the higher the DC current injected by the bipolar station to the DC link, the faster the decay rate and the higher the frequency of the oscillatory mode.

Therefore, based on the above analysis, although similar factors affect both modes, the real mode is much more dependent on the dynamics of the earth current, which depend primarily on the grounding impedance and secondarily on the DC voltage droop regulation of the bipolar station.

On the other hand, the DC voltage droop regulation of the bipolar station and the dynamics of the DC voltage are the main aspects affecting the oscillatory mode.

Hence, besides the grounding impedance already analysed, the principal factors for which the modes have shown great sensitivity are the initial operating point and the settings of the DC voltage droop controller of the bipolar station.

5.4.4. Influence of the operating point

This section addresses the impact of the operating point on the modes related to the asymmetrical DC operation. Since a large grounding resistance enhances the decay rate of both modes, it is set to zero to analyse the operating point so that the worst conditions from the stability point of view are considered. Thus, the grounding resistance and inductance are held constant at 0 and 1.63 p.u., respectively, during this section. Following the conclusions of the sensitivity analysis, the study of the operating point focuses on the impact that the initial magnitude of the DC current, DC voltage and AC voltage at the bipolar station have on the modes related to the asymmetrical DC operation.

As for the initial DC current, Figure 5.44 shows that its magnitude and direction influence more than two modes. It is important to note that the DC current is considered to have a positive direction when the active power flows from the monopolar station to the bipolar one. As expected from the sensitivity analysis, the initial DC current does not affect the real mode but the oscillatory mode related to the asymmetrical operation. In particular, the initial DC current modifies the decay rate of the oscillatory mode while hardly impacting its frequency. The worst damped mode not involved in the asymmetrical DC operation also worsens its damping ratio as the initial DC current increases.

Therefore, a high amount of active power flowing from the monopolar station to the bipolar station worsens system stability. However, it does not cause instability with the current parameterisation of the DC voltage droop controllers.

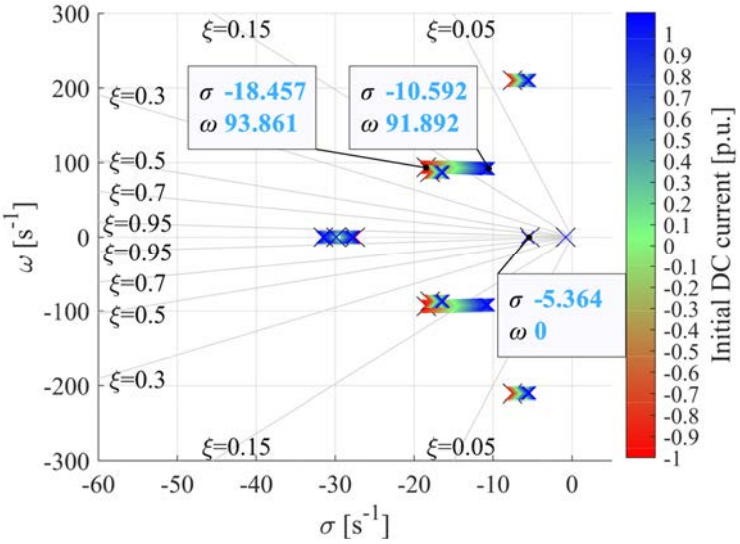

Figure 5.44. Root locus of the system as a function of the initial DC current.

Figure 5.45 shows that the magnitude and direction of the initial DC current hardly modify the participation of the states in the real and oscillatory modes involved in the asymmetrical DC operation.

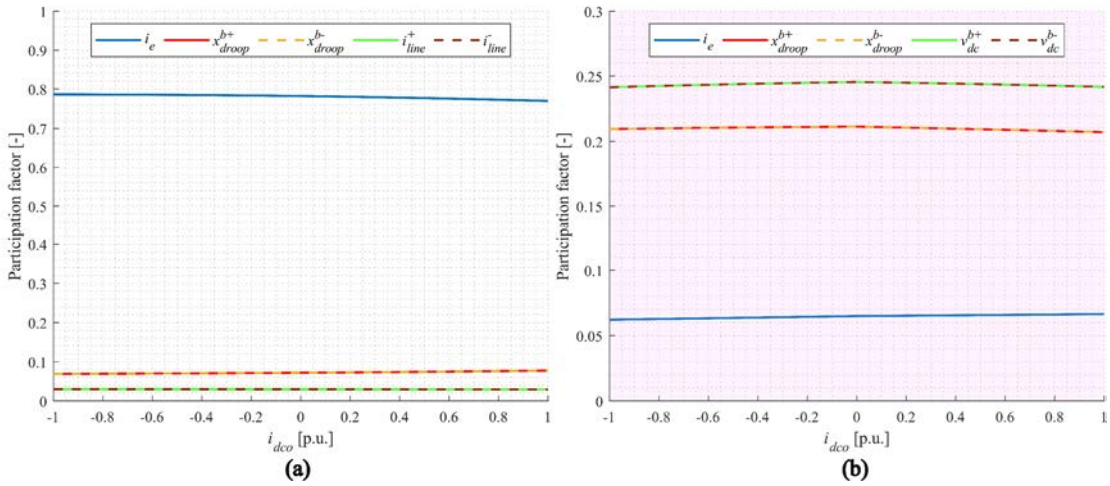

Figure 5.45. System variables with the highest participation factor in the real (a) and the oscillatory (b) mode as a function of the initial DC current. The white zone stands for a real and stable mode; the red zone represents an underdamped mode.

Concerning the initial DC voltage, Figure 5.46 shows the trajectories of the eigenvalues as a function of the initial DC voltage. According to Figure 5.46, high DC voltages improve the decay rate of the real mode and reduce the frequency of the oscillatory one. However, the effect on the real part of the oscillatory mode depends on the DC current direction.

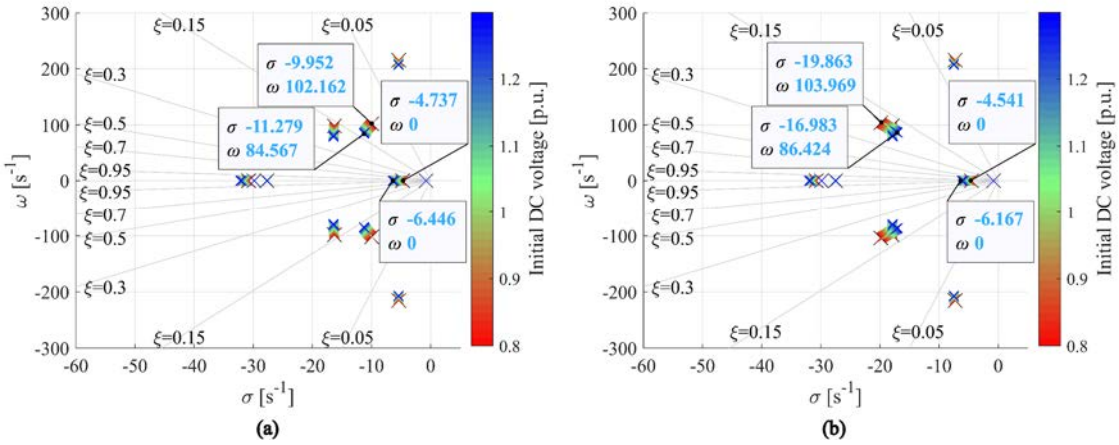

Figure 5.46. Root locus of the system as a function of the initial DC voltage for both directions of the DC current: a) positive DC current direction and b) negative DC current direction.

Therefore, the operating point of the DC system does not significatively affect the real mode. Moreover, although the initial DC voltage affects its decay rate, the impact is much smaller than that of the grounding impedance. By contrast, the operating point of the DC system has a higher effect on the oscillatory mode than the grounding impedance, especially the magnitude and direction of the DC current.

To finish with the operating point study, the initial magnitude of the AC voltage at the bipolar station is analysed next. Figure 5.47 shows the movement of the eigenvalues for a range of initial AC voltage magnitudes at the bipolar station. Both the real and oscillatory modes increase their decay rate as the AC voltage magnitude rises, but the

frequency of the oscillatory mode hardly changes. However, as in the case of the initial DC current and DC voltage, the effect on the real mode is small compared to the influence of the grounding impedance. The impact on the oscillatory mode is modest but more significant than the real one. However, it is not a crucial factor either.

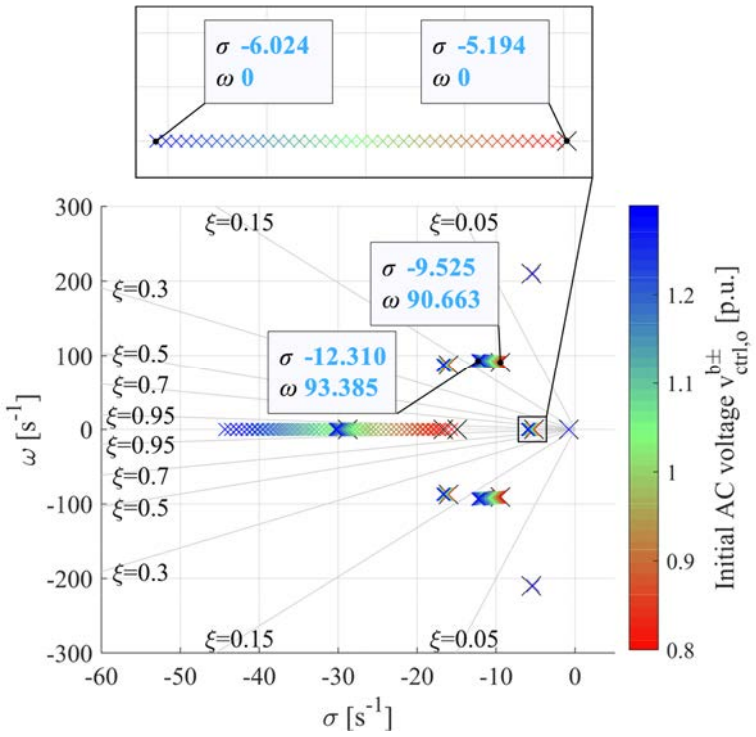

Figure 5.47. Root locus of the system as a function of the initial magnitude of the AC voltage.

After analysing the influence of the operating point on the modes involved in the asymmetrical DC operation, it can be concluded that this point hardly impacts the real mode, being its impact higher on the oscillatory mode, especially the DC current.

5.4.5. Influence of the DC voltage droop controller

According to the sensitivity analysis presented in Figure 5.42 and Figure 5.43 for the real and the oscillatory modes, the adjustment of the DC voltage droop controllers of the bipolar station influence both modes. In particular, the proportional $\left(kp^{b}_{droop}\right)$ and integral $\left(ki^{b}_{droop}\right)$ gains of the PI regulator and the droop coefficient $\left(k^{b}_{droop}\right)$.

The influence of these gains is assessed using the operating point shown in Figure 4.4, while the grounding resistance and inductance are held constant at 0 and 1.63 p.u., respectively. First, the effect of the proportional gain kp^{b}_{droop} on the small-signal stability of the system during asymmetrical DC operation is examined. Figure 5.48 shows the trajectories of the eigenvalues as a function of this gain.

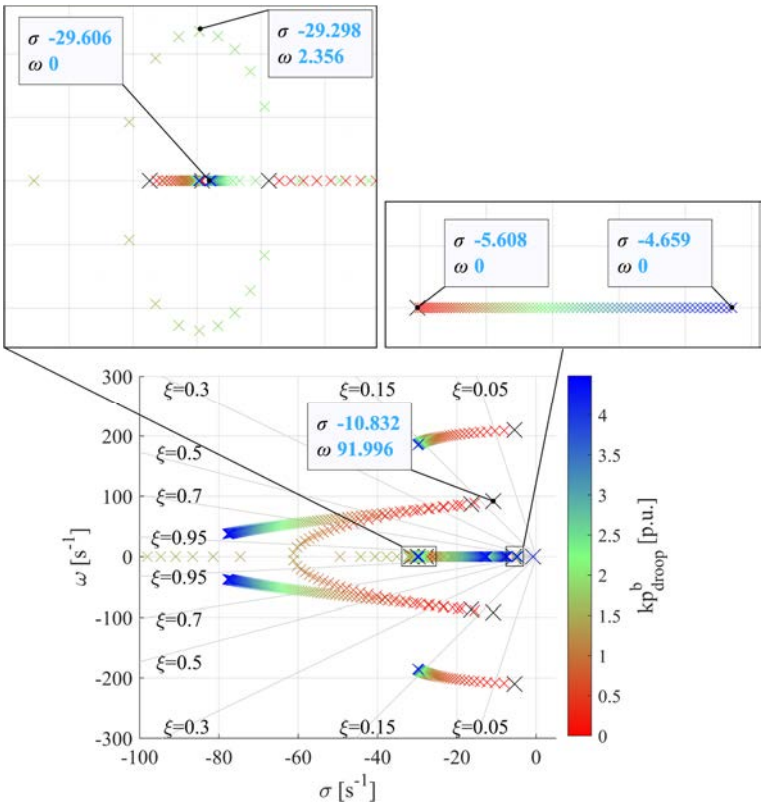

Figure 5.48. Root locus of the system as a function of kp^b_{droop}.

Several modes are influenced by the gain kp^b_{droop}, including the two modes involved in the asymmetrical DC operation, as the participation factors in Figure 5.49 prove. In addition, the worst damped mode unrelated to the asymmetrical DC operation also improves its damping ratio as the proportional gain kp^b_{droop} rises.

The effect that the gain kp^b_{droop} has on the two modes related to the asymmetrical DC operation is different. The real mode is not as sensitive as the oscillatory mode to the change in the gain and reduces its decay rate as the gain augments. In contrast, the oscillatory mode increases its damping ratio until it becomes an aperiodic mode as the gain increases. In addition, note that once the oscillatory mode becomes a real mode, it turns into an oscillatory mode again due to an interaction with another mode, although it is well-damped.

Therefore, Figure 5.48 proves that a small or zero proportional gain kp^b_{droop} of the DC voltage droop controller of the bipolar station worsens system stability, not only during asymmetrical DC operation but also during regular operation.

Figure 5.49 shows the participation factors of the two modes related to the asymmetrical DC operation as a function of the gain kp^b_{droop}. The earth current is the main variable that participates in the real mode, although its participation diminishes in favour of the participation of the states of the DC voltage droop controllers of the bipolar station as the gain augments. On the other hand, the participation factors of the oscillatory mode involved in the asymmetrical DC operation exhibit abrupt changes as the gain increases. Clearly, they show the interaction with the reactive power controller.

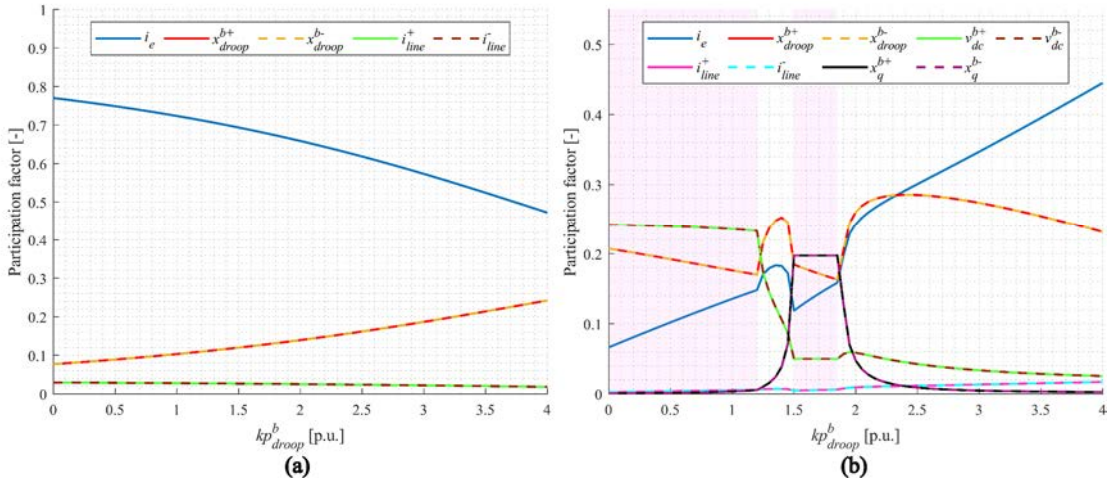

Figure 5.49. System variables with the highest participation factor in the real (a) and the oscillatory (b) mode as a function of the proportional gain of the DC voltage droop controller. The white zone stands for a real and stable mode, and the red zone represents an underdamped mode.

Figure 5.50 shows the variables where these two modes are observable as a function of the proportional gain of the DC voltage controller. Both modes are observable in the DC voltages, the DC current, the earth current, the AC active current at the bipolar station, and the states of the DC voltage droop controllers of the bipolar station for every value of gain. However, the observability graph of the oscillatory mode shows that during the interaction with the mode related to the reactive power controller of the bipolar station, the observability in the AC reactive current at the bipolar station also rises.

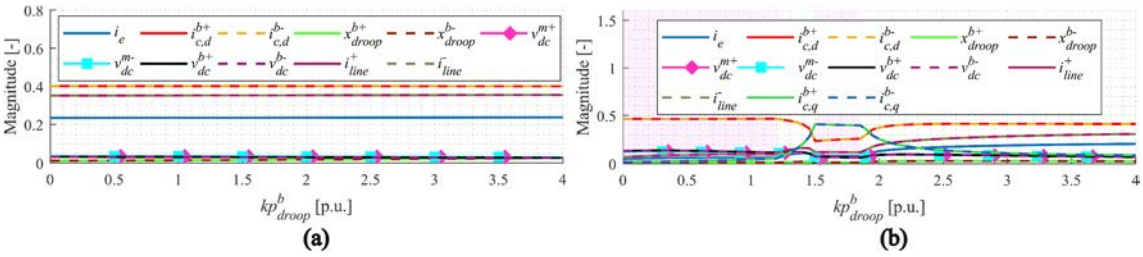

Figure 5.50. Observability of the real (a) and the oscillatory (b) mode as a function of kp^b_{droop}. The white zone stands for a real and stable mode, and the red zone represents an underdamped mode.

According to the results, the proportional gain of the DC voltage droop controller of the bipolar station $\left(kp^b_{droop}\right)$ is a critical parameter that influences not only the asymmetrical DC operation but also other system dynamics. Therefore, this gain should be tuned aiming for the proper dynamic behaviour of the system in different circumstances, including the asymmetrical DC operation.

Similarly, Figure 5.51 shows that the integral gain of the DC voltage droop controller of the bipolar station $\left(ki^b_{droop}\right)$ also affects several modes in the system. One of the oscillatory modes affected by this gain is unstable for small values of this gain.

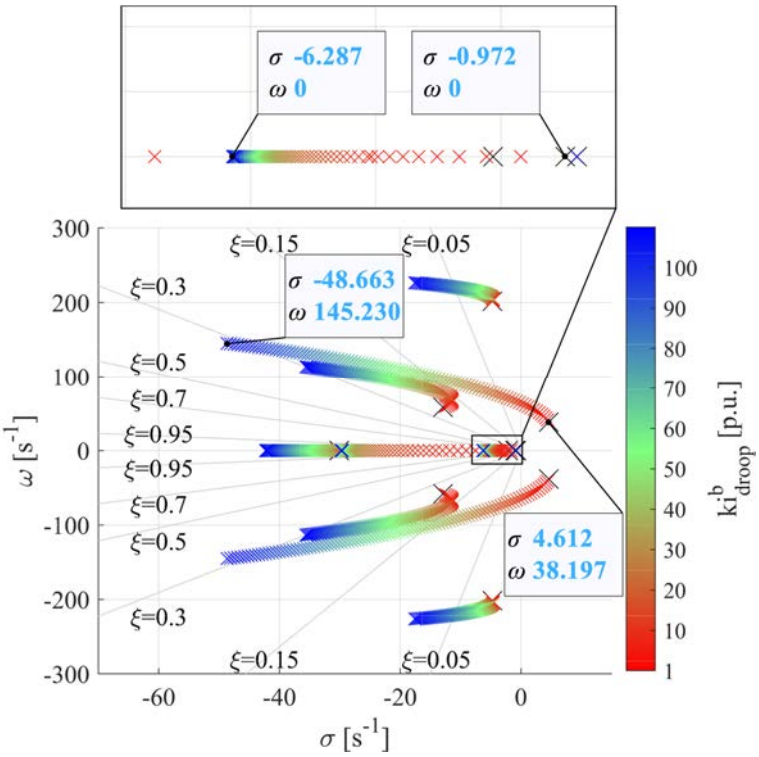

Figure 5.51. Root locus of the system as a function of ki^b_{droop}.

The participation factors shown in Figure 5.52 demonstrate that the real mode and the unstable oscillatory mode affected by the integral gain of the DC voltage droop controller are the two modes related to the asymmetrical DC operation. Furthermore, the oscillatory mode with a damping ratio lower than 5% enhances its damping ratio as the integral gain augments.

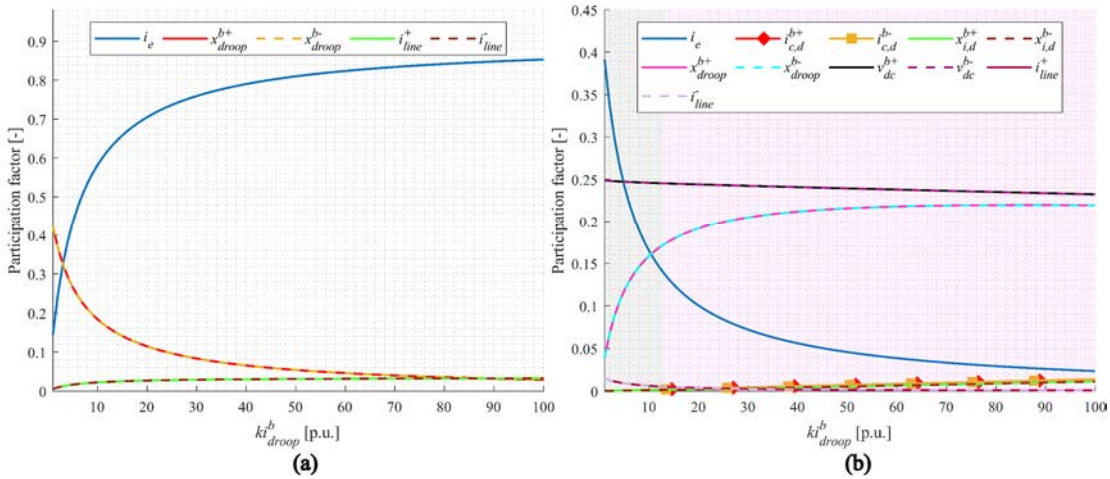

Figure 5.52. System variables with the highest participation factor in the real (a) and the oscillatory (b) mode as a function of ki^b_{droop}. The white zone stands for a real and stable mode, the red zone for an underdamped mode, and the grey zone for an unstable mode.

Therefore, the integral gain should be adjusted considering its impact on the modes related to the asymmetrical DC operation to avoid instability or a very slow transient.

To finish with the analysis of the influence of the DC voltage droop controller on the modes involved in the asymmetrical DC operation, the effect of the droop coefficient is analysed below.

Previously, the droop coefficient of both stations has been kept constant at 0.1 p.u., according to the value in Appendix B. Below, the impact of the droop coefficients on the system stability is analysed. Figure 5.53 (a) shows the movement of the eigenvalues when the droop coefficient of the monopolar station changes and those of the bipolar station are kept constant at 0.1 p.u. On the other hand, Figure 5.53 (b) shows the eigenvalues movement for changes in the droop coefficient of the bipolar station while maintaining at 0.1 p.u. the one of the monopolar station.

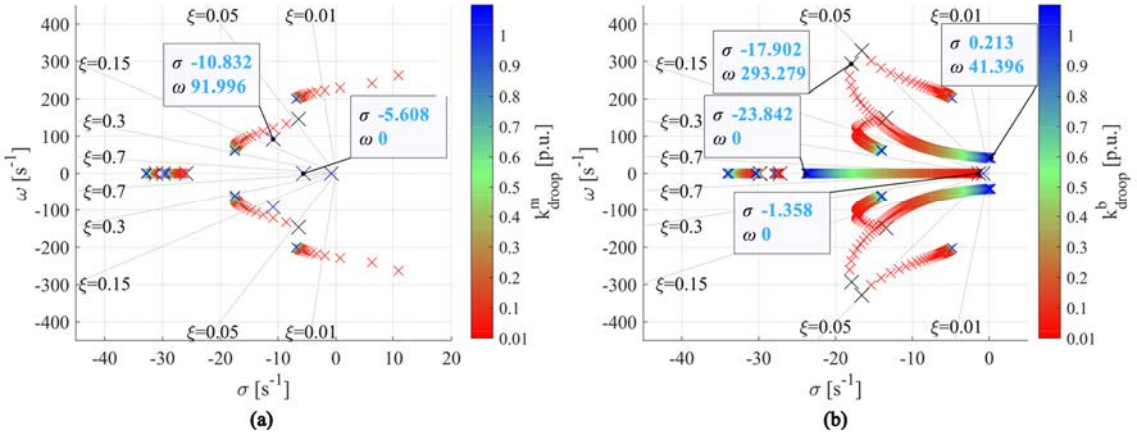

Figure 5.53. Root locus of the system as a function of the droop coefficient of a) the symmetrical monopolar HVDC station and b) the bipolar HVDC station.

Figure 5.53 (a) shows that the droop coefficient of the monopolar station $\left(k_{droop}^{m}\right)$ affects several modes in the system. Particularly, the worst damped mode unrelated to the asymmetrical DC operation becomes a non-stable oscillatory mode for small droop coefficients of the monopolar station. However, as expected from the results of the sensitivity analysis in Figure 5.42 and Figure 5.43, the two modes related to the asymmetrical DC operation are not affected by this droop coefficient. Nonetheless, it can be concluded that higher values for the droop coefficient of the monopolar station improve the system stability.

On the other hand, Figure 5.53 (b) shows that the droop coefficient of the bipolar station $\left(k_{droop}^{b}\right)$ also affects several modes in the system, including the two modes involved in the asymmetrical DC operation, as evidenced by the participation factors depicted in Figure 5.54. Note that the oscillatory mode related to the asymmetrical DC operation becomes a non-stable oscillatory mode for high values of the droop coefficient, whereas the real mode notably increases its decay rate. Therefore, the droop coefficient of the bipolar station causes an opposite effect on both modes. Furthermore, observe that for small droop coefficients, the real mode approaches the imaginary axis and turns into a very slow mode. In contrast, the oscillatory mode decreases its damping ratio but remains stable. The increment of the droop coefficient of the bipolar station also diminishes the

damping ratio of the other oscillatory mode that is not involved in the asymmetrical DC operation.

High droop coefficients in the bipolar station imply that this station loses its ability to control the DC voltage effectively, which explains why the oscillatory mode related to the asymmetrical DC operation turns unstable.

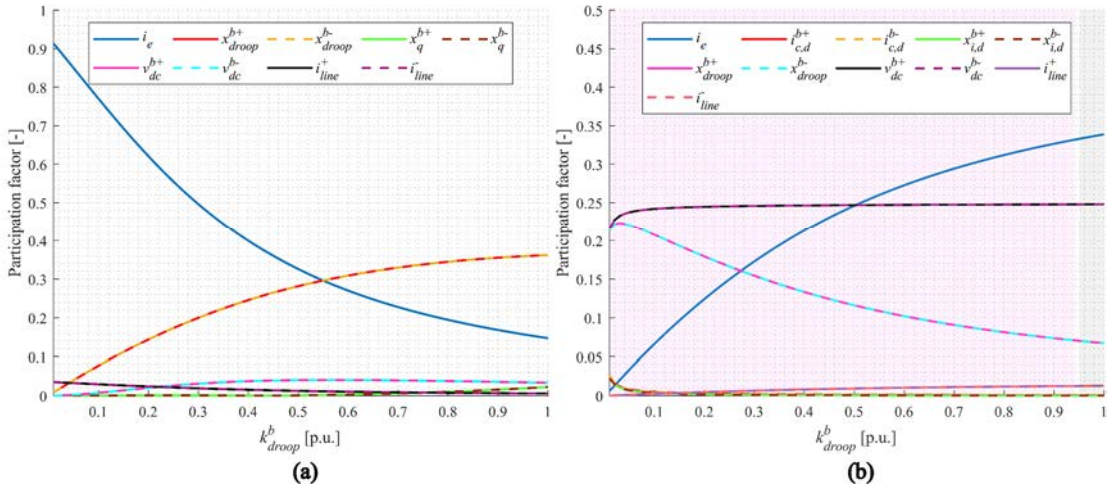

Figure 5.54. System variables with the highest participation factor in the real (a) and the oscillatory (b) mode as a function of k^b_{droop}. The white zone stands for a real and stable mode, the red zone for an underdamped mode, and the grey zone for an unstable mode.

The analysis of this section demonstrates that the DC voltage droop controller settings affect significatively to the stability of the system, not only from the point of view of the asymmetrical DC operation. However, the two modes involved in the asymmetrical DC operation are only influenced by the DC voltage droop controller settings of the bipolar station.

The proportional $\left(kp^b_{droop}\right)$ and integral $\left(ki^b_{droop}\right)$ gains affect more significatively the oscillatory mode and, to a lesser extent, the real mode. Small values for these gains generally decrease the damping ratio of the oscillatory mode, making it more unstable. However, large values of the proportional gain may cause the real mode to approach the imaginary axis, resulting in a slow transient during asymmetrical DC operation. Similarly, the droop coefficient value $\left(k^b_{droop}\right)$ should be chosen carefully, paying attention that high values make the system unstable and low values lead to poorly damped oscillatory modes and a real mode close to the origin, implying very slow transients. Therefore, unlike the case where the monopolar station controls the DC voltage, the correct tune of the DC voltage droop controllers is important to achieve stability during asymmetrical DC operations.

5.4.6. Impact of the zero–sequence controller

The zero-sequence controller introduced to enhance system stability during asymmetrical DC operations is unnecessary when the system implements a distributed DC voltage droop control strategy since the system stability depends on the correct tuning of the DC

voltage droop controller. Nevertheless, from the controllability and observability studies, this zero-sequence controller can control both modes related to the asymmetrical DC operation. Therefore, the impact of this controller in the symmetrical monopolar HVDC station on the stability and the dynamic response when the distributed DC voltage droop control regulates the DC grid is assessed below.

The effect of the gain k_{d0} in the modes of the system is shown in Figure 5.55 (a). On the one hand, the controller introduces a new real mode that moves from $\sigma = -3.3333\ s^{-1}$ to the right in the complex plane as the gain increases, implying a very slow transient in the system during asymmetrical operation. On the other hand, the real and the oscillatory modes increase their decay rate, although the latter is not significant.

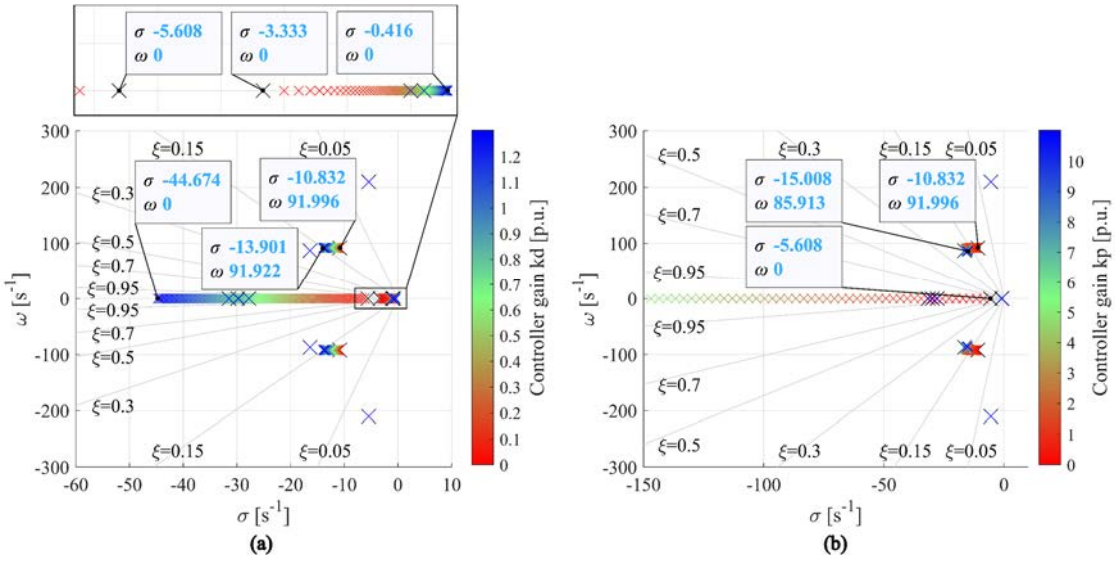

Figure 5.55. Root locus of the system for a sweep of the gain k_{d0} (a) and k_{p0} (b) of the zero-sequence voltage controller.

As for the proportional gain k_{p0}, it behaves as a virtual grounding resistance moving the mode, as shown in Figure 5.55 (b). This improves the decay rate of the real and the oscillatory mode but modifies the steady state during a permanent asymmetrical DC operation.

5.5. Conclusions

This chapter has analysed the small-signal stability of a heterogeneous DC system under asymmetrical DC operation using the model developed in Chapter 4.

The analysis has demonstrated that the small-signal stability during the asymmetrical DC operation is very dependent on the control strategy of the system and the specific control implemented in each topology.

When the system implements a centralised voltage control in the symmetrical monopolar HVDC station, the main factors that influence the stability during asymmetrical DC operation are a) the grounding impedance and b) the point of operation, particularly the direction of the DC current in the system. It is also important to highlight that under this

control strategy, the controllers of the HVDC stations do not have any impact on the stability related to the asymmetrical operation.

In addition, in the case of the bipolar station is responsible for the DC voltage regulation, the small-signal analysis has identified that two main factors influence the system stability during the asymmetrical DC operation: a) the grounding impedance and b) the tuning of the DC voltage controller. Besides, under this scenario, the voltage controller of the bipolar station affects the stability of other modes different from those related to the asymmetrical DC operation.

Finally, when a distributed DC voltage control is implemented, the main aspects that impact the stability during asymmetrical operation are a) the grounding impedance and b) the settings of the DC voltage droop controller of the bipolar station. Although the droop controller of the monopolar station does not influence the stability during asymmetrical DC operation, it affects the stability due to interactions with the controller of the bipolar HVDC station.

Therefore, since the grounding impedance is a common factor that directly affects the small-signal stability of the system during asymmetrical operation, it should be designed incorporating the stability constraints as an additional design criterion.

In addition, due to the influence that the parameterisation of the controllers has over the stability under asymmetrical operation, their configuration and design must consider this type of functioning and avoid a design based solely on symmetrical operation scenarios.

Furthermore, the small-signal model may also be used to develop controllers that improve the dynamic response of the system during asymmetrical DC operation, tune them, or select their best location in the case of large DC systems.

Future works should explore the implications of the asymmetrical DC operation in larger DC grids.

CHAPTER 6. CONCLUSIONS

This final chapter summarises the main conclusions and contributions of the thesis and points out possible continuation lines for future work.

6.1. Summary

The primary objective of this thesis has been to analyse the asymmetrical operation of DC systems formed by different HVDC station topologies with varying grounding systems and working with different control strategies. The study has been carried out from various approaches that encompass the load-flow calculation, the dynamic EMT simulation, the small-signal modelling, and the small-signal stability analysis. The assessment from these different perspectives has identified the main aspects involved in the asymmetrical DC operation and the operational issues that the asymmetrical DC operation poses for the correct working of the whole system. The main contributions of the thesis are presented in section 6.2; the main conclusions drawn from each chapter are gathered in section 6.3; and, finally, recommendations for future work are provided in section 6.4.

6.2. Contributions

- Load-flow-based assessment of a DC system composed of different topologies of HVDC stations, grounding systems and DC-DC converters that identifies the main parameters that participate in the asymmetrical DC operation steady state and their impact on the complete system while different control strategies are considered.
- Dynamic evaluation of a system composed of different HVDC stations topologies and grounding systems, which identifies the main parameters involved in the transient response during asymmetrical DC operation and their impact on the system considering different control strategies.
- Assessment of the impact that the connection of a symmetrical monopolar station to a bipolar system has over the existing protections considering different grounding impedances.
- Development of small-signal models suitable for analysing the asymmetrical DC operation and their validation against EMT dynamic simulations considering different controllers and grounding impedances.
- Small-signal stability assessment of a system composed of different HVDC station topologies and grounding schemes, which identifies the main system variables and control parameters involved during asymmetrical operation considering different control strategies.
- Development of a controller that enhances the system stability when existing controllers are insufficient.

6.3. Main conclusions

The main conclusions of each chapter of the thesis are gathered below.

6.3.1. Conclusions on the load flow analysis

Chapter 2 has dealt with the asymmetrical operation of a meshed DC grid composed of different MMC-VSC-based station topologies and DC-DC converters from a load-flow approach for the first time in the literature.

It has been found that the main aspects that influence the steady state after an asymmetrical contingency are: a) the grounding resistance of each symmetrical monopolar HVDC station; b) the control role of each bipolar HVDC station, which can be approximated as an equivalent resistance for the steady-state analysis, and its point of operation; and c) the ability of DC-DC converters to provide galvanic isolation or not.

Results in this chapter demonstrate that different combinations of the previously listed aspects cause other DC voltage and current asymmetries along the DC system, which are related to component overloading and excessive voltage deviations.

Therefore, this chapter highlights the importance of performing this type of N-1 analysis to identify potential issues after the occurrence of certain asymmetrical contingencies in the DC network. Furthermore, this methodology can be used to plan and design remedial action schemes and point out grid elements needed for reinforcement.

In addition, this steady-state approach can be used as an additional criterion for the design of the grounding scheme, the control strategy of the DC network, or to decide which type of DC-DC converter topology can be suitable in a specific location.

6.3.2. Conclusion on the EMT dynamic analysis

In Chapter 3, the asymmetrical DC operation of a DC system composed of MMC-VSC-based bipolar and symmetrical monopolar stations is analysed through dynamic simulations for the first time.

The analysis identifies that the transient response during asymmetrical DC operation is strongly determined by the grounding impedance, the role of the converter suffering the contingency and the control strategy of the complete system.

The diverse combinations of grounding resistance and control strategies can cause overvoltages, overcurrents, converter saturation, oscillations at the DC and AC side of the converter, and instability. In general, solid or high grounding symmetrical monopolar stations conduct the system to any of the situations described above, so a specific value of grounding resistance is recommended from the point of view of the asymmetrical DC operation.

In addition, it is also found that the grounding impedance of a symmetrical monopolar station connected to an existing bipolar system does not affect the performance of the existing protections if they present fast actuation.

6.3.3. Conclusions on the small-signal modelling

A new small-signal stability model valid for the analysis of DC systems working during asymmetrical DC operation is presented in Chapter 4. The small-signal model is validated

against EMT dynamic simulations using different control strategies, grounding impedance values and control parameters.

This model can diagnose stability issues related to the asymmetrical operation that cannot be detected with other small-signal models. Furthermore, it can be used to study the stability of large DC systems avoiding the high computational burden of EMT simulations.

6.3.4. Conclusions on the small-signal analysis

Chapter 5 addresses the small-signal stability analysis of a DC system composed of a bipolar and a symmetrical monopolar station.

The main findings are that the system stability during asymmetrical DC operation is highly determined by the control strategy of the system and the grounding impedance of the symmetrical monopolar station. Furthermore, depending on the control strategy, other important factors from the stability point of view are identified:

- The DC current direction plays a crucial role in the stability when the symmetrical monopolar station controls the DC voltage. However, the parameters of the controllers of both stations do not affect the asymmetrical response.
- The proportional and integral gains of the DC voltage controller have a high weight on the system stability when the bipolar HVDC station controls the DC voltage.
- When a distributed control is implemented, only the droop coefficient and the proportional and integral gains of the droop controller of the bipolar HVDC station affect the system stability.

Furthermore, a new controller is proposed based on the small-signal analysis results to improve the system stability when the symmetrical monopolar station controls the DC voltage.

The results obtained from the small-signal analysis of such a heterogeneous system have provided additional criteria for designing the grounding impedance and configuring and designing the controllers.

6.4. Future works

To widen the scope of the work presented in this thesis, some topics for future investigation are proposed below.

Load flow analysis

Development of standard methodologies considering the asymmetrical DC operation for system planning, grounding impedance design, remedial action schemes design or selection and optimisation of the location of DC-DC converters considering its galvanic isolation capability. In addition, the analysis could be extended to systems with VSC and LCC-based technology.

Dynamic analysis

Analysis of the asymmetrical DC operation in larger systems, incorporating other elements such as different topologies of DC-DC converters. Furthermore, the effect of varying topologies in the protection system could also be assessed.

Small-signal modelling for the analysis of the asymmetrical DC operation

Develop suitable small-signal models for other components, such as DC-DC converters or LCC topologies.

Small-signal stability analysis of the asymmetrical DC operation

Study the small-signal stability of larger and more complex DC systems under asymmetrical DC operation, considering other components and new controllers. Assess the impact of other grid components, the location of the grounding point or new control strategies on the small-signal stability.

REFERENCES

[1] "2030 Climate Target Plan." https://climate.ec.europa.eu/eu-action/european-green-deal/2030-climate-target-plan_en (accessed Feb. 17, 2023).

[2] L. Michi *et al.*, "New HVDC technology in Pan-European power system planning," *2019 AEIT HVDC Int. Conf. AEIT HVDC 2019*, May 2019, doi: 10.1109/AEIT-HVDC.2019.8740544.

[3] D. Van Hertem and M. Ghandhari, "Multi-terminal VSC HVDC for the European supergrid: Obstacles," *Renew. Sustain. Energy Rev.*, vol. 14, no. 9, pp. 3156–3163, 2010, doi: 10.1016/j.rser.2010.07.068.

[4] E. Pierri, O. Binder, N. G. A. Hemdan, and M. Kurrat, "Challenges and opportunities for a European HVDC grid," *Renew. Sustain. Energy Rev.*, vol. 70, pp. 427–456, Apr. 2017, doi: 10.1016/J.RSER.2016.11.233.

[5] D. Van Hertem, O. Gomis-bellmunt, and J. Liang, *HVDC grids: for offshore and supergrid of the future*. John Wiley & Son, 2016.

[6] M. H. Okba, M. H. Saied, M. Z. Mostafa, and T. M. Abdel- Moneim, "High voltage direct current transmission - A review, part I," in *2012 IEEE Energytech*, May 2012, pp. 1–7. doi: 10.1109/EnergyTech.2012.6304650.

[7] S. Mirsaeidi, A. Giramata, D. Tzelepis, J. He, D. M. Said, and K. M. Muttaqi, "An Introspective Review on Commutation Failure Inhibition Strategies in LCC-HVDC Transmission Networks," *Conf. Rec. - IAS Annu. Meet. (IEEE Ind. Appl. Soc.*, vol. 2022-October, 2022, doi: 10.1109/IAS54023.2022.9939962.

[8] M. Kurtoğlu, F. Eroğlu, A. O. Arslan, and A. M. Vural, "Recent contributions and future prospects of the modular multilevel converters: A comprehensive review," *Int. Trans. Electr. Energy Syst.*, vol. 29, no. 3, p. e2763, Mar. 2019, doi: 10.1002/ETEP.2763.

[9] B. Gemmell, J. Dorn, D. Retzmann, and D. Soerangr, "Prospects of multilevel VSC technologies for power transmission," in *2008 IEEE/PES Transmission and Distribution Conference and Exposition*, Apr. 2008, pp. 1–16. doi: 10.1109/TDC.2008.4517192.

[10] Y. Tian, H. R. Wickramasinghe, Z. Li, J. Pou, and G. Konstantinou, "Review, Classification and Loss Comparison of Modular Multilevel Converter Submodules for HVDC Applications," *Energies 2022, Vol. 15, Page 1985*, vol. 15, no. 6, p. 1985, Mar. 2022, doi: 10.3390/EN15061985.

[11] M. N. Sakib, S. P. Azad, and M. Kazerani, "A Critical Review of Modular Multilevel Converter Configurations and Submodule Topologies from DC Fault Blocking and Ride-Through Capabilities Viewpoints for HVDC Applications," *Energies 2022, Vol. 15, Page 4176*, vol. 15, no. 11, p. 4176, Jun. 2022, doi: 10.3390/EN15114176.

[12] S. Gordon, "Supergrid to the rescue [electricity supply security]," *Power Eng.*, vol. 20, no. 5, p. 30, 2006, doi: 10.1049/pe:20060505.

[13] D. Van Hertem, M. Ghandhari, and M. Delimar, "Technical limitations towards a SuperGrid - A European prospective," *2010 IEEE Int. Energy Conf. Exhib. EnergyCon 2010*, pp. 302–309, 2010, doi: 10.1109/ENERGYCON.2010.5771696.

[14] R. Adapa, "High-wire act: HVdc technology: The state of the art," *IEEE Power Energy Mag.*, vol. 10, no. 6, pp. 18–29, 2012, doi: 10.1109/MPE.2012.2213011.

[15] P. L. Francos, S. S. Verdugo, H. F. Alvarez, S. Guyomarch, and J. Loncle, "INELFE — Europe's first integrated onshore HVDC interconnection," in *2012 IEEE Power and Energy Society General Meeting*, Jul. 2012, pp. 1–8. doi: 10.1109/PESGM.2012.6344799.

[16] X. Li, Z. Yuan, J. Fu, Y. Wang, T. Liu, and Z. Zhu, "Nanao multi-terminal VSC-HVDC project for integrating large-scale wind generation," in *2014 IEEE PES General Meeting | Conference & Exposition*, Jul. 2014, pp. 1–5. doi: 10.1109/PESGM.2014.6939123.

[17] Y. Pipelzadeh, B. Chaudhuri, T. C. Green, Y. Wu, H. Pang, and J. Cao, "Modelling and Dynamic Operation of the Zhoushan DC Grid: Worlds First Five-Terminal VSC-HVDC Project," in *International High Voltage Direct Current 2015 Conference*, Oct. 2015. doi: 10.13140/RG.2.1.3449.3202.

[18] A. H. Manchola, T. Priebe, M. Hölzer, and M. Dommaschk, "VSC HVDC active damping for the Sylwin 1 offshore wind power plants," *J. Eng.*, vol. 2019, no. 18, pp. 4748–4753, Jul. 2019, doi: 10.1049/JOE.2018.9240.

[19] "Petrofac Hands over BorWin3 Offshore Wind Grid Connection Project to TenneT," *Gulf Oil & Gas*. SyndiGate Media Inc, Cairo, 2020.

[20] B. D. Railing *et al.*, "Cross sound cable project second generation VSC technology for HVDC," in *Cigré conference*, Aug. 2004.

[21] S. E. Schrader and F. E. Benth, "A stochastic study of carbon emission reduction from electrification and interconnecting cable utilization. The Norway and Germany case," *Energy Econ.*, vol. 114, p. 106300, Oct. 2022, doi: 10.1016/J.ENECO.2022.106300.

[22] European Network of Transmission System Operators for Electricity (ENTSO-e), "HVDC Links in System Operations," 2019, Accessed: Sep. 26, 2021. [Online]. Available: https://eepublicdownloads.entsoe.eu/clean-documents/SOC documents/20191203_HVDC links in system operations.pdf

[23] European Network of Transmission System Operators for Electricity (ENTSO-E), "Documents - TYNDP," 2023. https://tyndp.entsoe.eu/documents/ (accessed Feb. 18, 2023).

[24] D. Van Hertem *et al.*, "Substations for Future HVdc Grids: Equipment and Configurations for Connection of HVdc Network Elements," *IEEE Power Energy Mag.*, vol. 17, no. 4, pp. 56–66, Jul. 2019, doi: 10.1109/MPE.2019.2909006.

[25] A. Alassi, S. Bañales, O. Ellabban, G. Adam, and C. MacIver, "HVDC Transmission: Technology Review, Market Trends and Future Outlook," *Renew. Sustain. Energy Rev.*, vol. 112, pp. 530–554, Sep. 2019, doi: 10.1016/J.RSER.2019.04.062.

[26] G. Tang, Z. He, H. Pang, X. Huang, and X. Zhang, "Basic topology and key devices of the five-terminal DC grid," *CSEE J. Power Energy Syst.*, vol. 1, no. 2, pp. 22–35, Jul. 2015, doi: 10.17775/CSEEJPES.2015.00016.

[27] C. Guo, Z. Yin, C. Zhao, and R. Iravani, "Small-signal dynamics of hybrid LCC-VSC HVDC systems," *Int. J. Electr. Power Energy Syst.*, vol. 98, pp. 362–372, Jun. 2018, doi: 10.1016/J.IJEPES.2017.12.010.

[28] X. Guo, Y. Zhou, N. Mei, and B. Zhao, "Construction and Characteristic Analysis of Zhangbei Flexible DC Grid," *Dianwang Jishu/Power Syst. Technol.*, vol. 42,

no. 11, pp. 3698–3707, Nov. 2018, doi: 10.13335/J.1000-3673.PST.2017.2461.

[29] M. Wang *et al.*, "Review and outlook of HVDC grids as backbone of transmission system," *CSEE J. Power Energy Syst.*, vol. 7, no. 4, pp. 797–810, Jul. 2021, doi: 10.17775/CSEEJPES.2020.04890.

[30] V. Akhmatov *et al.*, "Technical guidelines and prestandardization work for first HVDC Grids," *IEEE Trans. Power Deliv.*, vol. 29, no. 1, pp. 327–335, 2014, doi: 10.1109/TPWRD.2013.2273978.

[31] M. Wang, J. Beerten, and D. Van Hertem, "DC fault analysis in bipolar HVDC grids," *Proc. IEEE YRS 2016*, vol. 8, no. 1, p. 1, 2016, Accessed: Jul. 12, 2021. [Online]. Available: https://lirias.kuleuven.be/1731368

[32] S. De Boeck, P. Tielens, W. Leterme, and D. Van Hertem, "Configurations and earthing of HVDC grids," *IEEE Power Energy Soc. Gen. Meet.*, pp. 1–5, 2013, doi: 10.1109/PESMG.2013.6672808.

[33] W. Leterme, P. Tielens, S. De Boeck, and D. Van Hertem, "Overview of grounding and configuration options for meshed HVDC grids," *IEEE Transactions on Power Delivery*, vol. 29, no. 6. 2014. doi: 10.1109/TPWRD.2014.2331106.

[34] M. K. Bucher and C. M. Franck, "Comparison of fault currents in multiterminal HVDC grids with different grounding schemes," in *2014 IEEE PES General Meeting | Conference & Exposition*, 2014, pp. 1–5. doi: 10.1109/PESGM.2014.6938990.

[35] M. Muniappan, "A comprehensive review of DC fault protection methods in HVDC transmission systems," *Prot. Control Mod. Power Syst. 2021 61*, vol. 6, no. 1, pp. 1–20, Jan. 2021, doi: 10.1186/S41601-020-00173-9.

[36] L. Chen *et al.*, "Combinatorial Multi-Objective Optimization of Resistive SFCL and DC Circuit Breaker in Hybrid HVDC Transmission System," *IEEE Trans. Appl. Supercond.*, vol. 31, no. 8, Nov. 2021, doi: 10.1109/TASC.2021.3094430.

[37] F. Mohammadi *et al.*, "HVDC Circuit Breakers: A Comprehensive Review," *IEEE Trans. Power Electron.*, vol. 36, no. 12, pp. 13726–13739, Dec. 2021, doi: 10.1109/TPEL.2021.3073895.

[38] M. Barnes, D. S. Vilchis-Rodriguez, X. Pei, R. Shuttleworth, O. Cwikowski, and A. C. Smith, "HVDC Circuit Breakers-A Review," *IEEE Access*, vol. 8, pp. 211829–211848, 2020, doi: 10.1109/ACCESS.2020.3039921.

[39] M. J. Pérez-Molina, D. M. Larruskain, P. Eguía López, and G. Buigues, "Challenges for Protection of Future HVDC Grids," *Front. Energy Res.*, vol. 8, p. 33, Feb. 2020, doi: 10.3389/FENRG.2020.00033.

[40] J. D. Paez, D. Frey, J. Maneiro, S. Bacha, and P. Dworakowski, "Overview of DC-DC Converters Dedicated to HVdc Grids," *IEEE Trans. Power Deliv.*, vol. 34, no. 1, pp. 119–128, Feb. 2019, doi: 10.1109/TPWRD.2018.2846408.

[41] D. Jovcic, M. Taherbaneh, J. P. Taisne, and S. Nguefeu, "Developing regional, radial DC grids and their interconnection into large DC grids," *IEEE Power Energy Soc. Gen. Meet.*, vol. 2014-Octob, no. October, Oct. 2014, doi: 10.1109/PESGM.2014.6939425.

[42] G. P. Adam, I. A. Gowaid, S. J. Finney, D. Holliday, and B. W. Williams, "Review of dc–dc converters for multi-terminal HVDC transmission networks," *IET Power*

Electron., vol. 9, no. 2, pp. 281–296, Feb. 2016, doi: 10.1049/IET-PEL.2015.0530.

[43] S. Dey and T. Bhattacharya, "Operation of a Modular DC-DC Converter for Hybrid Interconnection of Monopolar and Bipolar HVDC Links," *IEEE Trans. Ind. Appl.*, vol. 58, no. 4, pp. 4943–4954, 2022, doi: 10.1109/TIA.2022.3173269.

[44] D. Gomez, "DC-DC Converters for HVDC Heterogeneous Interconnections," Ph.D. dissertation, Universitat Politècnica de Catalunya, Barcelona, 2022.

[45] A. J. Agbemuko, J. L. Dominguez-Garcia, E. Prieto-Araujo, and O. Gomis-Bellmunt, "Advanced Impedance-Based Control Design for Decoupling Multi-Vendor Converter HVDC Grids," *IEEE Trans. Power Deliv.*, vol. 35, no. 5, pp. 2459–2470, Oct. 2020, doi: 10.1109/TPWRD.2020.2968761.

[46] A. Egea-Alvarez, J. Beerten, D. Van Hertem, and O. Gomis-Bellmunt, "Hierarchical power control of multiterminal HVDC grids," *Electr. Power Syst. Res.*, vol. 121, pp. 207–215, 2015, doi: 10.1016/j.epsr.2014.12.014.

[47] T. K. Vrana, J. Beerten, R. Belmans, and O. B. Fosso, "A classification of DC node voltage control methods for HVDC grids," *Electr. Power Syst. Res.*, vol. 103, pp. 137–144, 2013, doi: 10.1016/j.epsr.2013.05.001.

[48] R. Eriksson, J. Beerten, M. Ghandhari, and R. Belmans, "Optimizing DC Voltage Droop Settings for AC/DC System Interactions," *IEEE Trans. Power Deliv.*, vol. 29, no. 1, pp. 362–369, Feb. 2014, doi: 10.1109/TPWRD.2013.2264757.

[49] M. Goertz, S. Wenig, S. Beckler, C. Hirsching, M. Suriyah, and T. Leibfried, "Analysis of Cable Overvoltages in Symmetrical Monopolar and Rigid Bipolar HVDC Configuration," *IEEE Trans. Power Deliv.*, vol. 35, no. 4, pp. 2097–2107, Aug. 2020, doi: 10.1109/TPWRD.2019.2960851.

[50] E. Berne, G. Bergna, P. Egrot, and Q. Wolff, "Earth currents in HVDC grids: An example based on 5 terminal bipolar configurations," in *2014 16th European Conference on Power Electronics and Applications, EPE-ECCE Europe 2014*, 2014. doi: 10.1109/EPE.2014.6910729.

[51] X. Shi, Z. Wang, B. Liu, Y. Li, L. M. Tolbert, and F. Wang, "Steady-State Modeling of Modular Multilevel Converter under Unbalanced Grid Conditions," *IEEE Trans. Power Electron.*, vol. 32, no. 9, pp. 7306–7324, Sep. 2017, doi: 10.1109/TPEL.2016.2629472.

[52] M. Guan and Z. Xu, "Modeling and Control of a Modular Multilevel Converter-Based HVDC System Under Unbalanced Grid Conditions," *IEEE Trans. Power Electron.*, vol. 27, no. 12, pp. 4858–4867, Dec. 2012, doi: 10.1109/TPEL.2012.2192752.

[53] H. Aji, M. Ndreko, M. Popov, and M. A. M. M. van der Meijden, "Investigation on different negative sequence current control options for MMC-HVDC during single line to ground AC faults," in *2016 IEEE PES Innovative Smart Grid Technologies Conference Europe (ISGT-Europe)*, Oct. 2016, pp. 1–6. doi: 10.1109/ISGTEurope.2016.7856182.

[54] A. M. Kulkarni and P. B. Darji, "Dynamic performance of a modular multi-level converter based HVDC terminal under unbalanced AC grid conditions," in *10th IET International Conference on AC and DC Power Transmission (ACDC 2012)*, 2012, pp. 22–22. doi: 10.1049/cp.2012.1964.

[55] G. Falahi and A. Huang, "Control of modular multilevel converter based HVDC

systems during asymmetrical grid faults," in *IECON 2014 - 40th Annual Conference of the IEEE Industrial Electronics Society*, Oct. 2014, pp. 4595–4600. doi: 10.1109/IECON.2014.7049195.

[56] Y. Liang, J. Liu, T. Zhang, and Q. Yang, "Arm Current Control Strategy for MMC-HVDC under Unbalanced Conditions," *IEEE Trans. Power Deliv.*, 2017, doi: 10.1109/TPWRD.2016.2554620.

[57] G. Li, J. Liang, F. Ma, C. E. Ugalde-Loo, H. Liang, and H. Li, "Analysis of single-phase-to-ground faults at the valve-side of HB-MMCs in bipolar HVDC systems," in *2017 IEEE Energy Conversion Congress and Exposition, ECCE 2017*, 2017. doi: 10.1109/ECCE.2017.8096501.

[58] Y. Yanchen, M. Shicong, and L. Yingbiao, "Analysis and control strategy of unbalanced power in MMC-HVDC grid," *J. Eng.*, vol. 2017, no. 13, pp. 2211–2214, Jan. 2017, doi: 10.1049/joe.2017.0723.

[59] X. Shi, Z. Wang, B. Liu, Y. Liu, L. M. Tolbert, and F. Wang, "Characteristic investigation and control of a modular multilevel converter-based HVDC system under single-line-to-ground fault conditions," *IEEE Trans. Power Electron.*, 2015, doi: 10.1109/TPEL.2014.2323360.

[60] Y. Tao, B. Li, and T. Liu, "Pole-to-ground fault current estimation in symmetrical monopole high-voltage direct current grid considering modular multilevel converter control," *Electron. Lett.*, vol. 56, no. 8, pp. 392–395, Apr. 2020, doi: 10.1049/EL.2019.4080.

[61] N. A. Belda, C. A. Plet, and R. P. P. Smeets, "Analysis of Faults in Multiterminal HVDC Grid for Definition of Test Requirements of HVDC Circuit Breakers," *IEEE Trans. Power Deliv.*, vol. 33, no. 1, pp. 403–411, Feb. 2018, doi: 10.1109/TPWRD.2017.2716369.

[62] E. Kontos, G. Tsolaridis, R. Teodorescu, and P. Bauer, "On DC Fault Dynamics of MMC-Based HVdc Connections," *IEEE Trans. Power Deliv.*, vol. 33, no. 1, pp. 497–507, Feb. 2018, doi: 10.1109/TPWRD.2017.2764162.

[63] J. Dragon, L. Werner, and J. Hanson, "Effects of DC voltage droop characteristics on contingency behaviour of AC/DC systems," *Proc. Univ. Power Eng. Conf.*, 2014, doi: 10.1109/UPEC.2014.6934686.

[64] A. K. Marten and D. Westermann, "Schedule for converters of a meshed HVDC grid and a contingency schedule for adaption to unscheduled power flow changes," *IEEE Power Energy Soc. Gen. Meet.*, pp. 1–5, 2013, doi: 10.1109/PESMG.2013.6672303.

[65] J. Hu, K. Xu, L. Lin, and R. Zeng, "Analysis and enhanced control of hybrid-MMC-based HVDC systems during asymmetrical dc voltage faults," *IEEE Trans. Power Deliv.*, vol. 32, no. 3, pp. 1394–1403, Jun. 2017, doi: 10.1109/TPWRD.2016.2568240.

[66] W. Xiang, W. Lin, J. Wen, and C. Luo, "Four-channel control of hybrid MMC with pole-to-ground DC fault ride through capability," *IEEE Power Energy Soc. Gen. Meet.*, vol. 2018-January, pp. 1–5, Jan. 2018, doi: 10.1109/PESGM.2017.8274677.

[67] W. Xiang, W. Lin, L. Xu, and J. Wen, "Enhanced Independent Pole Control of Hybrid MMC-HVdc System," *IEEE Trans. Power Deliv.*, vol. 33, no. 2, pp. 861–

872, Apr. 2018, doi: 10.1109/TPWRD.2017.2715040.

[68] M. Lu, J. Hu, R. Zeng, and Z. He, "Fundamental-Frequency Reactive Circulating Current Injection for Capacitor Voltage Balancing in Hybrid-MMC HVDC Systems during Riding Through PTG Faults," *IEEE Trans. Power Deliv.*, vol. 33, no. 3, pp. 1348–1357, Jun. 2018, doi: 10.1109/TPWRD.2017.2755505.

[69] F. Gonzalez-Longatt, J. L. Rueda, and M. A. M. M. Van Der Meijden, "Effects of grounding configurations on post-contingency performance of MTDC system: A 3-Terminal example," in *Proceedings of the Universities Power Engineering Conference*, 2015. doi: 10.1109/UPEC.2015.7339912.

[70] E. Prieto-Araujo, A. Junyent-Ferre, G. Clariana-Colet, and O. Gomis-Bellmunt, "Control of modular multilevel converters under singular unbalanced voltage conditions with equal positive and negative sequence components," *IEEE Trans. Power Syst.*, vol. 32, no. 3, pp. 2131–2141, May 2017, doi: 10.1109/TPWRS.2016.2598617.

[71] H. Zhang, H. R. Wickramasinghe, L. Jing, J. Li, J. Pou, and G. Konstantinou, "Circulating current control scheme of modular multilevel converters supplying passive networks under unbalanced load conditions," *Electr. Power Syst. Res.*, vol. 171, pp. 36–46, Jun. 2019, doi: 10.1016/J.EPSR.2019.01.041.

[72] A. Junyent-Ferre, P. Clemow, M. M. C. Merlin, and T. C. Green, "Operation of HVDC modular multilevel converters under DC pole imbalances," in *2014 16th European Conference on Power Electronics and Applications, EPE-ECCE Europe 2014*, 2014. doi: 10.1109/EPE.2014.6911011.

[73] Z. Liu, S. Miao, Z. Fan, K. Chao, and Y. Liu, "Characteristics analysis and improved arm control of modular multilevel converter under asymmetric operation conditions," *Int. J. Electr. Power Energy Syst.*, vol. 105, pp. 272–282, Feb. 2019, doi: 10.1016/J.IJEPES.2018.08.037.

[74] M. Changizian, A. R. Mizani, and A. Shoulaie, "Proposed a New Voltage Rebalancing Method for Pole-to-Ground Fault in Bipolar Two Level VSC-HVDC," *IEEE Trans. Ind. Electron.*, 2021, doi: 10.1109/TIE.2021.3068668.

[75] J. He, K. Chen, M. Li, Y. Luo, C. Liang, and Y. Xu, "Review of protection and fault handling for a flexible DC grid," *Prot. Control Mod. Power Syst.*, vol. 5, no. 1, Dec. 2020, doi: 10.1186/S41601-020-00157-9.

[76] Y. Wang, B. Yang, H. Zuo, H. Liu, and H. Yan, "A DC Short-Circuit Fault Ride Through Strategy of MMC-HVDC Based on the Cascaded Star Converter," 2018, doi: 10.3390/en11082079.

[77] M. Wang, W. Leterme, G. Chaffey, J. Beerten, and D. Van Hertem, "Pole Rebalancing Methods for Pole-to-ground Faults in Symmetrical Monopolar HVDC Grids," *IEEE Transactions on Power Delivery*, 2018. doi: 10.1109/TPWRD.2018.2853704.

[78] H. Wang, G. Tang, Z. He, and J. Yang, "Efficient grounding for modular multilevel HVDC converters (MMC) on the AC side," *IEEE Trans. Power Deliv.*, vol. 29, no. 3, pp. 1262–1272, 2014, doi: 10.1109/TPWRD.2014.2311796.

[79] M. Wang, J. Beerten, and D. Van Hertem, "Pole voltage balancing in HVDC systems: Analysis and technology options," *2019 IEEE Milan PowerTech, PowerTech 2019*, 2019, doi: 10.1109/PTC.2019.8810816.

[80] M. Wang, W. Leterme, G. Chaffey, J. Beerten, and D. Van Hertem, "Protection and pole voltage rebalancing for pole-to-ground faults in symmetrical monopolar HVDC grids," *IET Conf. Publ.*, vol. 2019, no. CP751, 2019, doi: 10.1049/CP.2019.0043.

[81] W. H. Weihuang Huang *et al.*, "A calculation method for maximum steady-state loss of VSC-HVDC grounding resistor in Luxi back-back HVDC interconnector," in *12th IET International Conference on AC and DC Power Transmission (ACDC 2016)*, 2016, pp. 24 (5 .)-24 (5 .). doi: 10.1049/cp.2016.0404.

[82] C. A. Charalambous, "Interference Activity on Pipeline Systems from VSC-Based HVDC Cable Networks with Earth/Sea Return: An Insightful Review," *IEEE Trans. Power Deliv.*, vol. 36, no. 3, pp. 1531–1541, Jun. 2021, doi: 10.1109/TPWRD.2020.3011128.

[83] C. A. Charalambous and A. I. Nikolaidis, "Complete Method to Assess the DC Corrosion Impact on Pipeline Systems during the Planning and Approval Stages of HVDC Systems with Earth Current Return," *IEEE Access*, vol. 10, pp. 127550–127562, 2022, doi: 10.1109/ACCESS.2022.3226940.

[84] X. He, B. Zuo, L. Sun, Z. Li, Y. Wang, and Z. Jiao, "Research on Grounding Current Distribution in HVDC System Operating in Monopolar Mode," *2nd IEEE Conf. Energy Internet Energy Syst. Integr. EI2 2018 - Proc.*, Dec. 2018, doi: 10.1109/EI2.2018.8582584.

[85] Cigré Working Group B4.57, *Guide for the Development of Models for HVDC Converters in a HVDC Grid*, vol. 604, no. December. 2014.

[86] P. Systems Engineering Committee of the IEEE Industry Applications Society, *IEEE Std 142-2007 (Revision of IEEE Std 142-1991) IEEE Recommended Practice for Grounding of Industrial and Commercial Power Systems*, vol. 2007. 2007.

[87] S. Liu, Z. Xu, W. Hua, G. Tang, and Y. Xue, "Electromechanical transient modeling of modular multilevel converter based multi-terminal hvdc systems," *IEEE Trans. Power Syst.*, vol. 29, no. 1, pp. 72–83, 2014, doi: 10.1109/TPWRS.2013.2278402.

[88] C. Li, Y. Cao, Y. Yang, L. Wang, F. Blaabjerg, and T. Dragicevic, "Impedance-based method for DC stability of VSC-HVDC system with VSG control," *Int. J. Electr. Power Energy Syst.*, vol. 130, p. 106975, Sep. 2021, doi: 10.1016/J.IJEPES.2021.106975.

[89] J. Beerten, S. D'Arco, and J. A. Suul, "Identification and Small-Signal Analysis of Interaction Modes in VSC MTDC Systems," *IEEE Trans. Power Deliv.*, vol. 31, no. 2, 2016, doi: 10.1109/TPWRD.2015.2467965.

[90] S. D. Tavakoli, E. Prieto-Araujo, E. Sánchez-Sánchez, and O. Gomis-Bellmunt, "Interaction Assessment and Stability Analysis of the MMC-Based VSC-HVDC Link," *Energies 2020, Vol. 13, Page 2075*, vol. 13, no. 8, p. 2075, Apr. 2020, doi: 10.3390/EN13082075.

[91] C. Guo, A. Zheng, Z. Yin, and C. Zhao, "Small-signal stability of hybrid multi-terminal HVDC system," *Int. J. Electr. Power Energy Syst.*, vol. 109, pp. 434–443, Jul. 2019, doi: 10.1016/J.IJEPES.2019.02.031.

[92] O. Kotb, M. Ghandhari, R. Eriksson, and V. K. Sood, "On small signal stability of an AC/DC power system with a hybrid MTDC network," *Electr. Power Syst. Res.*,

vol. 136, pp. 79–88, Jul. 2016, doi: 10.1016/J.EPSR.2016.02.004.

[93] Z. Hai-lin, Y. Shu-jun, and Z. Peng, "Research on small-signal stability of hybrid multi-terminal HVDC system and control system parameter design," *J. Eng.*, vol. 2017, no. 13, pp. 2401–2406, Jan. 2017, doi: 10.1049/JOE.2017.0760.

[94] B. Rehman, C. Liu, W. Wei, C. Fu, and H. Li, "Applications of eigenvalues in installation of multi-infeed HVDC system for voltage stability," *Int. Trans. Electr. Energy Syst.*, vol. 30, no. 12, p. e12645, Dec. 2020, doi: 10.1002/2050-7038.12645.

[95] Q. Fu, W. Du, H. Wang, B. Ren, and X. Xiao, "Small-Signal Stability Analysis of a VSC-MTDC System for Investigating DC Voltage Oscillation," *IEEE Trans. Power Syst.*, vol. 36, no. 6, pp. 5081–5091, Nov. 2021, doi: 10.1109/TPWRS.2021.3072399.

[96] W. Liu, B. Qin, R. Zhang, J. Liu, and H. Li, "Impact of control system on small-signal stability of MMC-based MTDC transmission system," *Energy Reports*, vol. 6, pp. 1130–1135, Dec. 2020, doi: 10.1016/J.EGYR.2020.11.064.

[97] T. Abedin *et al.*, "Dynamic Modeling of HVDC for Power System Stability Assessment: A Review, Issues, and Recommendations," *Energies 2021, Vol. 14, Page 4829*, vol. 14, no. 16, p. 4829, Aug. 2021, doi: 10.3390/EN14164829.

[98] B. Qin, W. Liu, R. Zhang, T. Ding, and J. Liu, "Small-signal stability analysis and optimal control parameters design of MMC-based MTDC transmission systems," *IET Gener. Transm. Distrib.*, vol. 14, no. 21, pp. 4675–4683, Nov. 2020, doi: 10.1049/IET-GTD.2020.0063.

[99] M. Amin, M. Molinas, J. Lyu, and X. Cai, "Impact of power flow direction on the stability of VSC-HVDC seen from the impedance nyquist plot," *IEEE Trans. Power Electron.*, vol. 32, no. 10, pp. 8204–8217, Oct. 2017, doi: 10.1109/TPEL.2016.2608278.

[100] Q. Fu, W. Du, H. F. Wang, and B. Ren, "Analysis of Small-Signal Power Oscillations in MTDC Power Transmission System," *IEEE Trans. Power Syst.*, vol. 36, no. 4, pp. 3248–3259, Jul. 2021, doi: 10.1109/TPWRS.2020.3043041.

[101] J. Zhu *et al.*, "Coherence Analysis of System Characteristics and Control Parameters for Hybrid HVDC Transmission Systems Based on Small-signal Modeling," *IEEE J. Emerg. Sel. Top. Power Electron.*, pp. 1–1, Aug. 2020, doi: 10.1109/JESTPE.2020.3014434.

[102] A. B. Iskakov and I. B. Yadykin, "Lyapunov modal analysis and participation factors applied to small-signal stability of power systems," *Automatica*, vol. 132, p. 109814, Oct. 2021, doi: 10.1016/J.AUTOMATICA.2021.109814.

APPENDIX A. HVDC SYSTEM CONFIGURATION

A.1. System parameters

System parameters and base values are presented in the following tables.

Table A.1. Rated values of the system

System	Nominal Voltage	Rated frequency	Rated Power
AC Onshore	380 kV RMS LL	50 Hz	1000 MVA
AC Offshore	145 kV RMS LL	50 Hz	
DC Symmetrical Monopole	+/- 200 kV	-	
DC Bipole	+/- 400 kV	-	

Table A.2. General HVDC station data

HVDC station		Cm-E1	Cm-B3	Cm-A1 Cm-B2	Cm-C1 Cm-F1	Cb-A1 Cb-B1 Cb-B2	Cb-C2	Cb-D1
Configuration		Symmetrical Monopolar				Bipolar		
Rated power per converter (MVA)		200	1200	800	800	1200	800	800
Converter Transformer	Reactance (mH)	139	23	35	35	23	69	35
	Resistance (Ω)	1.45	0.242	0.363	0.363	0.242	0.726	0.363
	Primary winding voltage (kV)	145	380	380	145	380	145	145
	Secondary winding voltage (kV)	220	220	220	220	220	220	220

Table A.3. DC-DC converter data

DC-DC converter	Rated transformation ratio	Rated power
Cd-B1	±400 kV/±400 kV	2000 MW
Cd-E1	±400 kV/±200 kV	1000 MW

Table A.4. Line parameters for power flow simulations

Line type	R [Ω/km]	L [mH/km]	C [μF/km]	G [μS/km]	Max. current [A]
DC OHL +/- 400kV	0.0114	0.9356	0.0123	-	3500
DC OHL +/- 200kV	0.0133	0.8273	0.0139	-	3000
DC cable +/- 400kV	0.011	2.615	0.1908	0.048	2265
DC cable +/- 200kV	0.011	2.615	0.2185	0.055	1962
AC cable 145kV	0.0843	0.2526	0.1837	0.041	715
AC OHL 380kV	0.0200	0.8532	0.0135	-	3555

A.2. Operational data

The default operation data of each element in the system is gathered in this section.

Table A.5. Operational data of AC generators

AC Generator	Rated LL RMS Voltage	Type	Control	Set points
G-A0	380 kV	Voltage source	AC voltage magnitude	1.00 p.u.
			AC voltage angle	0.00 º
G-A1	380 kV	Power source	Active power	2000 MW
			Reactive power	0 Mvar
G-B0	380 kV	Voltage source	AC voltage magnitude	1.00 p.u.
			AC voltage angle	0.00 º
G-B1	380 kV	Power source	Active power	1000 MW
			Reactive power	0 Mvar
G-B2	380 kV	Power source	Active power	1000 MW
			Reactive power	0 Mvar
G-B3	380 kV	Power source	Active power	1000 MW
			Reactive power	0 Mvar
G-C1	145 kV	Power source	Active power	500 MW
			Reactive power	0 Mvar
G-C2	145 kV	Power source	Active power	500 MW
			Reactive power	0 Mvar
G-D1	145 kV	Power source	Active power	1000 MW
			Reactive power	0 Mvar
G-F1	145 kV	Power source	Active power	500 MW
			Reactive power	0 Mvar

Table A.6. Operational data of AC loads

AC Load	L-A1	L-B1	L-B2	L-B3	L-E1
Active power	-1000 MW	-2200 MW	-2300 MW	-1900 MW	-100 MW
Reactive power	0 Mvar	0 Mvar	0 Mvar	0 Mvar	0 Mvar

Table A.7. Operational data of DC-DC converters

DC-DC converter	Active power setpoint
Cd-B1	600 MW (from Bb-B1x to Cb-B1)
Cd-E1	300 MW (from Bb-E1 to Bm-E1)

Table A.8. Operational data of HVDC stations in DC system DCS1

HVDC station	Control	Set points
Cm-A1	DC voltage control	1.00 p.u.
	Reactive power control	0.00 Mvar
Cm-C1	Active power control	-400 MW
	Reactive power control	0.00 Mvar

Table A.9. Operational data of HVDC stations in DC system DCS2

HVDC station	Control	Set points
Cm-B2	DC voltage droop control	k_{droop} = 0.2 p.u. (based on its rated power) P_{ref} = -105.86 MW v_{dc_ref} = 1.00 p.u.
	Reactive power control	0.00 Mvar
Cm-B3	DC voltage droop control	k_{droop} = 0.2 p.u. (based on its rated power) P_{ref} = 800.00 MW v_{dc_ref} = 1.00 p.u.
	AC voltage magnitude control	1.00 p.u.
Cm-E1	AC voltage magnitude control	1.00 p.u.
	AC voltage phase control	0.00 º
Cm-F1	AC voltage magnitude control	1.00 p.u.
	AC voltage phase control	0.00 º

Table A.10. Operational data of HVDC stations in DC system DCS3

HVDC station	Control	Set points
Cb-A1	DC voltage droop control	k_{droop} = 0.2 p.u. (based on its rated power) P_{ref} = -1942.06 MW v_{dc_ref} = 1.00 p.u.
	AC voltage magnitude control	1.00 p.u.
Cb-B1	DC voltage droop control	k_{droop} = 0.2 p.u. (based on its rated power) P_{ref} = 1500.00 MW v_{dc_ref} = 1.00 p.u.
	AC voltage magnitude control	1.00 p.u.
Cb-B2	DC voltage droop control	k_{droop} = 0.2 p.u. (based on its rated power) P_{ref} = 1700.00 MW v_{dc_ref} = 1.00 p.u.
	AC voltage magnitude control	1.00 p.u.
Cb-C2	AC voltage magnitude control	1.00 p.u.
	AC voltage phase control	0.00 º
Cb-D1	AC voltage magnitude control	1.00 p.u.
	AC voltage phase control	0.00 º

APPENDIX B. SMALL-SIGNAL MODELLING DETAILS[4]

[4] This appendix reproduces part of the content published in J. Serrano-Sillero and M. Á. Moreno, "Small-signal stability analysis of the asymmetrical DC operation in HVDC networks," *Electr. Power Syst. Res.*, vol. 214, p. 108942, Jan. 2023.

B.1. Parameters

Table B.1. System parameters

Description	Symbol	Value	Base values		
			Voltage V_b	Power S_b	Frequency ω_b
Grid frequency	ω_g	1 p.u.	-	-	100π rad/s
Equivalent impedance of AC networks	l_g	0.0265 p.u.	380 kV	800 MVA	
	r_g	0.0027 p.u.			
Equivalent impedance of transformers	l_{trf}^m	0.18 p.u.	380/200 kV		
	r_{trf}^m	0.006 p.u.			
	l_{trf}^b	0.36 p.u.			
	r_{trf}^b	0.012 p.u.			
Arm impedance of converters	l_{arm}^m	0.1815 p.u.	200 kV		
	r_{arm}^m	0.0605 p.u.			
	l_{arm}^b	0.363 p.u.			
	r_{arm}^b	0.121 p.u.			
Equivalent capacitance of converter submodules	c_c^m	28.8634 p.u.	± 350 kV	400 MVA	
(c_c^b also includes the capacitance of the DC line)	c_c^b	28.9817 p.u.			
Equivalent parameters of the DC line	c_{line}	0.1183 p.u.			
	r_{line}	0.0072 p.u.			
	l_{line}	0.1920 p.u.			
Resistance between the neutral point of the zig-zag transformer and ground (changed along Chapter 5)	r_e	0 p.u.			
Equivalent default inductance of the zig-zag transformer (changed along Chapter 5)	l_e	1.6327 p.u.			

Table B.2. Control parameters

Description	**Outer Controller**								**Inner Controller**			
Symbol	kp_{vdc}	ki_{vdc}	kp_p	ki_p	kp_{vac}	ki_{vac}	kp_q	ki_q	kp_i	ki_i	l_{cc}^m	l_{cc}^b
Value	7.465	253.81	0	33	0	30	0	30	0.48	149	0.27075	0.1815

B.2. Dynamic Equations

AC side equations of the symmetrical monopolar HVDC station:

$$\frac{d\Delta i_{g,d}^m}{dt} = \left(\frac{\Delta v_{g,d}^m}{l_g} - \frac{\Delta v_{ctrl,d}^m}{l_g} - \frac{r_g}{l_g}\Delta i_{g,d}^m + \omega_g \Delta i_{g,q}^m\right)\omega_b \tag{B.1}$$

$$\frac{d\Delta i_{g,q}^m}{dt} = \left(\frac{\Delta v_{g,q}^m}{l_g} - \frac{\Delta v_{ctrl,q}^m}{l_g} - \frac{r_g}{l_g}\Delta i_{g,q}^m - \omega_g \Delta i_{g,d}^m\right)\omega_b \tag{B.2}$$

$$\frac{d\Delta v_{ctrl,d}^m}{dt} = \left(\frac{\Delta i_{g,d}^m}{c_f} - \frac{\Delta i_{c,d}^m}{c_f} + \omega_g \Delta v_{ctrl,q}^m\right)\omega_b \tag{B.3}$$

$$\frac{d\Delta v_{ctrl,q}^m}{dt} = \left(\frac{\Delta i_{g,q}^m}{c_f} - \frac{\Delta i_{c,q}^m}{c_f} - \omega_g \Delta v_{ctrl,d}^m\right)\omega_b \tag{B.4}$$

$$\frac{d\Delta i_{c,d}^m}{dt} = \left(\frac{\Delta v_{c,d}^m}{l_c} - \frac{\Delta v_{ctrl,d}^m}{l_c} - \frac{r_c}{l_c}\Delta i_{c,d}^m + \omega_g \Delta i_{c,q}^m\right)\omega_b \tag{B.5}$$

$$\frac{d\Delta i_{c,q}^m}{dt} = \left(\frac{\Delta v_{c,q}^m}{l_c} - \frac{\Delta v_{ctrl,q}^m}{l_c} - \frac{r_c}{l_c}\Delta i_{c,q}^m - \omega_g \Delta i_{c,d}^m\right)\omega_b \tag{B.6}$$

$$\frac{d\Delta i_e}{dt} = \left(\frac{\Delta v_{dc}^{m-}}{2l_0} - \frac{\Delta v_{dc}^{m+}}{2l_0} - \frac{r_0}{l_0}\Delta i_e\right)\omega_b \tag{B.7}$$

AC side equations of the bipolar HVDC station:

$$\frac{d\Delta i_{g,d}^b}{dt} = \left(\frac{\Delta v_{g,d}^b}{l_g} - \frac{\Delta v_{com,d}^b}{l_g} - \frac{r_g}{l_g}\Delta i_{g,d}^b + \omega_g \Delta i_{g,q}^b\right)\omega_b \tag{B.8}$$

$$\frac{d\Delta i_{g,q}^b}{dt} = \left(\frac{\Delta v_{g,q}^b}{l_g} - \frac{\Delta v_{ctrl,q}^b}{l_g} - \frac{r_g}{l_g}\Delta i_{g,q}^b - \omega_g \Delta i_{g,d}^b\right)\omega_b \tag{B.9}$$

$$\frac{d\Delta v_{com,d}^b}{dt} = \left(\frac{\Delta i_{g,d}^b}{c_f} - \frac{\Delta i_{trf,d}^{b+}}{c_f} - \frac{\Delta i_{trf,d}^{b-}}{c_f} + \omega_g \Delta v_{com,q}^b\right)\omega_b \tag{B.10}$$

$$\frac{d\Delta v_{com,q}^{b}}{dt} = \left(\frac{\Delta i_{g,q}^{b}}{c_f} - \frac{\Delta i_{trf,q}^{b+}}{c_f} - \frac{\Delta i_{trf,q}^{b-}}{c_f} - \omega_g \Delta v_{com,d}^{b}\right)\omega_b \tag{B.11}$$

$$\frac{d\Delta i_{trf,d}^{b\pm}}{dt} = \left(\frac{\Delta v_{com,d}^{b}}{l_{trf}} - \frac{\Delta v_{ctrl,d}^{b\pm}}{l_{trf}} - \frac{r_{trf}}{l_{trf}}\Delta i_{trf,d}^{b\pm} + \omega_g \Delta i_{trf,q}^{b\pm}\right)\omega_b \tag{B.12}$$

$$\frac{d\Delta i_{trf,q}^{b\pm}}{dt} = \left(\frac{\Delta v_{com,q}^{b}}{l_{trf}} - \frac{\Delta v_{ctrl,q}^{b\pm}}{l_{trf}} - \frac{r_{trf}}{l_{trf}}\Delta i_{trf,q}^{b\pm} - \omega_g \Delta i_{trf,d}^{b\pm}\right)\omega_b \tag{B.13}$$

$$\frac{d\Delta v_{ctrl,d}^{b\pm}}{dt} = \left(\frac{\Delta i_{trf,d}^{b\pm}}{c_f} + \frac{\Delta i_{c,d}^{b\pm}}{c_f} + \omega_g \Delta v_{ctrl,q}^{b\pm}\right)\omega_b \tag{B.14}$$

$$\frac{d\Delta v_{ctrl,q}^{b\pm}}{dt} = \left(\frac{\Delta i_{trf,q}^{b\pm}}{c_f} + \frac{\Delta i_{c,q}^{b\pm}}{c_f} - \omega_g \Delta v_{ctrl,d}^{b\pm}\right)\omega_b \tag{B.15}$$

$$\frac{d\Delta i_{c,d}^{b\pm}}{dt} = \left(\frac{\Delta v_{c,d}^{b\pm}}{\frac{l_{arm}}{2}} - \frac{\Delta v_{ctrl,d}^{b\pm}}{\frac{l_{arm}}{2}} - \frac{r_{arm}}{l_{arm}}\Delta i_{c,d}^{b\pm} + \omega_g \Delta i_{c,q}^{b\pm}\right)\omega_b \tag{B.16}$$

$$\frac{d\Delta i_{c,q}^{b\pm}}{dt} = \left(\frac{\Delta v_{c,q}^{b\pm}}{\frac{l_{arm}}{2}} - \frac{\Delta v_{ctrl,q}^{b\pm}}{\frac{l_{arm}}{2}} - \frac{r_{arm}}{l_{arm}}\Delta i_{c,q}^{b\pm} - \omega_g \Delta i_{c,d}^{b\pm}\right)\omega_b \tag{B.17}$$

DC side equations:

$$\frac{dv_{dc}^{m+}}{dt} = \left[i_{dc}^{m+}\left(1 - \frac{1}{2 + \frac{2c_{line}}{c_c^m}}\right) - i_{line}^{+}\left(1 - \frac{1}{2 + \frac{2c_{line}}{c_c^m}}\right) - i_{dc}^{m-}\frac{1}{2 + \frac{2c_{line}}{c_c^m}} + i_{line}^{-}\frac{1}{2 + \frac{2c_{line}}{c_c^m}}\right]\frac{\omega_b}{c_{line}} \tag{B.18}$$

$$\frac{dv_{dc}^{m-}}{dt} = \left[i_{dc}^{m-}\left(1 - \frac{1}{2 + \frac{2c_{line}}{c_c^m}}\right) - i_{line}^{-}\left(1 - \frac{1}{2 + \frac{2c_{line}}{c_c^m}}\right) - i_{dc}^{m+}\frac{1}{2 + \frac{2c_{line}}{c_c^m}} + i_{line}^{+}\frac{1}{2 + \frac{2c_{line}}{c_c^m}}\right]\frac{\omega_b}{c_{line}} \tag{B.19}$$

$$\frac{di_{line}^{+}}{dt} = \left(v_{dc}^{m+} - v_{dc}^{b+} - i_{line}^{+} r_{line}\right)\frac{\omega_b}{l_{line}} \tag{B.20}$$

$$\frac{di_{line}^{-}}{dt} = \left(v_{dc}^{m-} - v_{dc}^{b-} - i_{line}^{-} r_{line}\right) \frac{\omega_b}{l_{line}} \tag{B.21}$$

$$\frac{dv_{dc}^{b+}}{dt} = \left(i_{line}^{+} - i_{dc}^{b+}\right) \frac{\omega_b}{c_c^b} \tag{B.22}$$

$$\frac{dv_{dc}^{b-}}{dt} = \left(i_{line}^{-} - i_{dc}^{b-}\right) \frac{\omega_b}{c_c^b} \tag{B.23}$$